FABRICATION AND CHARACTERIZATION OF SPRAY PYROLYSED CADMIUM SULPHIDE HOMOJUNCTION SOLAR CELLS

Thesis

submitted to

COCHIN UNIVERSITY OF SCIENCE AND TECHNOLOGY

for the award of the degree of

DOCTOR OF PHILOSOPHY

by

K. P. VARKEY

DEPARTMENT OF PHYSICS

COCHIN UNIVERSITY OF SCIENCE AND TECHNOLOGY

KOCHI - 682022, INDIA

AUGUST 1999

CERTIFICATE

Certified that the work presented in this thesis entitled ***"Fabrication and characterization of spray pyrolysed cadmium sulphide homojunction solar cells"*** is based on the bonafide research work done by Mr. Varkey.K.P under my guidance, at the Department of Physics, Cochin University of Science and Technology, and has not been included in any other thesis submitted previously for the award of any degree.

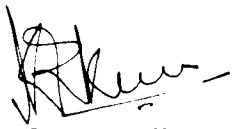

Cochin -22
11-08-1999

Prof. K. P. Vijayakumar

CONTENTS

Chapter 2

Preparation and characterization of thin films for solar cells

Chapter 3

Preparation and characterization of SnO_2, CdS and p-CdS:Cu thin films

Chapter 4

Fabrication and characterization of CdS homojunction solar cells

Preface

As the conventional energy sources are being depleted, especially the oil crisis in seventies, the entire world is searching for the alternative energy sources. Photovoltaic conversion of solar energy appears to be one of the most promising ways of meeting the increasing energy demands of the future. Enormous amount of work has been done on different techniques of fabrication of cells as well as material development. This has resulted in the lowering of the cost per peak watt of power generated from photovoltaic modules. But still this is prohibitively high, compared with the other sources of energy, making its wide spread use as a distant goal.

The main task of the scientists working in this area is to increase the efficiency of the devices and also to develop new materials with good opto electronic properties useful for energy conversion, keeping the idea of cost effectiveness. Earlier high efficiency cells coupled with solar concentrators were supposed to be the major solution for the problem of high cost. But thin film cells with moderate efficiencies and long life is considered to be the best solution for this problem.

In the material front, the photovoltaic technology was dominated by silicon mainly because of the availability of well-developed technology for material preparation and device fabrication. However as a solar cell material, silicon has certain inherent limitations. Most important one is that it is an indirect band gap semiconductor and hence it is not a good absorber of photons. Another factor is the high-tech process involved in the material purification of silicon and this is the major cause of the high cost of the silicon cells. Extensive research activities are going on in different laboratories all over the world, to develop new materials. As a result, materials like GaAs, InP, CdTe, $CuInSe_2$, $CuInS_2$ etc. have emerged as leading candidates with good opto-electronic

properties. All these materials have good optical absorption and band gaps are near ideal for maximum efficiency. These materials form heterojunction with wide gap semiconductors like cadmium sulfide (CdS) and cadmium-zinc sulfide($Cd_{1-x}Zn_x$)S. Very high efficiencies are reported for the thin film single junction solar cells fabricated using these semiconductors. It is also reported that costs of these cells are very low in comparison with silicon cells. But large scale production and marketing have not yet started.

One of the possible ways to reduce the cost is to prepare large area thin films by simple and low cost method. Usually Cadmium sulfide is used as a window material in several high efficient solar cells and the material is n-type. This is a direct band gap semiconductor having reasonably good optical absorption. There have been a few reports that p-type CdS can be prepared by proper doping. It is reported the vacuum evaporated CdS thin films can be converted in to p-CdS by copper doping. Same type of conversion is also reported on CdS thin films prepared by spray pyrolysis technique. Another report on CdS thin film by chemical bath deposition stated that the formation of p-type CdS by adding copper chloride solution in to the chemical bath. A third group reported the preparation of p-type CdS thin film in which laser ablation is applied to a mixed target of CdS and copper. In the present work, an attempt is made in fabricating a low cost homojunction solar cell using spray pyrolysed cadmium sulfide. Details of the fabrication procedure and different characterization techniques are presented in the thesis.

Cadmium sulfide can be prepared using different techniques such as vacuum evaporation, sputtering, electrodeposition, and sintering, chemical bath deposition and spray pyrolysis. Out of these, last two methods can provide large area films. It is to be specifically mentioned here that spray pyrolysis technique can be used to prepare stoichiometric films in large area and doping is also quite easy. Fabrication of homojunction in cadmium sulfide films using this

technique was not reported prior to our work by any group to the best of our knowledge. This was undertaken in the Thin Film Photovoltaic Division of the Dept. of Physics, CUSAT and forms the major part of the present work.

The thesis is organized in five chapters. Each chapter is self explanatory with its own introduction, conclusion and references. The chapter wise description of the contents is given below.

The chapter 1 begins with a general introduction, high lighting the present status of the solar cells prepared using compound and elemental semiconductors as well as the importance in the present work is mentioned in chapter. In the next part of the chapter theory of solar cell structures, with due importance to homojunction structures, is presented. The details of the solar cell parameters and cell characterization are also included in this chapter as it is essential to understand the device performance and its possible relationship with process parameters.

In the present work, for the fabrication of cadmium sulfide homojunction solar cells, we have used two techniques namely vacuum evaporation and spray pyrolysis. A detailed description about these techniques is given in first part of chapter 2, while the second part is dealing with the analytical techniques. Characterization of the materials using modern analytical instruments is an essential part of thin film research. A number of techniques are available for this .We made use of different techniques like x-ray diffraction (XRD), x-ray photon spectroscopy (XPS), and energy dispersive x-ray analysis (EDAX), at different stages, for analysing the homojunction. Optical absorption studies and Hall measurements were also used for the analysis. Depth profiling of the copper diffused cadmium sulfide (which was major analysis) was done by using auger electron spectroscopy (AES). These techniques are discussed in this part with due emphasis on their limitations and capabilities.

Details of fabrication of homojunction solar cells in cadmium sulfide, deposited by spray pyrolysis technique are given in detail in chapter 3. The results obtained from the characterization of these junctions are also described here. The first part of this chapter includes preparation and characterization of the transparent and conducting tin oxide films used as the lower electrode in the cells. For this an alcoholic solution of stannic chloride ($SnCl_4$ $0.5H_2O$) was sprayed on to hot substrate with compressed air as carrier gas. Even though this process is well known we had to standardize this process according to our laboratory conditions to get solar grade transparent conducting thin films.

Part II of chapter 3 describes the deposition of cadmium sulfide using spray pyrolysis on SnO_2 coated substrate. In order to get good quality and stoichiometric films we had to standardize the various deposition conditions. The films were prepared by spraying an aqueous solution of cadmium sulfide and thiourea on to the SnO_2 coated glass, with compressed air as carrier gas. Conductivity of the film was always found to be n-type. Resistivity was of the order of 3×10^2 Ω cm. These samples were analysed using XRD for getting information on structure, while the composition was analysed using EDAX and XPS. The surface nature was studied using SEM. Optical properties were obtained from absorption studies while electrical properties were obtained from Hall measurement. Details of all these studies are presented in this section.

Preparation of p-CdS film is described in third part of chapter 3. Thin copper film was deposited on the top surface of the n-CdS film using vacuum evaporation technique. The sample was then annealed at 300^0C under high vacuum (10^{-5} torr) for 45 minutes. Copper was completely diffused into the cadmium sulfide layer converting its top layer into p-type. AES depth profile analysis of the sample was done which indicated the existence of a layer of pure CdS below the p-type top layer. The bottom layer remained as n-type as there

was no copper in it. The structure of the film was investigated using XRD. Optical absorption and XPS studies were done in order to rule out the possibility of Cu_xS formation. Electrical characterization was done using Hall measurements and these details are included in this part.

Details of device fabrication and its characterizations are included in fourth chapter. Initial measurements on the homojunction gave encouraging results. So a complete device with the structure Glass /SnO_2 / n-CdS / p-CdS: Cu / In was fabricated. Indium was coated on the entire area of the cell. In order to improve and stabilize the characteristics of the devices, thermal treatments were given further. Finally the samples were tested for photovoltaic activity. The best cell from each batch is taken for studying the electrical properties. A detailed description of the experimental setup used for this purpose is also included here. Current - voltage characteristics under dark and illuminated conditions are presented in this chapter. Values of open circuit voltage and short-circuit current density with different annealing temperatures are presented. Spectral response curve for the best sample is also included in this part. For the best device fabricated the cell parameters were V_{oc} = 200 mV, J_{sc} = 5 mA/cm^2, FF = 0.44 and η = 0.73 % under an illumination of 60 mW/cm^2 on a cell of active area 5mm×5mm.

Optimization of the cell structure is one of the major processes in device fabrication for maximum efficiency. AES depth profile of the earlier sample showed that distribution of copper in the top layer of CdS was not uniform and the maximum copper content was existing very near to the top surface, resulting in the formation of a shallow junction. This must be an important factor for the low efficiency. So another layer of copper was again coated over the same active area of one of the cell by vacuum evaporation and the sample was annealed. The results of these cells were very much encouraging. Current - voltage characteristics under dark and illuminated conditions and the spectral

response curve of this cell was obtained. For the best device fabricated the open circuit voltage = 400 mV, J_{sc} = 12 mA/cm^2, FF = 0.49 and η = 3% under an illumination of 80 mW/cm^2. The active area of the cell is 5mm×4mm. The AES depth profile of this sample was taken to know the variation in the distribution of copper over the top p-CdS : Cu layer.

In the above two cases the fill factor of the device is low, which is due to the series resistance of the device fabricated. So we prepared a CdS film doped with indium over SnO_2 coated glass substrate. Then copper was diffused into this sample as described as earlier. Here also indium was the top electrode. The J-V characteristics of the best sample prepared under dark and illumination was drawn. The cell parameters for this were V_{oc} = 390 mV, J_{sc} = 13 mA/cm^2, FF = 0.55 and η = 3.5% under an illumination of 80 mW/cm^2 and the active cell area was 5mm×4mm. The spectral response curve of the device was also drawn.

In the last chapter, a summary of all the works done in developing the device are described. We have presented a method to fabricate a low cost solar cell. A number of problems have to be sorted out in order to improve the efficiency. Discussions of these problems are also included in this chapter.

Another problem discussed in this chapter is the environmental and safety uses related to the handling and commercial production of these devices. Future programmes to improve the efficiency of the devices in our laboratory are also discussed in this chapter.

List of papers published/presented/communicated in different journals/national seminars

1. Fabrication of homojunction using spray pyrolysed CdS thin film by copper diffusion
   K P Varkey and K P Vijayakumar, Jpn. J. Appl. Phys. 36(1997)L 394
2. Depth profiling of CdS homojunction using AES analysis
   K P Varkey ; K P Vijayakumar, Jun Imai, Toshijro Yoshida and Y Kashiwaba Bull. Mater.Sci. 20(1997)1085
3. Electrical studies on trap levels present in n and p-type spray pyrolysed CdS thin films
   N A Zeenath, K P Varkey and K P Vijayakumar, J. of Phys. Condensed Matter 10(9)(1998)2053
4. Spray pyrolysed thin film CdS homojunction solar cells with improved performance
   K P Varkey , K P Vijayakumar, Toshijro Yoshida and Y Kashiwaba, Renewable Energy (in press)
5. Effect of transparent conducting film on CdS homojunction
   Sunny Mathew, K P Varkey and K P Vijayakumar, Proc. of the National Solar Energy conf. (SEC), Trivandrum (1994)PV4
6. CdS homojunction by spray pyrolisis
   K P Varkey and K P Vijayakumar, Proc. National Seminar on Emerging trends in thin film technology and device fabrication (1995), CUSAT
7. Depth profile of CdS homojunction by AES analysis
   K P Varkey, K P Vijayakumar and Y Kashiwaba, Proc. Symposium on current status on solar energy material and systems, Anna University, Chennai (1997)p34

8. Spray pyrolysed thin film homojunction solar cells with improved performance
   K P Varkey and K P Vijayakumar, Renewable Energy 1999, ANERT National Conf., Trivandrum
9. Modification of window layer in spray pyrolysed CdS homojunction by indium doping
   K P Varkey , K P Vijayakumar, T Yoshida and Y Kashiwaba (communicated to Renewable Energy)

Chapter 1

General Introduction to solar cells

1.1. Introduction

For the last few decades of this century, the entire world is searching for an alternative to the conventional energy sources. Driving force for this is the realization that the traditional fossil energy sources such as coal, oil and gas are not only limited but also create environmental problems. So the world has to focus on nonconventional energy sources such as solar, wind, ocean, hydrothermal etc. Among these solar photovoltaic (PV) is the most effective because of this is abundant and free from pollution. From one square metre area, photovoltaic conversion can give 1000W, while wind energy and biomass conversion can give 500W and 50W respectively. At present, PV energy is used for both terrestrial and space applications. Infact, photovoltaic is the only convenient source of energy as far as the space application is concerned.

PV has many attractive features. As far as the conversion of light into electric energy is concerned, this is direct and instantaneous. It requires no additional fuel and there are no polluting by- products. PV systems are modular in nature and require only little maintenance. It can be physically located near the load and this reduces the transmission loss to a minimum. Above all, PV systems have no critical size.

Even after a few decades of research in PV technology, it is not matured enough to meet at least partially, the growing demands of energy for terrestrial applications. The foremost reason for this is that it is not cost effective when compared with other conventional energy sources. So the real problem before

the Scientists and Engineers working in this area is to develop PV systems that are economically viable. Keeping this goal in mind, researchers all over the world are focusing on the improvement of cell efficiency, development of low cost process for cell fabrication and low cost semiconducting materials.

There are mainly two different approaches adopted presently to reduce the cost of the existing devices. The first method is to make use of optical concentrating systems, so as to have high intensity of light falling over the cell. Here one uses cells of very high efficiency having small area to replace extensive solar cell areas with less expensive optics [1]. Highly efficient silicon and gallium arsenide solar cells have been now developed for this type of applications. The second approach makes use of low-cost polycrystalline semiconductor thin films for cell fabrication. This will reduce the quantity of material required for cell fabrication. Thin film photovoltaic modules may have greater potential for large scale power generation in future. Thin film technology generally provides high production capacity at reduced material consumption and energy, in the fabrication process [2]. For the production of low cost thin film cells, many materials have been developed recently [1]. So it seems that future of the PV technology depends on the development of thin film deposition techniques, suitable for the production of large area solar cells.

Several semiconducting materials have been tried for the last forty five years and now silicon has become the popular choice. Polycrystalline silicon can be used to fabricate cells having comparable efficiency at low cost, but the technology is not yet standardized. Hydrogenated amorphous silicon cells are commercially available now. Commercialization of high efficient thin film solar cells based on copper indium diselenide and cadmium telluride is now in progress. The technology for the fabrication of high quality single crystal silicon cells has been perfected and is presently readily available. The properties of the material are also studied in detail and the material is abundant and probably

echo-friendly. However one has to consider the inherent limitations of this material also. It is an indirect bandgap semiconductor, which means that during the process of optical absorption, considerable amount of photons will be lost as unabsorbed. A portion of the absorbed energy will be again lost as heat. Another disadvantage is that the optical absorption coefficient is low, which demands the use of a thick layer leading to higher cost and weight. Above all, the process of material purification is high-tech. All these limitations will ultimately affect the cell efficiency as well as the cost of the device. As a result, different new materials (both elemental and compounds) are being investigated today. The most prominent materials in the PV technology are a-Si:H, CdTe, GaAs, InP, $CuInSe_2$, $CuInS_2$, Cu(InGa)Se, CuIn(SeS) etc.

In the following section we will see the important properties of these leading materials in brief.

1.2. Solar Cell Materials

While selecting a solar cell material, one has to satisfy certain requirements. First of all, it should be a good absorber of the incident light with the optical absorption coefficient as high as possible. It should have a favourable band gap for maximum efficiency, i.e. near 1.55-1.6 eV. The material must have direct band gap. The methods of purification and preparation should be as simple as possible. Above all, the material should be easily available in large quantities and non toxic. Naturally it is very difficult to have materials with all these properties and the selection is usually done on relative merits.

1.2.1. Hydrogenated amorphous silicon (a-Si:H)

Hydrogenated amorphous silicon (a-Si:H) is currently emerging as an important material for solar cells, since this material has certain advantages. It has got a high optical absorption coefficient ($>10^5$ cm^{-1}) in the entire range of visible spectrum, which makes it suitable for thin film solar cells. Optical band

gap is nearly 1.6eV, ideal for high efficient solar cells. This can be varied between 1.1eV and 2eV by alloying with germanium or carbon [3]. This material can be prepared in thin film form having n and p-type conductivity. The resistivity of the material is usually very high (10^5 Ωcm), however by doping this can be brought to the order of 10^2 Ω cm. Deposition of amorphous silicon employs low temperatures (< 350°C) and can be easily scaled up to large areas (> m^2). Thin films of a-Si:H are prepared using a number of techniques like spray pyrolysis, sputtering, glow discharge etc. [4]. Properties of a-Si:H strongly depend on the deposition technique and the conditions prevailing during growth [4]. The best quality device films have been prepared by glow discharge of SiH_4 and solar cells made there of have exhibited better efficiencies [5]. The photovoltaic effect was observed in several types of device structures such as p/n, p/i/n and Schottky barrier junctions as well as heterojunctions. Maximum possible efficiency predicted for these cells is 15%. An efficiency of the order 12% was realised in recent times [6].

However there are some disadvantages also with this material. Device quality a-Si fabrication methods are vacuum based. Efforts are underway to speed up conventional glow discharge. Hot-wire technique is one technique that could be ten times or more faster than the existing glow discharge [7]. The main disadvantage is the gradual degradation in performance of the device as a result of continued light exposure or forward bias. This effect is known as Staebler Wronsky effect [2]. Light exposure has shown to increase the density of dangling bonds acting as recombination centers, which may be caused by breaking of the weak bonds [6,8]. Even though the degradation is easily reversed by heating at temperatures above 100°C [1], this still happens to be the most serious limitation to wide spread use of amorphous silicon. This disadvantage has restricted the usage of solar cells made up of a-Si:H to indoor application where there is no intense light. Production of a-Si modules presently amounts to 21% of the global PV module production of 62 MWp / year[2].

1.2.2. Cadmium Telluride (CdTe)

This is one of the most suitable materials in solar cell technology mainly because of its band gap. This II- VI binary semiconductor has got a favourable direct band gap of 1.44eV, ideal for maximum efficiency and a high optical absorption coefficient. This material crystallizes in Zinc blend structure (a=0.648nm). Heterojunction solar cells using CdTe is very effective, since it has got a matching electron affinity and lattice matching with certain window materials like cadmium sulphide. Highest conversion efficiency of 15.8% has been reported by Chu and Ferekides [9]. Majority of the highly efficient CdTe based solar cells use a structure of Glass/ITO/CdS/CdTe. A maximum efficiency of 18% is expected for these cells [10]. Homojunction solar cell structure is also possible for this material since it can be prepared in both conductivity type, but not much work is going on in this direction.

CdTe thin films can be prepared by different deposition techniques such as chemical spray, closed space sublimation, electrodeposition, sintering of screen printed films and vacuum evaporation [11-15]. One of the features of CdTe is the ability to form large grains in thin films, which is desirable in solar cell fabrication, independent of the deposition techniques. Jassim et al [16] have reported the formation of CdTe thin films with large grain size by closed space sublimation. A cadmium chloride treatment and a subsequent annealing in air at 400°C also promote the grain growth of the as deposited thin film. This annealing also enhances the interdiffusion of sulphur and tellurium, thus forming a mixed alloy Cd(S,Te) at the interface. This is believed to shift the actual p-n junction into the CdTe and to passivate the metallurgical hetero interface [2].

CdTe cell technology is at present closest to commercialization. Two American companies (Solar Cells Inc. and Golden Photon) have got manufacturing plants for CdTe. Inspite of all these advantages, some

environmental, safety and health risks are associated with the production and use of cadmium telluride modules on commercial basis. The CdTe-CdS modules have failed the toxicity characterizing leaching procedure (CTCLP Test) partially [17]. However, it is believed that reduced quantities of the material in the deposition process and careful recycling could overcome this problem.

1.2.3. Gallium Arsenide (GaAs)

It is a direct band gap semiconductor with optimum band gap (1.42eV), ideal for highly efficient solar cells. Good radiation resistance and significant annealing of radiation damages at 100-200°C makes it specifically suitable for space applications. GaAs crystallizes in Zinc blende structure.

GaAs thin films for solar cell applications have been grown using MOCVD, CVD, sputtering, MBE and vapour phase epitaxy [18]. GaAs based alloy films such as GaAlAs, GaAsP and GaInAs are also deposited by this deposition techniques. The most commonly used method is chemical vapour deposition.

Microstructural characteristics of the film is influenced by the deposition parameters like substrate temperatures, composition, flow rate of reactant gases and hydrogen chloride concentration at the surface [18]. The presence of hydrogen chloride reduces the rate of nucleation, promotes the growth of large crystallites and improves the bonding along the grain boundaries. The average grain size of GaAs films increases with increase in film thickness. GaAs exhibits a strong orientation along <110> direction at low arsine concentration and <111> preferred orientation at high arsine concentration, when the temperature is low. GaAs is usually n type with carrier concentration in the range of $5x10^{16}$ to 10^{17} cm^{-3} [18].

Several groups showed that germanium single crystal is a suitable substrate for CVD grown GaAs cells, since these two materials have good matching in thermal and lattice properties. Efficiencies approaching 21% were obtained for cells having an area of 4 to 16 cm^2 [19]. Some recent developments in GaAs cell technology based on improved analysis modeling and improved surface passivation are being tried on production of cells.

1.2.4. Indium Phosphide (InP)

InP has an energy gap of 1.35 eV, near the optimum value for high efficiency cells. Evaluation and characterization of InP cells have been made ever since 1960s. Since efficiency was not high (~ 10% AM0), chances of using this type of cells in terrestrial applications is probably low. InP thin films have been grown by evaporation, CVD, MOCVD and planar reactive deposition [20]. This material has a sphalerite structure at room temperature with lattice constant a=0.68nm [20]. Depending on the deposition process parameters, both amorphous and crystalline materials are obtained. Interestingly single source evaporation of InP results in amorphous and crystalline structure. Two source evaporation involving elemental deposition of In and P yields single phase InP films with grain size exceeding 1 mm at a substrate temperature of 500 K. But InP layers grown using CVD are polycrystalline and randomly oriented. InP films deposited on carbon substrates exhibit larger grains than those deposited on Mo substrates [20].

The high radiation resistance of these cells offers great promise for space applications, particularly with the prospects of continuous annealing of radiation damages by solar illumination [21]. The high radiation resistance is partly the result of low defect creation and the comparatively easy removal of defects through annealing. It is also able to retain high power output even at high radiation levels.

InP fabricated on ITO has shown an efficiency of 15.5%, while MOCVD $n^+/p/p^+$ structure had 18% efficiency [21]. In some cases p-InP was grown on p^+ InP substrates and p-n junctions were formed by ion implantation (S or Se) or by sputtered ITO layers. Workable contacts and coatings have been developed. The projected estimate of efficiency is 20% [6].

1.2.5. Copper Indium Diselenide ($CuInSe_2$)

This is one of the most suitable candidates for the solar cell because of its material properties [22] and it is evident from the fact that the heterojunctions fabricated using this material could exhibit the highest efficiency. The optical absorption coefficient of this material is the highest one reported ($\sim 3\text{-}6\times10^5$ cm^{-1}) [22] for any semiconductor. This results in the advantage that a very thin layer of material is needed, which inturn reduces the material consumption and final cost of the cell. It has a direct band gap of ~ 1 eV, near to the value of band gap for maximum efficiency. Cell structure can be hetero junction or homojunction, since copper indium diselenide (CIS) can be prepared in n and p-type. As far as the heterojunction is concerned the electron affinity of this appears to be compatible with that of window layer materials like CdS, (CdZn)S and indium tin oxide. There is also good lattice match with CdS and (CdZn)S, minimizing interfacial state density. It has very high radiation resistance which makes it ideal for space applications also.

Thin films of copper indium diselenide have been prepared by a variety of techniques like evaporation, rf sputtering, flash evaporation, spray pyrolysis, molecular beam epitaxy [23] and chemical bath deposition [24]. CIS based thin film solar cells have shown efficiencies as high as 17.7% [25] and very recently it is understood that this value has gone to 19% [26] and this is the highest value reported for a single junction polycrystalline thin film cell. The progress of CIS based solar cell efficiency from 5% to 19% with in a period of about 25 years is remarkable. CIS based solar cells have demonstrated very good outdoor stability

also. The NREL data on CIS modules (Siemens solar industries) have been exceptionally good, with no degradation by any modules, even after outdoor experiment for six years [7].

1.2.6. Copper Indium Sulphide ($CuInS_2$)

Just like other copper ternary semiconductors like $CuInSe_2$ and $CuInTe_2$, $CuInS_2$ is another direct band gap material, with a band gap of 1.55 eV, which is most ideal for maximum efficiency. It crystallizes in a diamond like lattice with a face centered tetragonal unit cell. It can be prepared in n and p-types, allowing homojunction formation as well as a variety of heterojunction types. It has got exceptional properties for terrestrial photovoltaic applications. The electron affinity and lattice constants are comparable with semiconductors like CdS and (CdZn)S. Another advantage is that it does not contain the toxic element selenium.

Thin films of $CuInS_2$ have been prepared by a variety of techniques like sputtering [27], co-evaporation[28], molecular beam epitaxy [29], electrodeposition [30] and chemical bath deposition [31]. $CuInS_2$ films prepared using rf sputtering shows absorption coefficient more than 10^4 cm^{-1} and this means that thin films of this material are suitable for the fabrication of solar cells [27]. $CuInS_2$ based solar cells have shown efficiencies of more than 12% in recent times [32].

1.2.7. Copper sulphide (Cu_xS)

The review on highly efficient solar cells is not complete without considering the Cu_2S solar cells because this is the pioneer one in the thin film PV industry. Moreover, the cell fabricated using this material (i.e. Cu_2S/CdS) is still considered to be the cheapest and simplest to fabricate. Interestingly, works of this heterojunction cell and silicon homojunction cell were started almost together.

The research on Cu_2S/CdS cell began with the work of D.C.Reynolds and Co-workers [33-35]. From the late 1950s, for a period of almost 20 years, the only all-thin-film-photovoltaic cell available was the heterojunction between p-type Cu_xS and n-type CdS. There were some difficulties in the functioning of this cell which can be summarised as a list in the following manner. 1) The interface between these two materials with different electron affinities, band gaps and crystal structures had lot of defects. 2) The interdiffusion of components caused defect states at or near the interface that strongly affected the junction properties. 3) A variety of Cu_xS phases can exist at room temperature, each with different photovoltaic properties. Changes from one to another may occur during cell fabrication and on extended operation because of loss of copper by oxidation. This affected the cell performance and life. In addition to these, there were problems like grain boundary defects, grain size and grain orientation which are common for all polycrystalline thin film devices.

An optimum cell structure was not designed even during 1960s, since little information was available about the material parameters and on the physics of the cell. But in 1970s some research groups began a systematic programme, setting targets for the open-circuit voltage, short-circuit current and fill factor guided by theoretical studies and the available information on the problems in photon absorption and carrier mechanisms [36]. This led to the production of the cells having efficiency more than 9% [37]. Certain workers tried to increase open-circuit voltage using $Zn_{0.1}Cd_{0.9}S$ as the window layer [38].

The CdS films were deposited by physical vapour deposition, spray pyrolysis, sputtering and sintering of screen printed layers. The most widely used procedure for producing Cu_2S layer is the topotaxial conversion. In this, CdS surface is treated with cuprous chloride solution through immersion [39].

The advantage of the process lies in its simplicity and speed. Another technique (known as dry process) was reported in which a film of cuprous chloride deposited on the CdS surface was allowed to react to form Cu_xS [40]. Sputtering of copper in H_2S atmosphere was also reported [41].

From the very beginning of the research work on Cu_2S/CdS cells, the problem of instability was also there. As knowledge of cell performance was improved it became clear that there were at least two primary causes for decay of performance with exposure to atmosphere. The first one was regarding the loss of short-circuit current. It was found that oxidation of the copper was the cause of this and may be avoided by proper protection of Cu_2S from the atmosphere. The second one was about the decomposition of Cu_2S. It was observed that Cu_2S, (under a sufficient high applied potential) would electrochemically decompose to produce metallic copper and reduced stoichiometry sulphide [42,43]. Little progress was made in solving this difficulty. Many published reports indicated that Cu_2S/CdS cell exposed to illumination at the maximum power point or higher voltages would degrade, particularly at open-circuit voltages, resulting in the formation of copper nodules [44].

Different research groups carried out extensive work to develop a stable cell and there by commercializing it. Stability data was not so encouraging, since the cell was not entirely free of degradation of open-circuit voltage. There were some reports indicating better performance in the case of back wall cells. However these cells had much lower efficiencies than that of the front wall design.

1.3. Solar Cell Structures

A common solar cell can mainly be divided into three distinct regions. First one is the absorber region where most of the incident solar spectrum is

absorbed to create electron-hole pairs; second one is the junction region where photogenerated carriers are separated due to the built-in electrostatic potential and the third is the collector region where the minority charge carriers become majority carriers and are fed in to the external load delivering power.

Basically there are three types of junctions; 1) metal- semicondutor 2) p-n homojunction (modification of this can be in p/i/n form also) and 3) p-n hetero junction. The basic principles involved in the last two types of junctions are discussed briefly. But a detailed study of the homojunction is required here because such a junction is selected in the present study.

1.3.1. Metal-Semiconductor Junctions

This is also known as Schottky barrier, which is the simplest one in structure to give a junction. It is made up of a thin metal film deposited on a semiconductor [45] and the energy band diagram of the junction made up of a p-type semiconductor with a metal is shown in Fig.1.1. When light is incident on the metal surface, photons with energy greater than the work function can excite holes from the metal over the barrier into the semiconductor. Since the metal film is thin, a large fraction of light enters the semiconductor and those photons with energy $h\nu > E_g$ produce electron-hole pairs in the neutral semiconductor as well as in the depletion region. Photo generated electrons are collected by the junction, while the holes move towards the back contact causing a photocurrent across the diode. The photocurrent is opposed by the dark current of the diode, which arises from the thermionic emission of holes from the semiconductor into the metal. Since dark current in a Schottky barrier diode is of a few orders of magnitude higher than that in the p-n junction diode with the same area, V_{oc} is reduced and this reduces the efficiency. The main advantage of the Schottky barrier solar cell is that it does not require any high temperature processing and is easy to fabricate. This reduces the cost of production considerably.

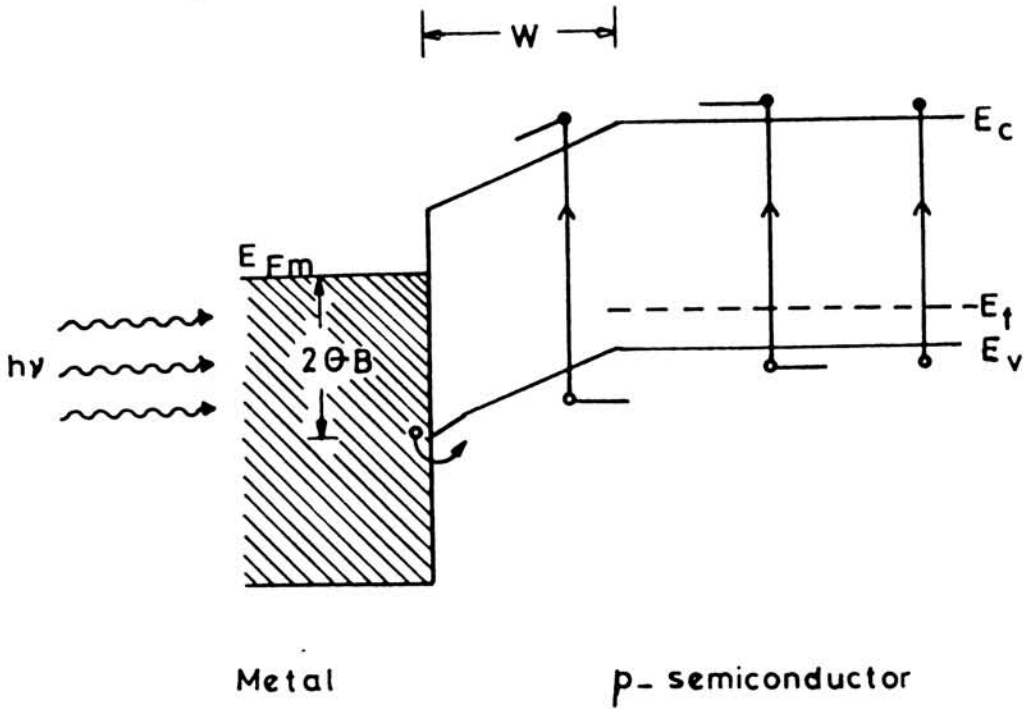

Fig. 1.1 . Energy band diagram of metal- semiconductor junction

Dark current is found to be reduced while V_{oc} gets increased due to the insertion of thin insulating layer between metal and semiconductor. This structure is known as Metal-Insulator-Semiconductor (MIS) solar cell. But the introduction of the resulting layer may reduce short circuit current. When the insulating layer is thick (> 2nm), the short circuit current will be reduced considerably [45].

1.3.2. Homojunctions

Homojunction is essentially a junction between the n and p-type portions of the same material formed by different impurity doping. The junction is termed as abrupt or graded, depending upon whether the impurity concentration in the material changes abruptly or gradually at the junction region. When two layers of semiconductor materials of opposite carrier types are intimately joined, an exchange of charge carriers take place and Fermi level becomes continuous in both the layers. Electrons from n-type portion adjacent to the junction flow into the p- side while holes from p-type to n side and this flow is due to density gradient. Then there will be some uncompensated stationary charges forming a dipole array, leading to the barrier formation. This equalizes the Fermi levels and prevents further flow of charges to either side [46]. The energy band diagram of p-n abrupt junction is shown in Fig.1.2

The sunlight incident on a p-n junction solar cell causes the absorption of photons in the semiconductor, resulting in the production of electron-hole pairs. A fraction of the photo generated carriers diffuse to the edges of the junction depletion region and is swept across the junction by the built-in electric field. Thus holes are collected on the p-side and electrons on the n-side where they are the majority carriers. The collection of charge and conversion into majority carriers give rise to photocurrent through a load connected across the cell.

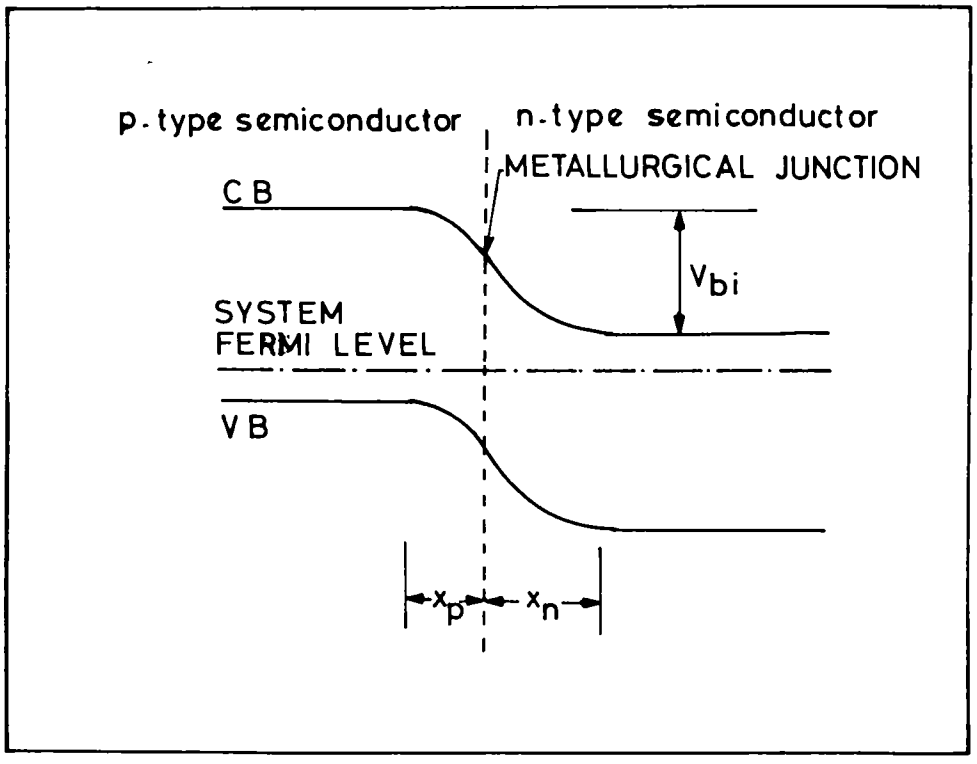

Fig. 1.2. Energy band diagram of p-n homojunction

The above description gives the picture of an ideal cell. But there are several loss mechanisms in the process and these are briefly listed in this paragraph. When light falls on the surface of a semiconductor, all the photons will not be absorbed by the material. A fraction of it is reflected and a minor part is transmitted through the material, depending upon the absorption coefficient of the material and the layer thickness. Generally as the band gap of the material increases, the absorption coefficient decreases for a given photon energy. Another loss mechanism is the recombination of the photogenerated carriers. There are several ways of recombination and the major one is surface or interface recombination. This takes place near the metal- semiconductor contact region, on the surface of the semiconductor and also in the junction region. In addition to these there will be recombination in the bulk portion of semiconductor which is known as bulk recombination. This sort of recombination can be decreased by reducing majority carrier concentration. The surface recombination can be reduced by giving passivation of surface states or preventing the flow of minority carriers towards surface states through n^+/n or p^+/p structures.

A detailed description of theory of homojunction structure is discussed in section 1.4.1.1.

1.3.3. p/i/n structures

A thin layer of intrinsic semiconductor is interjected between two heavily doped regions. This will result in enhancing the built-in electric field and also carrier collection [47]. Energy band diagram of this system is shown in Fig.1.3. Presence of intrinsic layer essentially stretches out the electrostatic field region and hence allows more photogenerated carriers to be brought to the collecting region. In p/i/n structures there is less reliance in having photo carriers diffused into the high electrostatic field barrier region for collection.

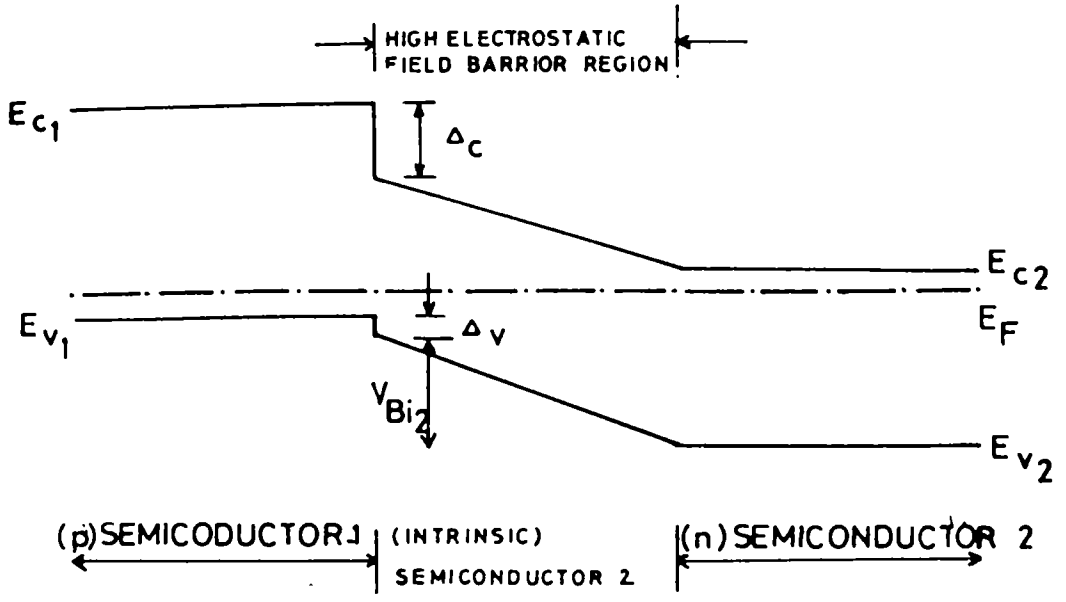

Fig. 1.3. Energy band diagram of p-i-n junction

In amorphous silicon solar cells, p/i/n structures exhibit good performance [48]. Basic problems with semiconductor like amorphous silicon are the low mobility of charge carriers and high density of recombination centers. With p/i/n structure the drift field enhances minority carrier collection, which will improve the efficiency.

1.3.4. Heterojunction

A junction formed between two semiconductors having different energy gaps and different chemical properties is termed a heterojunction. If the type of conductivity is the same in the two semiconductors, the heterojunction is called "isotype heterojunction". On the other hand, if the type of conductivity is different for the two semiconductors forming the junction, it is called "anisotropic heterojunction". Energy band diagram of an ideal heterojunction is shown in Fig. 1.4.

Some of the requirements for a good quality heterojunction are,

1. the lattice constant of the two material should be nearly equal
2. the electron affinities should be compatible
3. the thermal expansion coefficients should be close to each other.

Mismatch of lattice constants and thermal expansion coefficients will lead to interfacial dislocations at the heterojunction interface, giving rise to interface states which will act as trapping centers [49]. Heterojunction devices have certain advantages over the others for making economically feasible thin film solar cells [50]. Heterojunction structures allow the use of semiconductors that can be efficiently doped either as n-type or p-type and yet having attractive properties and reasonable cost. The use of a heterojunction with a large band gap window material and a small band gap absorber material is a means to minimize the surface recombination loss that might otherwise dominate in direct band-gap materials [51]. Heterojunctions have effective force fields due to the variation in electron and hole affinities, in addition to the electrostatic force

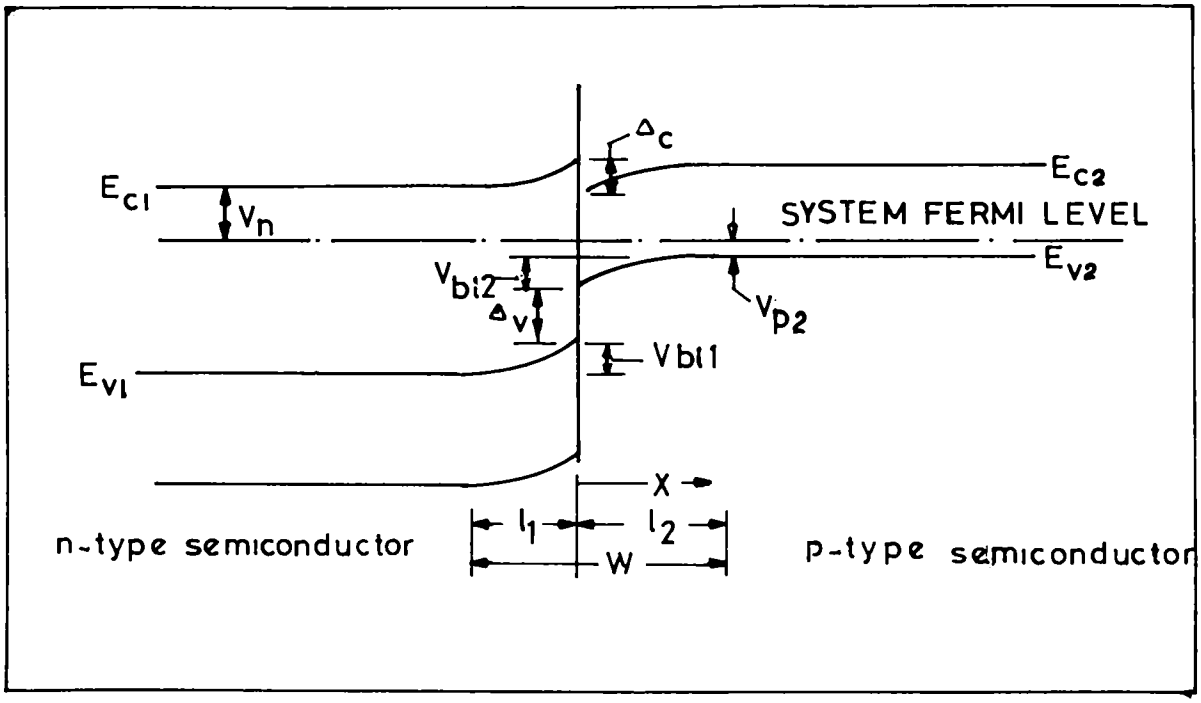

Fig.1.4. Energy band diagram of a p-n heterojunction

field and this may be used to aid in the collection of photo carries. The presence of these effective force fields can give rise to additional photovoltage.

It is interesting to note that, all the highest efficiency thin film solar cells are having heterojunction structures. Using CdTe [9], $CuInSe_2$ [25], and $CuInS_2$ [32] heterojunction structures have been made and studied. In all these cases, CdS was used as the window material because of its wide band gap, good lattice match and compatibility of electron affinity with these materials.

The absorption of photons from the incident radiation is greater in the case of heterojunction, when compared to homojunctions and this leads to better efficiency. The main disadvantage with the heterojunction is to find out a suitable material having compatible electron affinity and lattice matching as the window material. Otherwise the efficiency will be reduced. Such a problem does not arise in homojunction. A brief sketch of the theory of homojunction and heterojunction structures is included in the next section.

1.4. Theory of semiconductor solar cell structures

1.4.1. Basic theory of junction structures

Among the different structures of solar cell, homojunction and heterojunction are the most important and hence majority of research work is on these two structures. In order to know the junction behaviour and to evaluate the junction parameters of different cell structures, we should know the basic physics of these structures. In the next part of the section, physics of homojunction is given in detail, as the structure of the cells fabricated in the present work is also the same.

1.4.1.1. Homojunctions

Several workers have discussed the theory of homojunction in detail [52-55] and an overview of the work is presented in this section.

Fig.1.2 depicts a p-n homojunction in thermodynamic equilibrium. The built- in electrostatic potential energy V_{bi} is equal to the difference in work functions. Width of the space charge region in a p-n homojunction is $W = x_n + x_p$, where x_p is the extent of space charge region in the p-type material and x_n is the extent in the n-type material. For the homojunction, there are no effective forces present. There are no interface states at the metallurgical junction, since p-n homojunction is made by diffusing or implanting one dopant into oppositely doped materials.

The quantities W and the electric field, $\xi = \xi(x)$ may be obtained by applying Poisson's equation to the interface region. For the homojunction, the depletion assumption is made (neglecting all mobile charges in the depletion layer) and integrating the Poisson's equation, $\frac{d\xi}{dx} = \frac{\rho}{\varepsilon_s}$, (where ρ is the charge density and ε_s is the permittivity of the semiconductor) and assuming that N_D and N_A are constant with respect to the position, the electric field is given by

$$\xi(x) = \frac{-qN_A(x - x_p)}{\varepsilon_s} \quad \text{for } -x_p \le x \le 0 \qquad (1.1)$$

and

$$\xi(x) = \frac{qN_D(x - x_n)}{\varepsilon_s} \quad \text{for } 0 \le x \le x_n, \qquad (1.2)$$

under the assumption that the metallurgical junction is at $x = 0$ and by applying the boundary condition $\xi = 0$ at x_p and x_n. Here N_A and N_D are the acceptor and donor doping densities. The maximum electric field obtained at $x = 0$, is given by

$$\xi_m = \frac{qN_A x_p}{\varepsilon_s} = \frac{qN_D x_n}{\varepsilon_s} \tag{1.3}$$

The electrostatic potential is given by a second integration of $dV/dx = -\xi(x)$ and we will get,

$$V(x) = \frac{qN_A(x + x_p)}{2\varepsilon_s} \text{ for } -x_p < x < 0, \tag{1.4}$$

by setting V= 0, at x_p and

$$V(x) = \frac{qN_D(2xx_n - x^2)}{2\varepsilon_s} + \frac{qN_A x_p^2}{2\varepsilon_s}, \text{ for } 0 < x < x_n \tag{1.5}$$

At x_n, $V(x) = V_{bi}$, the junction built-in-voltage (diffusion voltage). So,

$$V_{bi} = \frac{q(N_D x_n^2 + N_A x_p^2)}{2\varepsilon_s} \tag{1.6}$$

From Eqn.1.6, by applying the condition that $N_A x_p = N_D x_n$,

$$x_n = \left[\frac{2\varepsilon_s V_{bi} N_A}{qN_D(N_A + N_D)}\right]^{1/2} \tag{1.7}$$

Similarly,

$$x_p = \left[\frac{2\varepsilon_s V_{bi} N_D}{qN_A(N_A + N_D)}\right]^{1/2} \tag{1.8}$$

So the depletion layer width,

$$W = x_n + x_p = \left[\frac{2\varepsilon_s V_{bi}(N_A + N_D)}{qN_A N_D}\right]^{1/2} \tag{1.9}$$

The above Eqns. 1.1 to 1.6 characterize a p-n homojunction with in the framework of depletion assumption.

If the material system of Fig.1.2 is driven out of thermodynamic equilibrium by bias, by light, by a temperature gradient etc., then V_{bi} becomes V_{bi}-V, where V is the band bending across the junction. If the equations resulting from the depletion assumption are used in this situation, then V_{bi} in equations 1.7 to 1.9 is replaced by $(V_{bi} - V)$.

From the above discussion, it follows that a p-n homojunction in an absorber can serve as a sink for photogenerated electrons diffusing out of the p-side and for photogenerated holes diffusing out of n-side, permitting current collection by diffusion.

i) Current transport

By making the following assumptions, we can obtain an expression for the current- voltage relationship for an ideal p/n junction. 1) abrupt depletion layer approximation 2) Boltzmann relations are valid throughout the depletion layer 3)injected minority carrier densities are small compared with the majority carrier densities 4) no generation currents exists in the depletion layer and the electron and hole currents are constant through the depletion layer.

At the thermal equilibrium, the Boltzmann relation is

$$n = n_i \exp\frac{E_F - E_i}{kT} = n_i \exp\frac{q(\psi - \phi)}{kT} \tag{1.10}$$

$$p = n_i \exp\frac{E_i - E_F}{kT} = n_i \exp\frac{q(\phi - \psi)}{kT} \tag{1.11}$$

where ψ and ϕ are the potential corresponding to the band edges and Fermi level respectively. When a voltage is applied, thermal equilibrium is disturbed and the minority carrier densities on both sides of the junction change. Thus $pn \neq n_i^2$. Denoting the quasi Fermi levels for electrons and holes as ϕ_n and ϕ_p respectively, the minority carrier densities are given by

$$n = n_i \exp\frac{q(\psi - \phi_n)}{kT} \tag{1.12}$$

$$p = n_i \exp\frac{q(\phi_p - \psi)}{kT} \tag{1.13}$$

and

$$pn = n_i^2 \exp\frac{q(\phi_p - \phi_n)}{kT} \tag{1.14}$$

For forward bias $\phi_p - \phi_n > 0$ and $pn > n_i^2$. At reverse bias $\phi_p - \phi_n < 0$ and $pn < n_i^2$.

The electrostatic potential difference across the junction is

$$V = \phi_p - \phi_n \tag{1.15}$$

By combining Equations 1.14 and 1.15, the expression for the electron density at the boundary of the depletion layer region on the p-side ($x = -x_p$) can be expressed as

$$n_p = \frac{n_i^2}{p_p} \exp\frac{qV}{kT} = n_{p0} \exp\left(\frac{qV}{kT}\right) \tag{1.16}$$

Similarly the hole density at $x = x_n$ on the n-side is given by

$$p_n = p_{n0} \exp\left(\frac{qV}{kT}\right) \tag{1.17}$$

The above equations 1.16 and 1.17 define the boundary conditions for the ideal current- voltage equation. Since the carrier transport is controlled by diffusion,

$$J_n = qD_n \frac{\partial n_p}{\partial x} \quad \text{at } -x_p$$

$$\text{i.e. } J_n = \frac{qD_n n_{p0}}{L_n}\left[\exp(\frac{qV}{kT}) - 1\right] \tag{1.18}$$

Where D_n is the diffusion coefficient for electrons and L_n is the diffusion length for electrons. Similarly for holes

$$J_p = -qD_p \frac{\partial p_n}{\partial x} \quad \text{at } x_n.$$

$$\text{i.e. } J_p = \frac{qD_p p_{n0}}{L_p}\left[\exp(\frac{qV}{kT}) - 1\right] \tag{1.19}$$

The total current is expressed by the well known Shockely equation

$$J = J_p + J_n = J_s\left[\exp(\frac{qV}{kT}) - 1\right] \tag{1.20}$$

$$\text{where } J_s = \frac{qD_p p_{n0}}{L_p} + \frac{qD_n n_{p0}}{L_n} \tag{1.21}$$

1.4.1.2. Semiconductor- semiconductor heterojunctions

The basic physics underlying in the working of heterojunctions were discussed by several workers [52-57] and here we will give a brief sketch of these junctions. Figure 1.4 gives an ideal anisotype heterojunction structure in thermodynamic equilibrium. The injection current model was first developed by Anderson [58]. The barrier heights of the junction are evaluated in terms of the energy band profile. In Anderson model the effects of dipoles and interface states are neglected. The n-type material has an electron affinity χ_1 and a hole affinity χ_1+Eg_1.The p-type material has an electron affinity χ_2 and hole affinity $\chi_2+ Eg_2$. The work function of the material 1 is $\phi_{n1} = \chi_1+ V_{n1}$ and the work function of the material 2 is $\phi_{p2} = \chi_2 + E_{g2}-V_{p2}$. It is assumed that $\phi_{p2} > \phi_{n1}$.

The band bending Vb_{i1} in material 1 and the band bending Vb_{i2} in material 2 represent the electrostatic potential energy required to equate the Fermi levels across this interface; i.e., $V_0 = V_{bi1} + V_{bi2}$

They must obey the condition

$$V_{bi1} + V_{bi2} = \phi_{p2} - \phi_{n1} \qquad (1.22)$$

The discontinuity in the conduction band edge Δ_c and discontinuity in the valence band edge Δ_v are given by

$$\Delta_c = \chi_2 - \chi_1 \qquad (1.23)$$

$$\Delta_v = \chi_2 + E_{g2} - (\chi_1 + E_{g1}) \qquad (1.24)$$

To further characterize the junction, the extent of the charge regions and the electrostatic field and band bending as a function of position should be determined. If the depletion assumption is valid (neglect of mobile charge), then Poisson equation is easily solved in each region of the structure. The Poisson's equation is integrated easily with the depletion assumption and we will get the following result.

$$E_{Fi1} = \frac{qN_D x^2}{2\varepsilon_{s1}} + \frac{qN_D l_1 x}{\varepsilon_{s1}} + \frac{qN_D l_1^2}{2\varepsilon_{s1}} \quad \text{for } -l_1 \le x \le 0 \qquad (1.25)$$

and

$$E_{Fi2} = \frac{-qN_A x^2}{2\varepsilon_{s2}} + \frac{qN_A l_2 x}{\varepsilon_{s2}} \text{ for } 0 \le x \le l_2 \qquad (1.26)$$

These equations use the intrinsic Fermi level to express the electrostatic potential energy or band bending variation as a function of position for each material. The boundary conditions applied here are $|Q_b^+| = |Q_b^-|$ and $\xi_0(-l_1) = \xi_0(l_2) = 0$. In addition, E_{Fi1} has been set equal to zero at $x = -l_1$ and thus it equals V_{bi1} at $x = 0$. Correspondingly E_{Fi2} has been set equal to zero at $x = 0$ and thus it equals V_{bi2} at $x = l_2$. The electrostatic field ξ_0 present in thermodynamic equilibrium is just the derivative of Eqns. (1.25) and (1.26).

We can also determine the values of l_1 and l_2 as

$$l_1 = \left[\frac{2\varepsilon_{s1}\varepsilon_{s2}N_A(\phi_{p2} - \phi_{n1})}{qN_D(\varepsilon_{s2}N_A + \varepsilon_{s1}N_D)}\right]^{1/2} \qquad (1.27)$$

$$l_2 = \left[\frac{2\varepsilon_{s1}\varepsilon_{s2}N_D(\phi_{p2} - \phi_{n1})}{qN_A(\varepsilon_{s2}N_A + \varepsilon_{s1}N_D)}\right]^{1/2} \qquad (1.28)$$

Also we can find Vb_{i1} and Vb_{i2} as

$$V_{bi1} = \frac{qN_D l_1^2}{2\varepsilon_{s1}} \qquad (1.29)$$

$$V_{bi2} = \frac{qN_A l_2^2}{2\varepsilon_{s2}} \qquad (1.30)$$

The maximum electric field existing in the interface region is seen to occur at $x = 0$ and is given by

$$\xi_{max} = \frac{qN_D l_1}{\varepsilon_{s1}} = \left[\frac{2qN_D V_{bi1}}{\varepsilon_{s1}}\right]^{1/2} \qquad (1.31)$$

or

$$\xi_{max} = \frac{qN_A l_2}{\varepsilon_{s2}} = \left[\frac{2qN_D V_{bi1}}{\varepsilon_{s1}}\right]^{1/2} \qquad (1.32)$$

Equations (1.25) to (1.32) characterize a heterojunction in thermodynamic equilibrium, if the depletion assumption is valid. If the junction is driven out of thermodynamic equilibrium by bias, by light or by a temperature gradient, then

the band bending in material 1 becomes $V_{bi1} - V_1$ and that in material 2 becomes $V_{bi2} - V_2$. These quantities replace V_{bi1} and V_{bi2} in equations (1.31) and (1.32). Since there is no interface states, we have $N_D l_1 = N_A l_2$. Then from Eqns. (1.29) and (1.30), we get

$$[N_D \varepsilon_{s1}(V_{bi1} - V_1)]^{1/2} = [N_A \varepsilon_{s2}(V_{bi2} - V_2)]^{1/2} \qquad (1.33)$$

and total change in band bending V is

$$V = V_1 + V_2 \qquad (1.34)$$

V_1 and V_2 can be expressed simply in terms of V, the bias developed or impressed on the junction, by using Eqns. (1.33) and (1.34).

1.4.2. Current- Voltage characteristics

In darkness, a solar cell behaves like a rectifying junction with the current given by (after including the effects of series resistance R_s and shunt resistance R_{sh}),

$$I = \left[1 + \frac{R_s}{R_{sh}}\right]^{-1} [I_0 \exp a(V - IR_s) + \frac{V}{R_{sh}} - I_0] \qquad (1.35)$$

where $a = q/AkT$, I_0 is the reverse saturation current and A is the diode quality factor.

Under illumination, the current voltage characteristics are translated (by the amount of the light generated current) as illustrated in the Fig. 1.5a. The current for the solar cell under illumination is given by

$$I = \left[1 + \frac{R_s}{R_{sh}}\right]^{-1} [I_0 \exp a(V - IR_s)] + \frac{V}{R_{sg}} - I_0 - H(V) I_L \qquad (1.36)$$

where I_L is the light generated current and $H(V)$ is a collection function that expresses the voltage dependence of the collection of photogenerated carriers. The form of the I-V curve in light is different from that in the dark due to the increased current through the series resistance, $H(V)$. For an ideal junction with $R_s = 0$, $R_{sh} = \infty$, $H(V) = 1$, Eqn. (1.32) reduces to

$$I = I_0 \exp(aV) - I_0 - I_L \qquad (1.37)$$

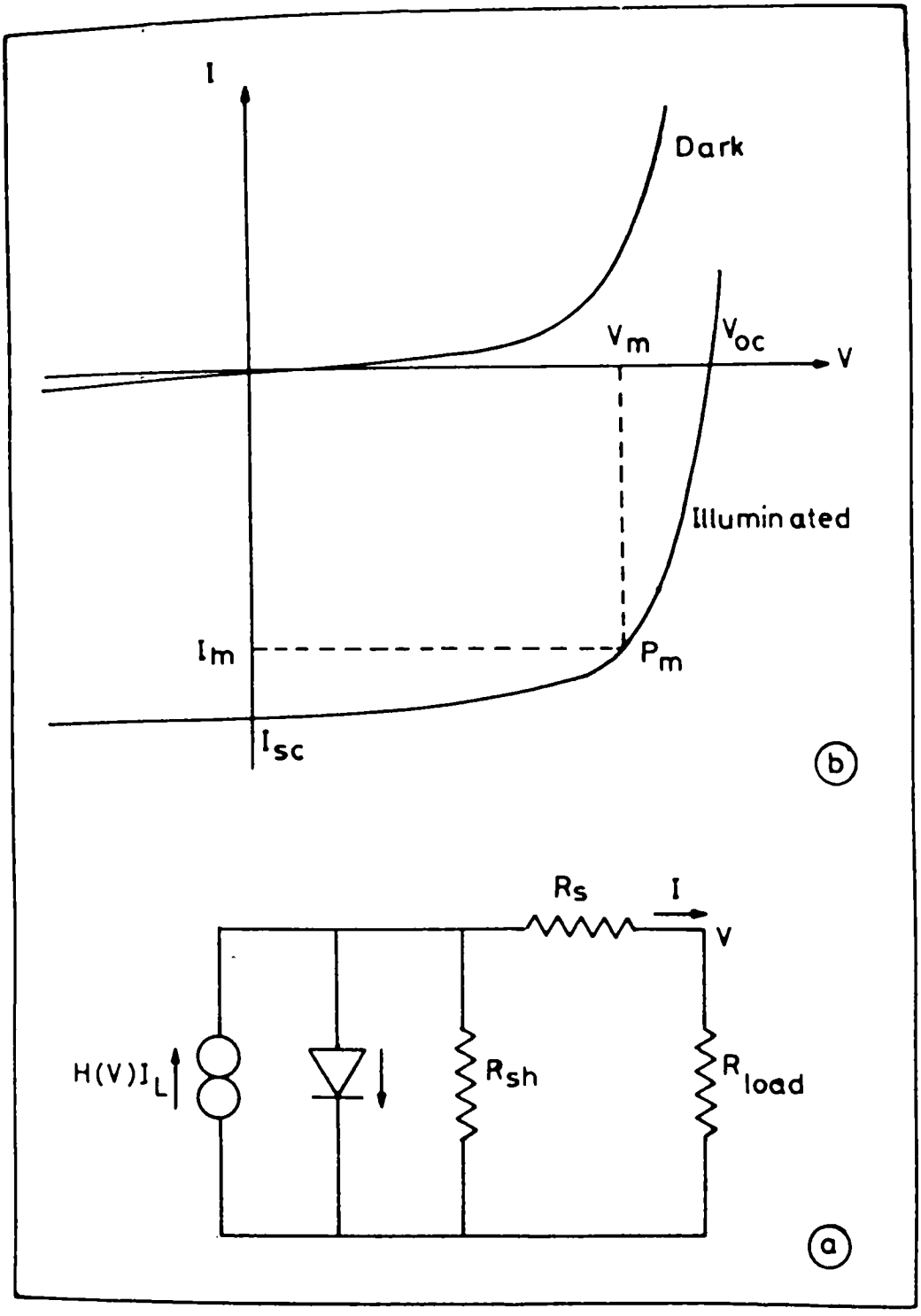

Fig. 1.5.a) The equivalent circuit for a solar cell

b) The dark and illuminated I-V curve for a solar cell

The short circuit current I_{sc} is defined as the current that flows through the junction under illumination at zero applied bias ($V = 0$) and the voltage when $I = 0$ is known as the open circuit voltage (V_{oc}). The maximum power available from the cell is

$$P_m = V_m I_m \tag{1.38}$$

where I_m and V_m are the current and voltage corresponding to the maximum power point. The ratio of the maximum power to the product of the open-circuit voltage and short circuit current is defined as fill factor (FF), i.e.,

$$FF = \frac{P_m}{I_{sc} V_{oc}} \tag{1.39}$$

The efficiency η of the solar cell for conversion of light energy into electrical energy is defined as

$$\eta = \frac{I_m V_m}{P_{in}} = \frac{I_{sc} V_{oc} FF}{P_{in}} \tag{1.40}$$

where P_{in} is the input power to the cell. The input power is given by

$$P_{in} = A_t \int_0^\infty F(\lambda) \frac{hc}{\lambda} d\lambda \tag{1.41}$$

where A_t is the total device area, $F(\lambda)$ is the number of photons per square per second per unit bandwidth incident on the device at wavelength λ and (hc/λ) is the energy associated with each photon.

An equivalent circuit of the solar cell is shown in Fig.1.5b. The rectifying junction is in parallel with the current generator, $H(V)\, I_L$, and a shunt resistance R_{sh}. The current to the external load, R_{load}, encounters a series resistance R_s

For the ideal cell, the maximum power point current I_m is given by

$$I_m = -(1 - B)(I_0 + I_L) \tag{1.42}$$

where

$$B = (1 + aV_m)^{-1} \tag{1.43}$$

For the general condition, the maximum power point is given by

$$I_m = -\left(1+\frac{R_s}{R_{sh}}\right)^{-1}(1-B)(I_0+GI_L) \tag{1.44}$$

where

$$G = H(V_m) - \frac{1}{a}(\partial H/\partial V)_{Vm} + (aI_L R_{sh})^{-1}(2-B)^{-1} \tag{1.45}$$

for the ideal solar cell $G = 1$

For the ideal case, the open circuit voltage and the short-circuit current are given by

$$V_{oc} = (1/a)\ln\left(\frac{I_L + I_0}{I_0}\right) \tag{1.46}$$

$$I_{sc} = -I_L \tag{1.47}$$

and for the general case,

$$V_{oc} = \frac{1}{a}\ln[\frac{H(V_{oc})I_L + I_0 V_{oc}/R_{sh}}{I_0}] \tag{1.48}$$

and

$$I_{sc} = (1+R_s/R_{sh})^{-1}[I_0\exp(-aI_{sc}R_s) - I_0 - H(0)I_L] \tag{1.49}$$

For the ideal case, the fill factor is given by

$$FF = \frac{(1-B^2)(1+I_0/I_L)/B}{\ln(1+I_L/I_0)} \tag{1.50}$$

For the general case, the fill factor is given by

$$FF = \frac{[(1-B)^2/B]G}{H(0)\ln[H(V_{oc})I_L/I_0]} \tag{1.51}$$

assuming the diode eqn. in light is of the form

$$I = I_0\left(\exp\frac{qV}{AkT} - 1\right) - I_{sc} \tag{1.52}$$

where

$$I_0 = I_{00}\exp\left(\frac{-qV_b}{AkT}\right) \tag{1.53}$$

the open circuit voltage can be calculated from

$$I_m = -\left(1+\frac{R_s}{R_{sh}}\right)^{-1}(1-B)(I_0+GI_L) \tag{1.44}$$

where

$$G = H(V_m) - \frac{1}{a}(\partial H/\partial V)_{Vm} + (aI_L R_{sh})^{-1}(2-B)^{-1} \tag{1.45}$$

for the ideal solar cell $G = 1$

For the ideal case, the open circuit voltage and the short-circuit current are given by

$$V_{oc} = (1/a)\ln\left(\frac{I_L + I_0}{I_0}\right) \tag{1.46}$$

$$I_{sc} = -I_L \tag{1.47}$$

and for the general case,

$$V_{oc} = \frac{1}{a}\ln[\frac{H(V_{oc})I_L + I_0 V_{oc}/R_{sh}}{I_0}] \tag{1.48}$$

and

$$I_{sc} = (1+R_s/R_{sh})^{-1}[I_0\exp(-aI_{sc}R_s) - I_0 - H(0)I_L] \tag{1.49}$$

For the ideal case, the fill factor is given by

$$FF = \frac{(1-B^2)(1+I_0/I_L)/B}{\ln(1+I_L/I_0)} \tag{1.50}$$

For the general case, the fill factor is given by

$$FF = \frac{[(1-B)^2/B]G}{H(0)\ln[H(V_{oc})I_L/I_0]} \tag{1.51}$$

assuming the diode eqn. in light is of the form

$$I = I_0\left(\exp\frac{qV}{AkT} - 1\right) - I_{sc} \tag{1.52}$$

where

$$I_0 = I_{00}\exp\left(\frac{-qV_b}{AkT}\right) \tag{1.53}$$

the open circuit voltage can be calculated from

$$V_{oc} = \frac{Ak}{q} \ln\left(\frac{I_{sc}}{I_{00}}\right) T + V_b \qquad (1.54)$$

The value of I_0 increases exponentially with decreasing ($1/T$) causing V_{oc} to decrease almost linearly with increasing T [46,59].

1.4.3. Capacitance-Voltage (C-V) characteristics

The built-in potential V_{bi} and potential distribution V(x) are expressed as

$$V(x) = \xi_m \left(x - \frac{x^2}{2W} \right) \qquad (1.55)$$

$$V_{bi} = \frac{\xi_m}{2}(l_1 + l_2)\frac{\xi_m W}{2} \qquad (1.56)$$

where W is the total depletion width. From Eqns.(1.7) and (1.8), we obtain for a two sided abrupt junction,

$$W = \left[\frac{2\varepsilon_s V_{bi}(N_A + N_D)}{qN_A N_D} \right]^{1/2} \qquad (1.57)$$

For a one sided abrupt junction,

$$W = \left[\frac{2\varepsilon_s V_{bi}}{qN_B} \right]^{1/2} \qquad (1.58)$$

where $N_B = N_D$ or N_A depending up on $N_A \gg N_D$ or $N_A \ll N_D$. If the junction is forward biased with a voltage V, the depletion layer width for a two side abrupt junction becomes

$$W = \left[(V_{bi} - V) \frac{2\varepsilon_s (N_A + N_D)}{qN_A N_D} \right]^{1/2} \qquad (1.59)$$

and for a one sided abrupt junction "W" becomes,

$$W = \left[\frac{(V_{bi} - V) 2\varepsilon_s}{qN_B} \right]^{1/2} \qquad (1.60)$$

The depletion layer capacitance per unit area, defined by $C = dQ_c/dV$ is the incremental increase in charge per unit area for an incremental change of the applied voltage dV. For one sided abrupt junction,

$$C = \frac{dQ_c}{dV} = \left[\frac{q\varepsilon_s N_B}{2(V_{bi} - V)}\right]^{1/2}$$

or

$$\frac{1}{C^2} = \frac{2(V_{bi} - V)}{q\varepsilon_s N_B} \tag{1.61}$$

The net acceptor density N_A can be calculated from the slope of a C^{-2} Vs. applied voltage plot and the built-in voltage V_b found from the voltage intercept. For a linearly graded junction, the electric field distribution is given by

$$\xi_x = \frac{-qa}{2\varepsilon\varepsilon_0}\left[(W/2)^2 - x^2\right] \tag{1.62}$$

The maximum field at $x = 0$ is given by

$$|\xi_m| = \frac{qaW^2}{8\varepsilon\varepsilon_0} \tag{1.63}$$

where 'a' is the impurity gradient. The built-in potential can be expressed as

$$V_{bi} = \frac{qaW^3}{12\varepsilon\varepsilon_0} \tag{1.64}$$

The depletion layer capacitance relation in this case is

$$C = \frac{dQ_c}{dV} = \left[\frac{qa\varepsilon^2\varepsilon_0^2}{12(V_{bi} - V)}\right]^{1/3} \tag{1.65}$$

1.4.4 Spectral Response

The spectral response measurement can provide information about the nature of the junction and the contribution to the various cell components to the output of the device. The photocurrent collected at each wavelength relative to the number of photons incident on the surface at that wavelength determines the spectral response of the device. The internal spectral response, $SR(\lambda)$, is the number of electron-hole pairs collected under short -circuit conditions relative to the number of photons entering the material and is given by

$$SR(\lambda) = \frac{J_p(\lambda)}{qF(\lambda)[1 - R(\lambda)]} + \frac{J_n(\lambda)}{qF(\lambda)[1 - R(\lambda)]} + \frac{J_{dr}(\lambda)}{qF(\lambda)[1 - R(\lambda)]} \tag{1.66}$$

while the external response $SR(\lambda)_{ext.}$ is the internal response modified by reflection losses for the surface of the device and is represented as

$$SR(\lambda)_{ext} = SR(\lambda)[1 - R(\lambda)] \qquad (1.67)$$

Where $J_p(\lambda)$, $J_n(\lambda)$, $J_{dr}(\lambda)$ are the hole diffusion, electron diffusion and depletion region contribution, respectively, to the total photocurrent density J_L, $F(\lambda)$ is the number of photons per square centimeter per second per unit band width incident on the device at wavelength λ, and $R(\lambda)$ is the fraction of these photons reflected from the surface.

1.4.5. Collection Function [*H(V)*]

The collection function $H(V)$ can be expressed as the product of two terms $h(V)$ and $g(\lambda,V)$, where $g(\lambda,V)$ represents the fraction of photogenerated minority carriers arriving at the junction interface, and $h(V)$, the fraction of photogenerated minority carriers that safely pass through the junction interface upon reaching it. Recombination in junction interface states created during fabrication of the cell (due to the presence of defects or the lattice mismatch between the window and absorber layers) reduces $h(V)$ from unity. The two terms in the collection function are given by

$$g(\lambda,V) = 1 - \exp\left(\frac{-\alpha(\lambda)W(V)}{1+\alpha(\lambda)L}\right) \qquad (1.68)$$

$$h(V) = \frac{1}{1 + S_I / \mu\xi} \qquad (1.69)$$

where α is the absorption coefficient, L the bulk minority carrier diffusion length, W the depletion layer width in the absorber, S_I the interface recombination velocity, μ the local mobility and ξ the electric field at the junction.

The electric field at the interface is given by [46]

$$\xi = \frac{2(V_b - V)}{W(V)} \qquad (1.70)$$

and the depletion layer width

$$W(V)=\left[\frac{2\varepsilon_s(V_b-V)}{qN_A}\right]^{1/2} \qquad (1.71)$$

where V_b is the built-in voltage, ε_s the permitivity of the absorber, q the electron charge and N_A the acceptor concentration. The term $h(V)$ is independent of the wavelength of the light.

1.5. Conclusion

From the above discussion, it is quite clear that thin film solar cells of moderate efficiency with reasonably good area are a solution to achieve the goal of low cost photovoltaic technology. An over view of the current photovoltaic materials is included in this chapter. The basic physics underlying the different solar cell structures with an emphasis to homojunction structure is also described.

References

1. L D.Partain (Ed), *Solar Cells and their Applications*, John Wiley & Sons, Inc., New York (1995)
2. W .H. Bloss, F. Pfisterer, M. Schubert and T. Walter, Progress in Photovoltaics: Research and Applications, **3** (1995) 3-24
3. Jeffrey C. Yang, Progress in Photovoltaics: Research and Applications, **3** (1995) 181
4. K .L. Chopra and S.R. Das, *Thin Film Solar Cells*, Plenum Press, New York (1983) 433
5. K .L. Chopra and S.R. Das, *Thin Film Solar Cells*, Plenum Press, New York (1983) 429
6. C .J. Winter, R.L. Sizman and L.L. Vant-Hull (Eds), *Solar Power Plants*, Springer-Verlag, Berlin (1991)
7. Ken Zweibel, Progress in Photovoltaics: Research and Applications, **3** (1995) 279-293
8. L .D. Partain (Ed), *Solar Cells and their Applications*, John Wiley & Sons, Inc., New York (1995) 163
9. T .L. Chu, S. Chu, J. Britt, G. Chen, C. Ferekids, N. Schultz, C. Wang and C. Wu, *Proc. 11th EC Photovoltaic Solar Energy Conf.*, Montreux, Switzerland, 1992, Harwood Academic Publishers, Switzerland (1993) 988
10. X .X. Liu, I. L. Eisgruber and J.R. Sites, *Proc. 23rd IEEE Photovoltaic Specialist Conference*, Louisville, KY, 1993, IEEE, New York (1993) 405
11. S .P. Albright, B. Ackerman and J.F. Jordan, IEEE Trans. Electron Devices **37** (1990) 434
12. C .Ferekids, J. Britt, Y. Ma and L. Killian, *Proc. 23rd IEEE Photovoltaic Specialist Conference*, Louisville, KY, 1993, IEEE, New York (1993) 389
13. J . Barker, S.P. Binns, D.R. Johnson, R.J. Marshall, S. Oktik, M.E. Ozsan, M.H. Patterson, S.J. Ransome, S. Roberts, M. Sadeghi, J. Sherborne, A.K. Turner and J.M. Woodcock, Int. J. Sol. Energy **12** (1992) 79

14. N . Suyama, N. Ueno, K. Omura, H. Takada, Y. Kita, S. Kitamura, T. Hibino, and M. Murazono, *Proc. 19th Photovoltaic Specialist Conference*, New Orleans, LA, 1987, IEEE, New York(1987) 1470
15. G .K.M. Thutupalli, and S.G. Tomlin, J. Phys. D: Appl. Phys., **9** (1976) 128
16. M .M. Al Jassim, F.S. Hasoon, K.M. Jones, B.M. Keyes, R.J. Matson and H.R. Moutinho, *Proc. 23rd IEEE Photovoltaic Specialist Conference*, Louisville, KY, 1993, IEEE, New York (1993) 459
17. W .H. Bloss, F. Pfisterer, M. Schubert and T. Walter, Progress in Photovoltaics: Research and Applications, **3** (1995) 15
18. K .L. Chopra and S.R. Das, *Thin Film Solar Cells*, Plenum Press, New York (1983) 294
19. L .D. Partain (Ed), *Solar Cells and their Applications*, John Wiley & Sons, Inc., New York (1995) 114
20. K .L. Chopra and S.R. Das, *Thin Film Solar Cells*, Plenum Press, New York (1983) 403
21. L .D. Partain (Ed), *Solar Cells and their Applications*, John Wiley & Sons, Inc., New York (1995) 116
22. L .L. Kazmerski in *Current topics in photovoltaics*, Academic Press, London (1985) 43
23. K .L. Chopra and S.R. Das, *Thin Film Solar Cells*, Plenum Press, New York (1983) 317
24. P .K. Vidyadharan Pillai, K.P. Vijayakumar, P.S. Mukerjee, J. Mater. Sci. Lett., **13** (1994) 1725
25. M . Bodegard, L. Stoltz and J. Hedestrom, *Proc. 12th European Photovoltaic Solar Energy Conf.*, Amsterdam, Kluwer Scientific, The Netherlands (1994) 1749
26. K .L. Chopra's personal communication on a seminar at CUSAT, Kochi (1999)
27. Y .Yamamoto, T. Yamaguchi, T. Tanaka, N. Tanahashi and A. yoshida, Solar Energy Materials and Solar Cells, **49** (1997) 402

28. K .Topper, J. Krauser, J. Bruns, R. Scheer, A. Weidinger and D. Brauning, Solar Energy Materials and Solar Cells, **49** (1997) 383

29. H . Metzner, Th. Hahn, Chr. Schmiga, J.H. Bremer, D. Borchett, W.R. Fahrner and M. Seibt, Solar Energy Materials and Solar Cells, **49** (1997) 337

30. S . Nakamura and A. Yamamoto, Solar Energy Materials and Solar Cells, **49** (1997) 415

31. S . Bini, K. Bindu, M. lakshmi, C. Sudha Kartha and K.P. Vijayakumar, Proc. DAE Solid State physics Symposium, **41**(1998) 489

32. T . Walter, D. Braunger, D. Hariskos, Ch. Koble and H.W. Schock, *Proc.13th European Photovoltaic Solar Energy Conf.*, Nice (1995) 597

33. D .C. Reynolds and G. M. Leies, Electr. Eng. **73** (1954) 734

34. D .C. Reynolds, G. M. Leies, L.I. Antes and R.E. Marburger, Phys. Rev., **96** (1954) 533

35. D .C. Reynolds and S.J. Czyzak, Phys. Rev., **96** (1954) 1705

36. T .J. Coutts and J.D. Meakin (Eds.), *Current topics in photovoltaics*, Academic Press, London (1985) 228

37. J .A. Bragagnolo, A.M. Barnett, G.M. Storti and J.D. Meakin, IEEE Trans. Electron Devices, ED-**27** (1980) 645

38. W . Paltz, J.Besson, T. Nguyen Duy and J. Vedol, Proc. 10th IEEE Photovoltaic Specialist Conference (1973) 69

39. J . Echigoya and J.W. Edington, Phys. Status Solidi **A 72** (1982) 304

40. T .S. Te Velde, Energy Convers., **15** (1975) 111

41. G .A. Armantrout, D.E. Miller, K.E. Vindelov and T.G. Brown, J.Vac.Sci.Technol., **16** (1979) 212

42. D .T.Bernatowicz and H.W. Brandhorst.Jr., *8th IEEE Photovoltaic Specialist Conference* (1970) 24

43. H .J. Mathieu, K.K. Reinhartz and H. Rickert, Proc. *10th IEEE Photovoltaic Specialist Conference* (1973) 93

44. T .J. Coutts and J.D. Meakin (Eds), *Current topics in photovoltaics*, Academic Press, London (1985) 241

45. M . Tyagi, *Semiconductor materials and devices*, John Wiley & Sons (1991) 348

46. A .L. Fahrenbruch and R.H. Bube, *Fundamentals of solar cells*, Academic press, New York (1983) 109

47. K .W. Boer, *Survey of semiconductor Physics*, Vol.2, Van Nostrand Reinhold, New York (1992) 820

48. K .L. Chopra and S.R. Das, *Thin film solar cells*, Plenum Press, New York (1983) 445

49. K .L. Chopra and S.R. Das, *Thin film solar cells*, Plenum Press, New York (1983) 83

50. S .J. Fonash and A. Rowthwarf in *Current topics in photovoltaics*, Academic Press, London (1985) 6

51. A .L. Fahrenbruch and R.H. Bube, *Fundamentals of solar cells*, Academic press, New York (1983) 130

52. S .J. Fonash, *Solar cell device Physics*, Academic Press, New York (1981)

53. A .L. Fahrenbruch and R.H. Bube, *Fundamentals of solar cells*, Academic press, New York (1983)

54. K .L. Chopra and S.R. Das, *Thin film solar cells*, Plenum Press, New York (1983)

55. S .M. Sze, *Physics of semiconductor devices*, 2nd Edition, Wiley Eastern Ltd., New Delhi (1981)

56. H .J. Hovel, *Semiconductors and semimetals, Vol.11, Solar cells*, Academic press, New York (1975)

57. A .G. Milnes and D.L Feucht, *Heterojunctions and Metal semiconductor junctions*, Academic press, New York (1972)

58. R .L. Anderson, Solid State Electronics **5** (1962) 341

59. J .J. Wysocki and P. Rappaport, J.Appl.Phys., **31**(1960) 571

Chapter 2

Preparation and characterization of thin films for solar cells

2.1. Introduction

Thin films have got wide applications in science and industry. During the last few decades, a number of experimental techniques have been developed for the preparation of thin films of different types of materials, mainly due to the increase in the application of thin films. For the elemental and structural analysis of the films, a large variety of characterization techniques are also developed. Vacuum evaporation, various sputtering techniques, spray pyrolysis, electrodeposition, ion beam assisted coating, molecular beam epitaxy and chemical bath deposition are the prominent techniques developed during the last fifty years [1]. Each technique has got its own advantages and limitations.

In the present work, we mainly used spray pyrolysis and vacuum evaporation techniques for the preparation of thin films used for solar cells.

The properties of the thin film depend on its structure (crystal structure, grain structure, nature of grain boundary and type defects) and composition, which in turn mainly depend on the method of preparation and variation of the parameters of the technique. So it becomes essential that the thin film samples have to be analysed using the modern analytical techniques to know the structure, chemical composition, surface nature etc. for standardizing the deposition procedure.

This chapter gives a detailed description of the techniques, for the preparation and characterization of cadmium sulphide thin films used in the present work for the fabrication of homojunction solar cell. As stated earlier, the two techniques used for sample preparation were spray pyrolysis and vacuum evaporation. Doping of the film was done through diffusion of impurity atoms using thermal annealing.

In the first part of this chapter, a brief description of major techniques used for thin film preparation is included with due importance to the two techniques relevant to the present work. The second part deals with detailed description of different analytical techniques used.

2.2. Thin film deposition techniques

A thin film deposition process involves three steps:

1) Creation of atomic/molecular/ ionic species.

2) Transport of these species through a medium

3) Condensation of the species

Depending on whether the atomic/molecular/ ionic species has been created using a physical process (such as thermal evaporation and sputtering), or by a chemical, electroless, or electrochemical process, we can broadly classify the deposition techniques under the following headings; 1) physical vapour deposition and 2) chemical vapour deposition, 3) electroless or solution growth, and 4) electrochemical deposition. By combining physical methods with CVD, hybrid techniques such as reactive evaporation/ sputtering and plasma deposition have been established. Basic principles of the techniques as well as the important properties of thin films prepared using these techniques are presently available in standard textbooks [2-5].

When one wants to deposit thin films for photovoltaic applications, it is necessary to exploit the most promising technique that satisfies the criteria of

simplicity, cost effectiveness and the capability of producing uniform films of large area with well defined physical properties. It is well known that spray pyrolysis technique satisfies many of these requirements. Hence in this work we used this technique for the preparation of tin oxide and cadmium sulphide films (Here SnO_2 films were used as the lower electrode). So we gave due emphasis to this technique and is described in detail.

The other technique namely, vacuum evaporation was used for the deposition of the copper film and also the top electrode. Details of this technique are also included in this chapter while the other techniques are mentioned in brief.

2.2.1. Sputtering

It is well known that when a surface is bombarded with high velocity positive ions, ejection of surface atoms takes place. This process of ejecting atoms from the surface due to the bombardment of positive ions (usually of inert gases) is commonly known as sputtering. The ejected atoms can be made to condense on a substrate to form a thin film.

Sputtering technique has many advantages. Any material can be volatalised by sputtering, generally compounds are volatalised stoichiometrically, and thin film deposition rate can be made uniform over large areas. Therefore it is particularly suitable for compound semiconductor thin film deposition. Furthermore the kinetic energy distribution of sputtered atoms falls largely with in the energy window for displacing surface atoms on the depositing film without causing sub surface damage. Sputtering can also be used to clean the substrate prior to the deposition. The disadvantage with this process is that a small amount of intrinsic re-sputtering always occurs largely due to the impingement of fast materials reflected from the target material. Again, the

chance of the gaseous atoms getting embedded in the film is quite large. Sputtering is used for the deposition of many semiconductors [6,7].

2.2.2. Vacuum evaporation

It is the most widely used method for preparing stoichiometric thin films, as it is very simple and convenient. Here the only requirement is to have a vacuum environment in which sufficient amount of heat is given to the evaporant to attain the vapour pressure necessary for evaporation. Then the evaporated material is allowed to condense on a substrate kept at a suitable temperature.

Deposition consists of three distinguishable steps.

1) Transition of the condensed phase (solid or liquid) into the gaseous state.

2) Traversal of the vapour from the vapour source to the substrate.

3) Condensation of the vapour at the substrate.

When evaporation is made in vacuum, the evaporation temperature will be considerably lowered and the formation of the oxides and incorporation of impurities in the growing layer will be reduced. Evaporation is normally done at a pressure of 10^{-5} torr. At this pressure, a straight line path for most of the emitted vapour atoms is also ensured, for a substrate-to-source distance of nearly 10-50 cm. The details of this technique is also available in the standard books mentioned earlier [2-5]. Depending upon the nature of heating there are several types of vacuum evaporation techniques. The most popular types are briefly described in the following section.

2.2.2.1. Resistive Heating

This is the most well known physical vapour deposition technique. Material to be deposited is created in the vapour form by resistive heating. The vapour atoms thus created are transported through a vacuum of 10^{-5} torr to get deposited on substrate. The evaporant material is supported on a source. The

requirements for the source materials are that it should have a negligible vapour pressure at the vapourisation temperature of the evaporant and should not react with the evaporant. Even though more sophisticated techniques for the preparation of thin films have been developed, electrical heating is still commonly used in the laboratory and industry to prepare thin films of oxides [8], dielectrics [9] and semiconductor compounds [10.11].

2.2.2.2. Flash Evaporation

This technique has proved to be very useful for alloys and compounds. In this method, the material to be deposited is dropped continuously as fine particles from a hopper on to a hot source from which numerous discrete evaporation takes place. The net result of this discrete evaporation is a vapour stream whose composition is uniform and identical to that of the source material. Therefore the film composition can be controlled very effectively. The stoichiometry is achieved by evaporation of the constituents in the desired ratio. The thermal energy applied to the filament is high enough to evaporate even less volatile materials [12,13].

The other techniques employed to supply the heat of vapourisation of materials are electron beam evaporation, laser evaporation, arc evaporation, radio frequency heating etc.

2.2.3. Molecular Beam Epitaxy [MBE]

Epitaxy is the oriented or single crystalline growth of one substance over another having crystallographic relations between the deposit and the substrate. Epitaxial growth on to single crystal substrates, obtained by the condensation of one or more directed beams of atoms or molecules from an effusion source in an ultra high vacuum system is called "molecular beam epitaxy" (MBE).

The low density vapour beam is obtained from a high vapour pressure Knudsen type source. This is basically a low evaporation technique, used for the analysis of the structure, topography, composition and chemical state of the surface of the film during its growth. MBE technique has been used for the deposition of GaAs based compounds [14] and copper indium selenide [15]. Again this technique is very useful for the preparation of quantum well structures [16].

2.2.4. Chemical Vapour Deposition [CVD]

Chemical vapour deposition is an important and popular technique for the preparation of wide variety of materials (elements as well as compounds) on various substrates. CVD essentially involves exposure of the substrate to one or several vapourising compounds or reagent gases, some or all of which contain constituents of the desired substance. A chemical reaction is then initiated, at or near the substrate surface, producing the desired material as a solid phase reaction product, which condenses on the substrate. The chemical reaction may be activated by the application of heat, an rf field, light or X-rays, an electric arc, a glow discharge, electron bombardment or catalytic action of the substrate surface. CVD has many advantages over other methods of thin film deposition. Films with high degree of purity, better stoichiometry and doping levels can be prepared. The need for high expensive vacuum equipment can be avoided, since many reactions can be accomplished at ambient pressures. Higher deposition temperature improves crystal perfection.

2.2.5. Electrodeposition

Electrodeposition is the process of depositing a substance by the passage of the electric current through the electrolyte, producing a chemical change. The properties of the electrodeposited films depend on the electrolyte, the electrodes and current density. When a metal electrode is dipped in a solution containing ions of that metal, a dynamic equilibrium is set up:

$M \Leftrightarrow M^{+X} + Xe$

where M denotes the metal atom. The resultant potential between the electrode and electrolyte in the absence of an external voltage is called the electrode potential.

With the establishment of dynamic equilibrium the electrode gains a certain charge on itself which attracts oppositely charged ions and molecules, holding them at the electrode/electrolyte interface by electrostatic process. During deposition, ions reach the electrode surface, move to stable positions on it and release their charges and undergo electrochemical reactions. Using this method various metals like Cu, Ag, Au etc. are electroplated for electrical contacts in solar cells. CdS films are also deposited using this technique [17,18].

2.2.6. Chemical Bath Deposition (CBD)

CBD is a solution growth process used for depositing thin films of compound materials. An aqueous solution of a metal complex when mixed with a solution of chalcogen bearing compound, precipitation of the chalcogenide occurs under certain conditions. When the precipitation is controlled, the compound gets deposited on the wall of the container and surface of the substrate. This method has been successfully used to deposit binary [19-21] and ternary semiconductors [22]. The parameters that control the deposition process are temperature, pH value, concentration of the ions, the nature of the substrate, nature of the complexing agents and the salts used. The impurities that may be present in the starting chemicals have generally no effect on the growth process, unless its concentration is such that it satisfies the condition for precipitation. So high purity chemicals are not required in this process [23]. Moreover, large area films can be obtained and vacuum is not needed. So it is clear that this technique is very simple and low cost.

2.2.7. Spray pyrolysis process

This method, useful for the preparation of compound semiconductors, was first demonstrated by Chamberline and Skarman in 1966 [24]. Since then this has been extensively used for the preparation of several semiconductor materials and it is reviewed in detail by several authors [25,26].

2.2.7.1. Principle

Spray pyrolysis involves a thermally stimulated chemical reaction between constituent ions to form the required compound. In this technique, a solution containing the soluble salts of the constituent atoms of the required compound is sprayed on to a hot substrate in the form of fine droplets, using a sprayer. Usually compressed air will be the carrier gas. But compressed nitrogen is also used as carrier gas to avoid the prescence of oxygen. The sprayed droplets reaching the hot substrate surface undergo pyrolytic decomposition and form the compound as a thin film on the surface of the hot substrate. In fact it is the hot substrate which provides the thermal energy needed for the decomposition and subsequent recombination of the constituent species. The other volatile by-products and the excess solvents are converted into vapour phase and are removed from the site of chemical reaction by using an exhaust fan.

Carrier gas here plays an active role in the pyrolytic reaction process especially in the case of oxide films. Doping can be easily accomplished by simply dissolving the dopants in the required quantity in the spray solution. Only thing to be noted here is that the soluble salt of the dopant should be available. Such an attempt is made in the present work in order to prepare indium doped cadmium sulphide films. Here characterization of the film is required for knowing the quantity of dopant available in the film. Actually in our work, we varied the concentration of the dopant and the characterization of

the films was also done. Even multicomponent doping can be done on different layers of the film, using this technique.

2.2.7.2. Growth Kinetics

The aerodynamics of the atomization and droplet impact processes had been studied by Lampkin [27]. He could correlate the dynamic features of the spray process with the kinetics of film growth and surface topography. When the size and momentum of the spray droplets are uniform, optically good quality and smooth films are obtained in the case of CdS. Analysis of surface topography of sprayed CdS films using VASE (Variable Angle Spectroscopic Ellipsometry) [28] indicated that the film prepared at low temperature had high surface roughness and this roughness decreased with increase in substrate temperature. The surface roughness reaches a minimum for films prepared at 280-300°C and thereafter it increases slowly with temperature. As the substrate temperature increases, it is observed that the reaction completes before reaching substrate surface and hence the material is deposited in the form of powder. This results in the increase of surface roughness of the film. This work also revealed that the deposition rate decreases with increase in substrate temperature and as the substrate temperature goes above 300°C, the rate of deposition decreases rapidly. At low temperatures, growth (deposition) rate is very high leading to the formation of rough films.

Deposition process in spray technique is a combination of the following steps -

1. spreading of a drop into a disk. 2. pyrolytic reaction between the decomposed reactants. 3. evaporation of the solvent. 4. the repetition of the preceding processes with succeeding droplets. Consequently, the film generally contains disks interspersed into each other. The lateral mobility of the droplets and coalescence and sintering kinetics of the superimposed disks crystallite clusters

determine the growth kinetics and microstructural features of the spray pyrolysed films.

2.2.7.3. Chemical Aspects

The chemicals used for spray pyrolysis have to satisfy the following conditions.

1. On thermal decomposition, the chemicals in solution form must provide the species/complexes that will undergo a thermally activated chemical reaction to yield the desired thin film material 2. the remaining constituents of the chemicals, including the carrier liquid should be volatile at the spray temperature. For a given thin film material, the above conditions can be met by a number of combinations of chemicals. However, different deposition parameters are required for each of these combinations in order to get good quality (structurally) films.

2.2.7.4. Characteristic features of the spray pyrolysis process

The growth rate of the sprayed films depends upon the chemical and topographical nature and temperature of the substrate, the chemical nature and concentration of spray solution and its additives. Another factor that affects the growth rate is the spray parameters like scanning speed of the spray head, the distance of the spray head from the substrate, the angle of incidence of the droplet on the substrate etc. The thickness of the film increases almost linearly with spraying time, i.e. with the amount of sprayed solution. In general, the spray pyrolysis process affects the substrate surface. When it is not desirable for the substrate to take part in the pyrolytic reactions, neutral substrates such as glass/quartz, ceramics are employed.

The chemical composition of the film is found to depend on the kinetics of the pyrolytic process. Under appropriate conditions, stoichiometric sulphide and selenide films and nearly stoichiometric oxide films can be obtained. The

stoichiometry of the sulphide films does not vary appreciably with the metal-to-sulphur ion ratio in the spray solution for ratios ranging from 1:1 to 1:1.5, but the microstructure of the film is strongly influenced by this ratio [29]. But on the other hand, stoichiometry of oxide films is dependent on relatively more complex reactions. In the case of SnO_2, the deviation from stoichiometry (i.e., the number of oxygen vacancies) is equal to the number of Sn^{4+} species reduced to Sn^{2+} ions, and this is controlled by the water and alcohol content in the spray solution. The oxygen content in the film is also influenced by the rate of cooling of the films after the spray is over, owing primarily to the adsorption of oxygen [30].

The spray deposited films are strongly adherent, mechanically hard, free from pin hole and stable with time and temperature. Post deposition annealing of films generally affects the oxygen dominated electrical properties significantly. Islam and Hakim [31] annealed SnO_2 films at 250°C, both in air and vacuum. They observed no change in optical properties, whereas there is a significant improvement in electrical properties. This is due to the oxygen chemisorption/desorption mechanisms at grain boundaries. In the present work, we made use of this technique for the preparation of tin oxide thin films and cadmium sulphide thin films.

2.2.7.5. Film preparation

The experimental setup used in our laboratory for the preparation of SnO_2 and CdS thin films is shown in Fig.2.1. The spray head and the substrate with heater are kept inside a chamber provided with an exhaust fan for removing the gaseous by-products and other gases. The geometry of the nozzles for the carrier gases and the solution mainly determines the spray pattern, size and distribution of droplets. These parameters in turn, determine the quality of the films prepared using this technique. Out of the different spray head tried in our laboratory, we have selected the one with following description.

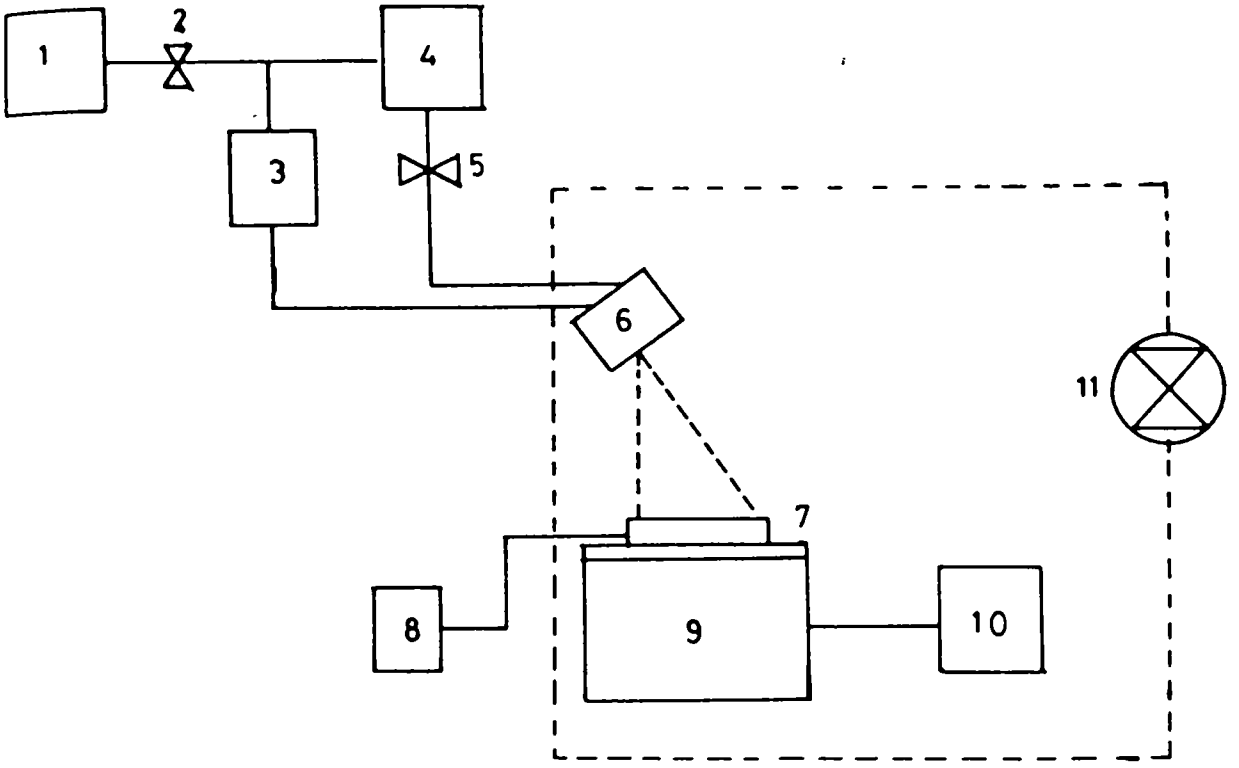

1. Air compressor
2. Gas flow control valve
3. Manometer
4. Solution reservoir
5. Solution flow control valve
6. Spray head
7. Substrate
8. Thermometer
9. Substrate heater
10. Heater control
11. Exhaust fan

Fig. 2.1. Schematic diagram of experimental set up for spray pyrolysis coating

A very fine capillary tube is used for carrying the solution and another tube with comparatively larger diameter is used for carrying the carrier gas. Both the tubes were intercepted at 80° which gives better results [28]. This avoids the formation of large size droplets in the spray. We conducted a number of experiments to optimize the spray parameters.

The cleanliness of the substrate surface has a decisive influence on the growth and adhesion of thin films. In order to get thin films of reproducible properties, a thoroughly cleaned substrate is a pre-requisite. Different cleaning methods are used depending up on the nature of the substrate, type of contaminants and degree of the cleanliness required. Usually the substrate surfaces are contaminated with finger prints, oil, lint and air borne particulate matter. Main aim of the substrate cleaning is that the bonds between the contaminant molecule and substrate surface are broken. This may be achieved in two ways: by solvent cleaning methods or by ion beam bombardment.

In the present work for the preparation of SnO_2 films, ordinary soda lime glass of dimension (7.5× 2.5× 0.2 cm^3) was used as the substrate as it is very cheap and easily available. These glass slides were cleaned using solvent cleaning method. In this technique slides were first dipped in freshly prepared chromic acid heated to 60°C. The nascent oxygen liberated from the fresh chromic acid cleanses the substrate surface. Then the slides were washed in flowing water. These glass slides were dipped in dilute alkaline detergent solution kept at 60°C. This removed the acid traces present on the surface. It was again washed in running water for some time followed by a wash in distilled water. Later ultrasonic cleaning was given, keeping the slides in distilled water. This gave scrubbing effect on the substrate surface and removed any dust particles still adhering to the surface. After this the slides were dipped in acetone for 10 minutes to remove any oil particles and water on the surface.

Finally the slides were dried in a hot air oven after which these were used as the substrate for depositing SnO_2 films by spray pyrolysis technique.

Glass slides (usually 6 in numbers) were placed on a hot plate made of thick iron block (16 × 9 × 1.25 cm^3) which can be heated to the required temperature with a controlled heater. The temperature of the substrate holder was measured using a digital thermometer (JUMO-TDAt, W.Germany). During spray, the temperature of the substrate was kept constant with an accuracy of ± 5°C. The pressure of the carrier gas was noted using a manometer and was kept at 90 ± 0.5 cms.of Hg (absolute). Usually for the preparation of SnO_2 films, hydrated stannic chloride dissolved in methanol was used as the solution and the temperature of the substrate holder was kept constant at 475°C for the good quality films. The exact details of the tin oxide films prepared in our laboratory are included in the next chapter.

For the preparation of cadmium sulphide using spray pyrolysis a mixture of aqueous solution of cadmium chloride and thiourea was sprayed on to a heated substrate. The droplet undergoes pyrolytic decomposition to form a stoichiometric cadmium sulphide film on the substrate. This takes place according to the chemical reaction

$$CdCl_2 + (NH_2)_2CS + 2H_2O \rightarrow CdS + 2NH_4Cl + CO_2$$

The setup of spray pyrolysis technique for the preparation of CdS films is exactly the same as that used for the preparation of SnO_2 films. There are a number of reports for the variation of substrate temperature and carrier gas used. But in our case we prepared CdS films at a temperature of 300°C with an accuracy of ± 5°C and air as the carrier gas. The pressure of the carrier gas was noted using a manometer and maintained at 90 ± 0.5 cms. of Hg. The spray head

had exactly the same design as that used for the preparation of tin oxide films. The exact details are included in the next chapter.

2.3. Annealing Process

In the present work of junction fabrication, we prepared p-CdS samples by the thermal annealing of copper deposited over n-CdS under high vacuum. Since this process forms the major part of our work, it needs an elaboration.

The annealing chamber was made of a glass tube over which nichrome wire was wound uniformly over the entire length of the tube. Length of the glass tube is such that three samples (5×1.2 cm^2) can be placed well inside the tube, so that a uniform heating was ensured for the samples. The tube was placed in the vacuum coating chamber and the pressure was measured using a penning gauge (Hindhivac, model STA 6P4M). Temperature was controlled by controlling the current through the nichrome wire connected to a variac and was measured using a Chromel-alumel thermocouple. The heating and cooling rate for all the annealing was kept at the rate of 2°C/minute.

2.4. Film Characterization Techniques

2.4.1. Measurement of Thickness

Film thickness can be measured by using either an in-situ monitoring technique or a post deposition technique. In the present investigation, thickness of the film was measured using gravimetric method with the help of a microbalance. Later a few cases were verified using "stylus" method. We found that, on an average, CdS films obtained by spraying 500 ml solution was having a thickness of 1μm. This was found to be true from ESCA depth profiling also.

2.4.1.1. Gravimetric Method

A microbalance (K-Roy, model K-15) with an accuracy of ± 1μg was used to measure the film thickness. A thoroughly cleaned substrate was weighed first. After depositing the film, mass of the substrate with film was determined and the difference gave mass of the film deposited. By knowing the dimension of the film and assuming bulk density, film thickness was estimated. This method of measurement was done only for the films whose thickness is greater than 300 nm. This was repeated several times to get an average value from which we could arrive at the earlier conclusion i.e., a film had a thickness of 1μm on spraying 500 ml solution. Thickness of the copper film deposited over CdS layer was obtained using a quartz crystal thickness monitor.

2.4.2. Composition analysis

Chemical analysis of thin films cannot be carried out using standard chemical methods used in the case of bulk samples. The main reason is that in this case thickness is in the range of a few hundred to few thousands of angstroms only, and hence, the quantity of material available is very less. As a result, here the normal methods of chemical analysis become difficult and one has to use sensitive instruments to know the chemical composition of thin film.

The basic principle of these sensitive techniques can be summarized as follows. The sample is irradiated with a probe beam of either particle or radiation. When the radiation interacts with the atoms of the sample material, it emits X-rays, electrons or some other radiation which are characteristic of the atoms of the materials in the film. Some of the emissions reveal the electronic or the chemical state of these atoms also. Hence by making measurements on the energies / wavelengths of these particles / radiation, it is possible to determine the elements present in the sample. In some cases the chemical state of the atoms can also be determined.

Analytical techniques like ESCA, ICP and EDAX were used in the present work and a brief description about these techniques are included in the following section.

2.4.3. Chemical / Depth profile analysis

2.4.3.1. Energy Dispersive X-ray Analysis (EDAX)

Here the sample is irradiated using electron beam and X-rays are emitted. The energy dispersive X-ray spectrometer measures the X-ray emission directly, producing a spectrum of counts versus energy. As each X-ray photon enters the detector, it produces photoelectrons, whose total number is linearly proportional to the energy of the entering X-rays. The photoelectron charge is collected using a bias voltage before the subsequent X-ray photon enters the detector. Charge collected from the detector is very small since the number of electrons produced by each X-ray photon is of the order of hundreds or at the maximum a few thousands. It is amplified using a pre- amplifier whose output voltage is proportional to energy of the x-rays[32].

The sample is usually mounted on the platform of EDAX. Characteristic peaks of X-rays emitted by constituent elements are recorded. The peaks are recorded after averaging the reading obtained from large number of counts. The surface of the film is scanned at different places to get the average counts.

In the present investigation, we used this technique for the analysis of cadmium sulphide films to compare or corroborate the results obtained from other analysis. The machine used was made by Horiba Co., model E Max.2770.

2.4.3.2. Electron Spectroscopy for Chemical Analysis (ESCA)

This method was developed in 1950s. Since then, this field has continued to grow rapidly. Now ESCA is much used in basic and applied research. It is an important tool for studying the binding energy of electrons of different

materials. Since the spatial sensitivity of this technique is limited to a very thin layer (of 50 A°), ESCA is particularly well suited for surface science and thin film applications.

In an ESCA experiment, the sample is irradiated by electromagnetic radiation of energy hν and electrons are emitted with kinetic energy

$$E_{kin} = h\nu - E_B - \phi \qquad (2.1)$$

where E_B is the binding energy (ionization energy) of a particular electron shell and ϕ is the spectrometer work function. Energy of the photoelectrons is analysed in the spectrometer and, since the photon energy is known, one can determine the characteristic binding energies of the sample material. Depending up on the energy of the incident light, it is common to denote the spectroscopy - either as UPS (ultra-violet photoelectron spectroscopy) for lower energies ($\leq$ 50 eV) or XPS (X-ray photoelectron spectroscopy) for higher photon energies ($\geq$ 1 keV). But ESCA is often used synonymously with XPS.

Depending on the applications, there are different designs of the machine. If it is vital to measure small chemical shifts and to resolve closely spaced lines, resolution is naturally the most essential parameter. In other applications where it is of prime interest to detect small concentrations of elements (like dopant), resolution can be sacrificed for intensity.

Photoelectron spectroscopy probes only the surface region of a sample. For electrons with kinetic energies in the range 100 to 1000 eV, the mean free path before an inelastic loss process is typically 5 to 20 A°, i.e., only a few interatomic spacing.

The intensity from a surface layer with thickness x can be written as

$$I(x) = I_0(1 - e^{-x/\lambda \sin\theta}) \qquad (2.2)$$

where I_0 is the total intensity and λ is the mean free path of the electron. θ is the angle between the direction of escaping electrons and the plane of the surface.

One of the main applications of ESCA is to make quantitative measurements of the concentration of different species in the surface region of a sample. The existence of chemical shifts of valence electrons of elements can be noted using this technique and this gives a clear idea about the chemical state of the ionized atom. The ESCA spectrum thereby provides information on the type of bonding formed. In other words the nature of the compound can be identified like oxide, nitride, halide etc. Combined with the surface sensitivity, this makes ESCA a surface sensitive analytical tool suitable for thin film and surface science applications. The machine used for the present analysis was ULVAC-PHI, model no: ESCA 5600 CIM.

2.4.3.3. Auger Electron Spectroscopy (AES)

In photoelectron spectroscopy, one measures the kinetic energies and thereby the binding energies of the photoelectrons. After the ionization process, the core holes decay by emitting either a radiation or auger electrons. A KLL auger transition means that the K level electron undergoes initial ionization. An L level electron moves into fill the K level vacancy and at the same time, gives up the energy of that transition to another L level electron which then becomes the ejected auger electron. The advantage of AES lies in its ability to give both a qualitative and quantitative non destructive analysis of the elements present in the immediate atomic layers, from a very small area of a solid surface. When combined with a controlled removal of surface layers by ion sputtering, AES becomes one of the most powerful analytical tools for the compositional analysis of thin films along the thickness.

In the present investigation, we used ESCA and AES for the detailed investigation of the samples prepared for the homojunction solar cells. Here we

used these techniques to know the variation of concentration of copper along the depth of the CdS layer and the chemical shifts of valence electrons of elements like Cu, Cd and S as a result of doping.

2.4.4. Structural Analysis

2.4.4.1. X-Ray Diffraction (XRD)

XRD is a precise and popular method for determining the crystal structures of thin films and it is essentially non-destructive. It gives information about the crystal structure, orientations, lattice constants, crystallite size and composition (with the help of JCPDS standards) of the sample. Analysis of the diffraction pattern obtained, by comparing with the standard JCPDS data can reveal the existence of different crystallographic phases in the film, their relative abundance and preferred orientations. From the width of the diffraction line the average grain size of the film can also be estimated.

The interplanar spacing d can be calculated from the X-ray diffraction profiles using the well known formula

$$2d\sin\theta = n\lambda \qquad (2.3)$$

where θ is the Bragg angle and n is the order of the spectrum, λ is the wavelength of X-rays. Using the d values the set of lattice planes (hkl) are identified from the standard data and the lattice parameters are calculated using the following relations.

For tetragonal systems,

$$\frac{1}{d^2} = \frac{h^2 + k^2}{a^2} + \frac{l^2}{c^2} \qquad (2.4)$$

and for hexagonal systems,

$$\frac{1}{d^2} = \frac{4(h^2 + hk + k^2)}{3a^2} + \frac{l^2}{c^2} \qquad (2.5)$$

where a and c are lattice parameters. The grain size L was evaluated using Scherrer's formula, [33]

$$L = \frac{k\lambda}{\beta \cos\theta} \qquad (2.6)$$

where k is a constant nearly equal to 1 and β the width usually measured in radians at intensity equal to half the maximum intensity of the peak (FWHM).

In the present work, this technique was used for identifying the structure of all the films prepared. The analysed range of "2θ" values was from 20° to 60° and the wavelength of the radiation was 0.15405 nm. The machine we used was Rigaku-Japan (Model D.Max.C).

2.4.4.2. Scanning Electron Microscope (SEM)

SEM is the most widely used instrument for obtaining microstructural and surface features of thin films. A finely focused electron beam is scattered over the surface of the specimen and the secondary electrons emanating from the specimen are used for imaging of the surface. To avoid charging problems, a thin layer of gold is deposited on the specimen surface without altering the surface features. The secondary electron mode (emissive mode) is generally preferred for determination of topographical features. Since these electrons come from surface layer (thickness of about 1nm), the picture obtained is a faithful reproduction of the surface features. Only the surface morphology of the film can be obtained by this technique.

We used this technique to find out the uniformity of the CdS films prepared and also for microstructure analysis.

2.4.5. Optical Properties

Optical measurements are performed for determining the band gap values of semiconductors. Photon induced electronic transitions occur between

valence band and conduction band which lead to the determination of energy band gap.

Band gap of the experimental film was determined from the absorption spectrum. Using photon energy and band gap E_g, the absorption coefficient α can be expressed as [34]

$$\alpha = (h\nu - E_g)^{\gamma} \qquad (2.7)$$

where γ is a constant. A plot of $(\alpha)^{(1/\gamma)}$ as a function of $h\nu$ yields a straight line with an intercept on the photon energy axis equal to the band gap of the material. In the one electron approximation γ=1/2 and 3/2 for allowed direct transition and forbidden direct transition respectively. The constant γ equals 2 for indirect allowed transitions where phonons are involved and equals 3 for forbidden indirect transition.

In the present work, optical absorption spectrum was taken mainly to study the change in band gap of CdS due to copper diffusion. This was also used to study the transmission spectrum of SnO_2 samples prepared. The instrument used was (Hitachi, 3410 UV-VIS-NIR). The wavelength range used for our studies was in the visible-near infra red region.

2.4.6. Electrical Properties

Knowledge of the electrical properties of semiconductor materials is necessary for understanding the factors limiting the performance of solar cells. The electrical properties of interest are the type of carriers, resistivity, mobility and carrier concentration. Here we describe the commonly used parameters.

2.4.6.1. Resistivity.

The most commonly used technique for measurement of resistivity of semiconductors is the "four probe method". Four collinear metal probes are

placed on the semiconductor. A constant current (I) is passed between the two outer probes and the voltage (V) between the inner two probes is measured. Resistivity is then calculated from the relation

$$\rho = \frac{2\pi S_0 V}{I} \qquad (2.8)$$

where S_0 is the distance between the probes.

Another parameter usually measured in thin film samples is the sheet resistance, which is expressed in Ω / □. This is measured using a simple two-probe method, selecting a square geometry for the specimen. The sheet resistivity is then calculated by multiplying the sheet resistance with the thickness of the film. The sheet resistance is independent of the size of the square we select.

2.4.6.2. Hot probe method

It is a simple method, which is widely used to determine the type of conductivity of a semiconductor specimen [35]. Two fine metal probes are placed on the semiconductor sample and a multimeter is connected between them to measure the voltage. One of the probes is kept at room temperature and the other is heated to 80°C. Hot probe heats the semiconductor immediately beneath it so that the kinetic energy of free carriers in this region is increased. Therefore the carriers diffuse out of the hot region at a faster rate than they diffuse into this region from adjacent low temperature regions. If the semiconductor is n-type, electron will move away from the hot probe leaving a positive charge region of donors and the hot probe becomes positive with respect to the cold probe. The current will flow from the hot probe to the cold probe. In a p-type semiconductor the direction of the current flow is reversed. Thus the polarity of the hot probe indicates whether the semiconductor is n-type or p-type. This method is not applicable for intrinsic semiconductors where the number of electrons and holes are nearly equal. This method is not reliable

when the resistance of the semiconductor is very high. In the present work, we often used this technique to identify the conductivity of p-type CdS film. Later this was verified using Hall measurements.

2.4.6.3. Hall Measurement.

In the conventional Hall measurement system, a rectangular bar of the specimen with thickness (d), length (l) and width (w) is placed in a magnetic flux (B). The Hall constant and Hall mobility are given by the equations

$$R_H = \frac{V_H d}{I_x B} \tag{2.9}$$

$$\mu_H = \frac{I V_H}{w V_x B} \tag{2.10}$$

where V_H is the measured Hall voltage, V_x is the applied voltage along the length l and I_x is the current.

For n-type semiconductor,

$$R_H = \frac{-1}{q n_0} \quad \text{and} \quad \mu_H = \mu_n \tag{2.11}$$

For p-type semiconductor,

$$R_H = \frac{1}{q p_0} \quad \text{and} \quad \mu_H = \mu_p \tag{2.12}$$

Density of carriers is given by

$$\eta = \frac{1}{\rho q \mu_H} \tag{2.13}$$

where ρ is the resistivity. Type of carriers is defined by the sign of the Hall mobility. If it is positive, then carriers are holes and negative indicates electrons. From the Hall measurements, the above parameters are calculated. In the present investigation, we used this technique for characterizing the n-CdS and p-CdS and SnO_2 samples. The equipment we used is Model H-50, of MMR Technologies, Inc., USA.

2.5. Conclusion

In this chapter a brief description of various preparation techniques used for thin film deposition is included, with emphasis to spray pyrolysis and vacuum evaporation. These two are the techniques mainly used for the present work. Since characterization of the prepared films is an equally important part of the current work, an account of different characterization techniques used is also described in this chapter.

References

1. K .L. Chopra and S.R. Das, *Thin Film Solar Cells*, Plenum Press, New York (1983) 195
2. K .L. Chopra, *Thin Film Phenomena*, Mc Graw Hill, New York (1969)
3. L .I. Maissel and R. Glang (Eds), *Hand Book of Thin Film Technology*, Mc Graw Hill, New York (1970)
4. Joy George, *Preparation of Thin Films*, Mercel Dekker Inc., New York (1992)
5. D .L. Smith, *Thin Film Deposition: Principles and Practice*, Mc Graw Hill, New York (1995)
6. K .L. Chopra, *Thin Film Phenomena*, Kreiger, New York (1979) 39
7. T . Serikawa and A. Okamoto, J.Vac.Sci.Technol., **A3** (1985) 1784
8. M .K. Jayaraj and C.P.G. Vallabhan, Thin Solid Films, **177** (1989) 59
9. J .D. Targove and A.R. Murphy, Thin Solid Films, **191** (1990) 47
10. K . Suzuki, Y. Ema and T. Hayashi, J.Appl.Phys., **60** (1986) 4215
11. R .D. Gould and C.J. Bowler, Thin Solid Films, **164** (1988) 281
12. E .K. Muller, J.Appl.Phys., **35** (1964) 580
13. E .G. Ellis, J.Appl.Phys., **38** (1967) 2906
14. S . Ueda, H. Kamohara, Y. Ishikawa, N. Tamura, S. Katoo and Y. Shiraki, J.Vac.Sci.Technol., **44** (1986) 602
15. Y . Korikashi, M. Kawasimha and Y. Yamaguchi, Jpn.J.Appl.Phys., **25** (1986) 868
16. Elizabeth Corcoran, *Vigyan, Scientific American* (Indian Edition), November (1990) 82
17. K .S. Balakrishnan and A.C. Rastogi, Thin Solid Films, **163** (1988) 279
18. E . Fates, P. Herrasti, F. Arjona, E.G. Camerero and M. Leon, J. Mater.Sci.Lett., **5** (1986) 583
19. M .T.S. Nair, P.K. Nair, R.A. Zingaro and E.A. Meyers, J.Appl.Phys., **75** (1994) 1557

20. M .T.S. Nair, P.K. Nair, H.M.K.K. Pathirana, R.A. Zingaro and E.A. Meyers, J.Electrochem.Soc., **140** (1993) 2987

21. C .A. Estrada, P.K. Nair, M.T.S. Nair, R.A. Zingaro and E.A. Meyers, J.Electrochem.Soc., **141** (1994) 802

22. P .K. Vidyadharan Pillai, *Ph.D.Thesis*, Cochin University of Science and Technology (1997)

23. P .K. Nair, M.T.S. Nair, V.M. Garcia, O.L. Arenas, Y. Pena, A. Castillo, I.T. Ayala, O. Gomezdaza, A. Sanchez, J. Campos, H. Hu, R. Suarez and M.E. Rincon, Solar Energy Materials and Solar cells, **52** (1998) 313

24. R .R. Chamberline and J.S. Skarman, J. Electrochem. Soc., **113** (1966) 86

25. B .R. Pamplin and S.R. Feigelson, Thin Solid Films, **60** (1979) 141

26. R . Krishnakumar, Y. Ramaprakash, V. Subramanian, K. Chandrasekhara Pillai and A.S. Lakshmanan, SPIE Opt. Mater.Tech. Energy Effic., Solar Energy Convers., **562** (1985) 187

27. C .M. Lampkin, Prog. Cry. Growth Characteristics, **1** (1979) 405

28. Sunny Mathew, *Ph.D.Thesis*, Cochin University of Science and Technology (1994)

29. Y .Y. Ma and R.H. Bube, J. Electrochem. Soc., **124** (1977) 1430

30. K .L. Chopra and S.R. Das, *Thin Film Solar Cells*, Plenum Press, New York (1983) 217

31. M .N. Islam and M.O. Hakim, J.Phys.D: Appl.Phys., **19** (1986) 615

32. H .H. Willard, L.L. Meritt Jr., John A. Dean and Frank A. Seattle Jr., (Eds.), *Instrumental Methods of Analysis*, 6th edition, CBS Publishers and Distributors, Delhi (1986)

33. B .D. Cullity, *Elements of X-ray Diffraction*, Addison-Wesley Publishing Company, Inc., Massachusetts (1967)

34. R .A. Smith, *Semiconductors*, 2nd Edition, Academic Publishers, Calcutta (1989)

35. M .S. Tyagi, Introduction to Semiconductor Materials and Devices, John wiley & Sons (1991)

Chapter 3

Preparation and characterization of SnO_2, CdS and P- CdS:Cu thin films

Preamble

Main objective of the present work is to develop a simple, low cost thin film solar cell using a very familiar semiconducting material like cadmium sulphide. We have successfully fabricated CdS homojunction solar cell with a structure of Glass/SnO_2/ n-CdS / p-CdS:Cu/In. Ordinary sodalime glass was used as the substrate. On this glass plate SnO_2 was deposited using spray pyrolysis technique, a simple and elegant process. This layer of SnO_2 acts as the lower electrode of the solar cell. Over this, a layer of cadmium sulphide was deposited again using spray pyrolysis method. A thin layer of copper was deposited on the cadmium sulphide surface using vacuum evaporation. Later the copper was diffused into the layer of cadmium sulphide by thermal annealing in high vacuum. Top layer into which copper was diffused acted as the p- type absorber and the bottom layer of CdS film remained n-type and acted as the window layer. Finally indium was deposited on the top of copper diffused layer, to act as the top electrode.

This chapter is divided into three parts, which give the details of experiments conducted for the preparation and characterization of SnO_2 and CdS in thin film form. Even though the process of preparation of these materials are well known, we had to standardize these processes in our laboratory conditions to get good quality homojunction. Moreover, to the best of our knowledge, there are only a few publications on p- type CdS thin films. Hence

we have given due emphasis on the preparation of this type of films in sprayed cadmium sulphide.

3.1. Part I Tin oxide (SnO_2)

3.1.1. Introduction

Transparent oxide thin films exhibit high electrical conductivity, high optical transmittance in the visible region and high reflectance in the IR region. It finds place in a variety of applications such as gas sensors [1-3], protective coatings [4], electrode materials in display devices [5-7] and solar cells [8,9]. The growth technique plays a significant role in governing the properties of these films, because the same material deposited by two different techniques usually have different physical properties [10]. Electrical and optical properties of these films strongly dependent on the structure, morphology and the nature of the impurities present.

SnO_2 is a material with a wide band gap of 3.5 - 4 eV and refractive index 1.9. Its conductivity can easily be controlled by proper doping and these films are extremely stable towards atmospheric exposure and highly adhesive, when prepared on glass substrates. SnO_2 has a tetragonal rutile structure with lattice parameters a = b = 4.737 A^o and c = 3.185 A^o[11]. The unit cell contains six atoms - two tin and four oxygen atoms. SnO_2 thin films can be deposited by various techniques such as CVD [12,13], spray pyrolysis [14-16], reactive evaporation [17], reactive sputtering [18] etc. The various methods of preparation of transparent conducting oxide films and their properties and applications are presented in several reviews [19,20]. In the present work, we have used SnO_2 thin films (prepared using spray pyrolysis technique) as the lower electrode in the solar cell fabricated. The preparation and characterization of these thin films are presented in detail. But before this, we present the basic principles of various deposition techniques of SnO_2 in the following sections.

Tin oxide films are usually deposited by vapourisation of suitable organo metallic compounds followed by insitu oxidation with O_2, H_2O and H_2O_2. In this type of deposition, tin is deposited first and then oxidation follows. These organo metallic compounds should be volatile, thermally stable at a temperature sufficiently high to produce an adequate vapour pressure and should dissociate at higher temperatures. Stannous and stannic chloride, tetramethyl tin, dimethyl tin chloride and di butyl tin diacetate are the most commonly used organo metallic compounds for the growth of tin oxide films. Tin oxide films grown on fused quartz substrate using CVD technique is always polycrystalline in nature [21]. However, the preferred orientation is a strong function of growth temperature and deposition rate. In order to improve the properties of SnO_2 films, doping with various elements such as antimony, phosphorous, arsenic etc. had been tried in this method of preparation [22].

SnO_2 thin films have been prepared by a wide range of vacuum evaporation techniques, such as direct evaporation of tin oxide sources using electron beam [23] and flash evaporation technique [24] and from a tin source through reactive evaporation [25]. This has also been prepared by annealing vacuum deposited tin films in oxygen atmosphere [26]. Post-oxidation is generally necessary in order to obtain conducting transparent tin oxide thin films. It has been observed that the as-evaporated films mainly have SnO phase, which is produced by the decomposition of SnO_2 molecules during evaporation. The oxidation of SnO to SnO_2 is carried out in an oxygen atmosphere at temperatures in the range 200 - 650°C.

Reactive sputtering of tin has been extensively used to grow good quality tin oxide films. The main advantage of this process is that the material can be supplied to the substrate in the desired proportion and with sufficient energy to ensure the reaction of the elements and the formation of a dense structure. Tin is sputtered in the presence of an oxygen-argon mixture. Rate of sputtering and

the ratio of oxygen to the total gas mixture decide the extent of tin oxidation. Films grown at lower substrate temperatures (< 200°C) are generally amorphous in nature and require post-deposition annealing, either in air or in vacuum. Various workers [27,28] have employed this process to prepare SnO_2 thin films. Annealing of these films improves their crystallanity and conductivity. Argon-oxygen reactive gas mixture ratio plays an important role in the formation of SnO_2 phase.

Tin oxide films have also been prepared by sputtering a tin oxide target rather than a metallic tin target. However, the presence of oxygen is essential in order to have predominantly SnO_2 phase instead of SnO in these films [29]. Introduction of oxygen and an increase of substrate temperature enhance the growth of SnO_2 phase.

CVD technique requires deposition temperatures of 400-600°C, where as a relatively lower temperature is sufficient in the case of spray process. On the other hand, it is possible to grow films at room temperature using sputtering and laser assisted deposition techniques. It is reported that SnO_2 films prepared using spray pyrolysis technique have better electrical and optical property [30]. So the spray pyrolysis technique was chosen for the preparation of SnO_2 films in the present work and the details are included in the next section.

3.1.2. Sample Preparation

Transparent conducting films of SnO_2 have been prepared by many workers using spray pyrolysis technique [31-33]. Basic principle involved in this technique is given in chapter 2. We can prepare tin oxide films doped with antimony, indium and fluorine using this method. Here we present the details of the experiments conducted and discuss the properties of the films prepared for the present work.

For the preparation of SnO_2 films, hydrated stannic chloride ($SnCl_4.5H_2O$) dissolved in methanol was used as the solution. 30 ml (0.5 M) solution was sprayed at a rate of 10 ml/minute for one set of samples. Once the spray head geometry is standardized, the important parameter that controls the properties of the film prepared is the temperature of the substrate. So the samples were prepared at different temperatures (425-525°C) to standardize the process. The films prepared below 450°C and above 500°C were found to be not so good in appearance and also in properties. So we had selected the films prepared at three temperatures 450°C, 475°C and 500°C for detailed study and the properties of these films were reported in the following section.

3.1.3. Characterization

Thickness of the film prepared can be found out by simple gravimetric method. For this the glass slide was weighed using a microbalance and SnO_2 was coated on this. It was again weighed and assuming the film to be uniform with density 6.99 gm/cm^3, the thickness of the film was calculated. This was later verified using stylus method. If we were using a solution of 30 ml, the thickness was found to be (on an average) 0.5 μm.

One of the major problems with the thin film solar cell fabrication is the poor adhesion of electrode with the substrate. When subjected to different thin film deposition steps and heat treatments, the electrode may peel off. So we have to test the adhesion when a new substrate is selected. This was done in the case of SnO_2 films using a cellophane tape. The tape is pasted uniformly on the film without having trapped air between the film and tape. The tape is then pulled off manually. If the film is not having good adhesion it will be peeled off and this never occurred in the case of the films prepared at substrate temperatures between 450 and 500°C.

In the present work, SnO_2 was used as the transparent conducting electrode. i.e. the light is entering into the absorber through the SnO_2 layer. So one of the most important parameters of interest is the percentage of transmission and second one is the electrical resistivity. These parameters were studied with the variation in substrate temperature. Resistivity of the material was calculated during the Hall measurements using Vander Pauws technique. In this measurements linearity between different points of the sample was done and by feeding the thickness of the sample, resistivity was calculated. It was found to be a minimum for the films prepared at 475°C.The percentage transmission of light was measured in the wavelength range 400-2500 nm using spectrophotometer and is depicted in Fig. 3.1. From the figure we can see that the percentage of transmission was more than 80 for all the films in the visible region and the film prepared at 450°C has a greater percentage of transmission. But the resistivity was found to be maximum for this film. Considering all these facts the film prepared at 475°C was selected for the present study.

Crystal structure of the films was analyzed using the XRD spectrum. This is shown in Fig.3.2. Films prepared at different temperatures are found to be crystalline and the pattern shows the presence of a sharp peak at $2\theta = 51.55°$, preferential growth along <211> direction for all the films prepared at different temperatures. The 'd' values are compared with the standard JCPDS data and are found to be very close to the standard value. The XRD data for the film prepared at 475°C is tabulated in Table 3.1.

Mobility, carrier concentration, resistivity and Hall coefficient were measured by Hall measurement using Vander Pauws technique in square geometry for samples prepared at different temperatures and the results of the measurements are shown in Table 3.2. Conductivity of the samples prepared at different temperatures was found to be n-type by Hall measurement. As

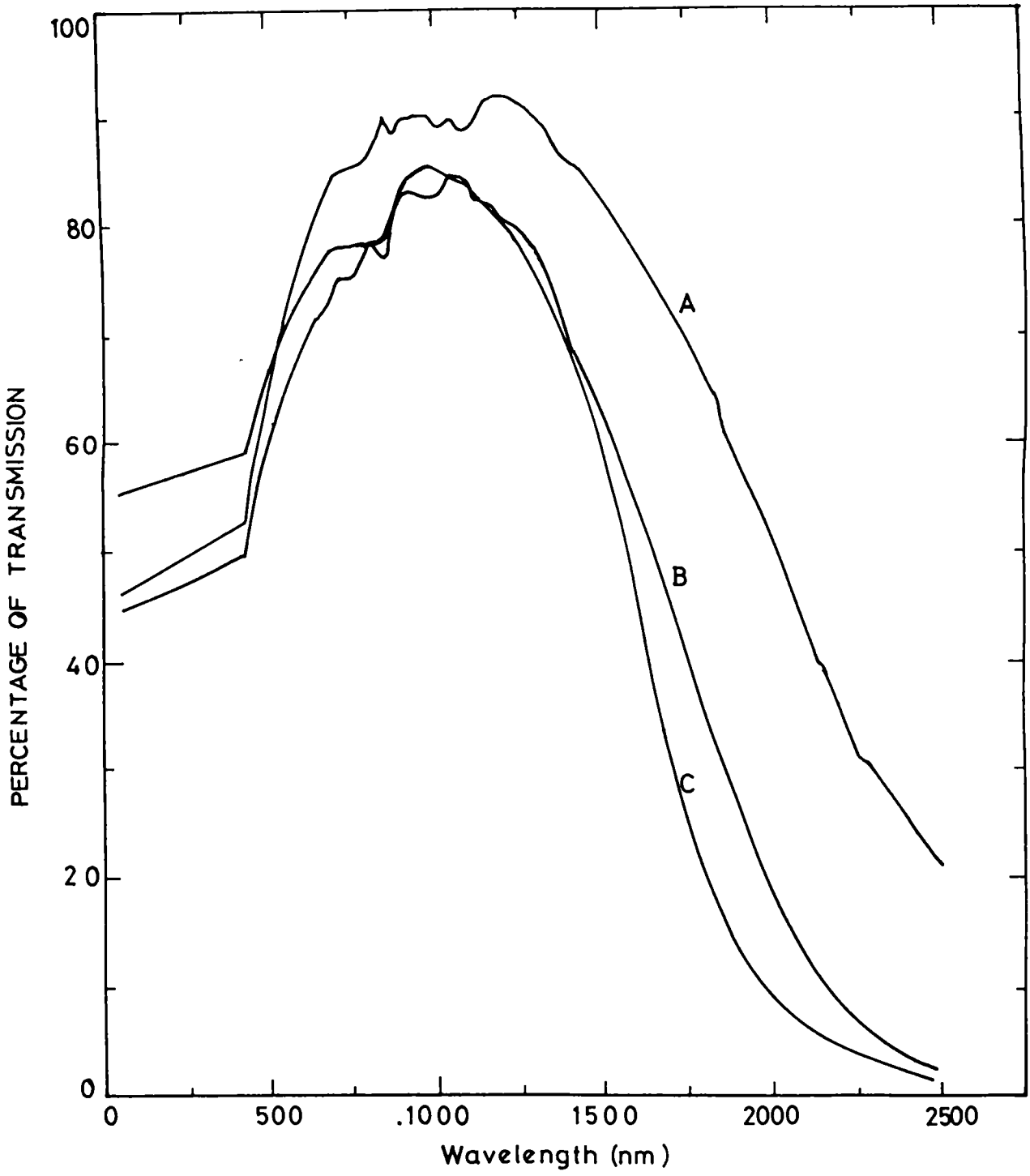

Fig. 3.1. Transmission spectra of SnO_2 films with substrate temperatures A) 450°C. B) 475°C. C) 500°C

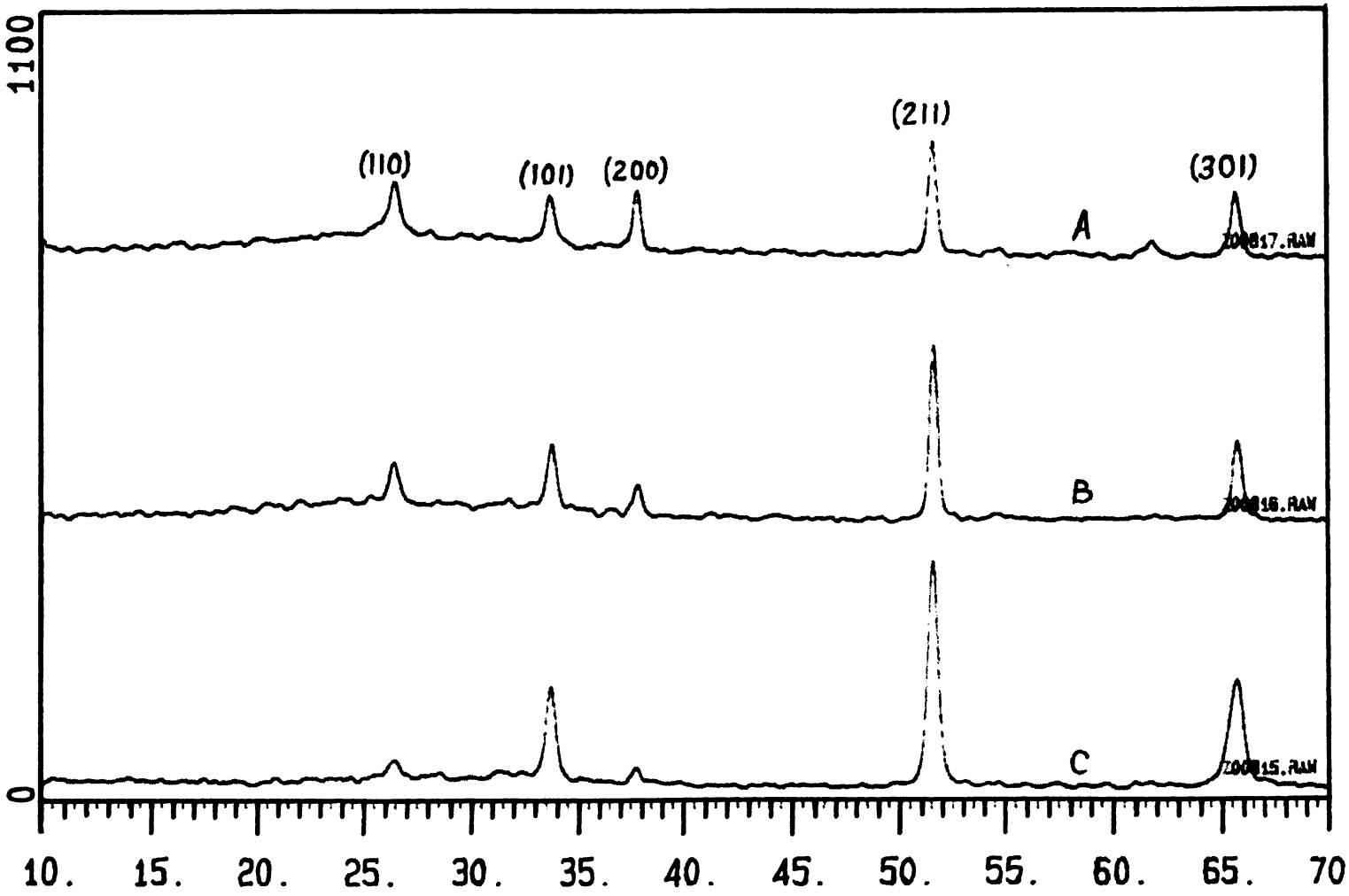

Fig.3.2. XRD spectra of SnO_2 films with substrate temperatures A) 450°C. B) 475°C. C) 500°C

temperature of the sample increases, the resistivity decreases and becomes a minimum at a temperature of 475°C beyond which it increases again.

Table 3.1.

XRD data of the SnO_2 film prepared at 475°C

Peak	2θ	d space A°		I (Rel)	plane
		observed	standard		
1	26.45	3.367	3.351	23.18	110
2	33.7	2.657	2.644	36.66	101
3	37.85	2.37	2.369	22	200
4	51.55	1.77	1.765	100	211
5	65.75	1.419	1.415	31.4	301

Table 3.2

Hall measurement values of SnO_2 samples prepared at different temperatures

Temperature °C	Resistivity Ω cm	Mobility $cm^2V^{-1}s^{-1}$	Carrier concentration cm^{-3}
450	1.512×10^{-3}	-14.29	9.7×10^{19}
475	5.680×10^{-4}	-63.28	1.449×10^{20}
500	8.718×10^{-4}	-73.79	1.74×10^{20}

Mobility and carrier concentration gradually increase as the substrate temperature is increased. More or less similar behaviour was observed by Vidyadharan Pillai [34] and Vasu et al [14]. Above results can be explained on the basis of grain boundary scattering. With an increase in substrate

temperature, the grain size increases causing a decrease in grain boundary potential and hence an increase in mobility [20]. Decrease in grain boundary potential is also responsible for an increase in carrier concentration with temperature [35].

Properties of the transparent conducting films used in the present work is summarized in Table 3.3. This type of SnO_2 film was used as the lower electrode in the solar cell fabrication.

Table 3.3

Properties of the SnO_2 films used in the present work

Thickness	500 nm
Composition	SnO_2
Grain orientation	Preferential along <211>
Resistivity	5.68×10^{-4} Ω cm
Mobility	-63.28 cm^2V^{-1} s^{-1}
Carrier concentration	1.449×10^{20} cm^{-3}
Transmission of light	80%
Typeness	n-type

3.1.4. Conclusion

Transparent conducting SnO_2 thin films were prepared on ordinary sodalime glass, well suited as lower electrode in the thin film solar cells. These were prepared using a simple and low cost process, viz., spray pyrolysis and were found to be having resistivity 5.68×10^{-4} Ω cm and 80% of optical transmission in visible region. These films were highly adhesive on glass substrates and solar cell material prepared on this also is highly adhesive.

3.2. Part II Cadmium Sulphide

3.2.1. Introduction

Extensive work have been done on this material because of its good optoelectronic properties. II-VI compound semiconductors have an important role in photovoltaic research field, since these semiconductors have direct band gaps extending from UV to far infra-red radiation. For direct band gap semiconductors the band to band absorption rises sharply and absorption coefficient is normally greater than 10^4 cm^{-1}. So the thickness of the material for the absorption of the solar radiation can be limited to ~ 1μm.

Cadmium sulphide is a semiconductor with a direct band gap of 2.42 eV. Normally the as-prepared CdS is n-type and with a typical carrier concentration in the range of 10^{16} - 10^{18} cm^{-3} [36] and mobility in the range 0.1 to 10 cm^2 V^{-1} s^{-1} [37]. Usually this is used as a window material in a variety of high efficient thin film solar cells because of its wide band gap. Most of the works in the cadmium sulphide films had been reviewed in the following section and an effort is made to highlight the properties of this semiconductor as a material for solar cell.

3.2.2. Summary of works on preparation and properties of CdS

Work on single crystal cadmium sulphide started in early 1950s. This material came to the attention of the scientific world when Reynolds et al [38] first observed the photovoltaic effect in single crystal CdS with various metal electrodes. Later R.H. Bube reported the observation of photoconductivity and crystal imperfections in CdS crystal [39]. High conductivity CdS crystals with chloride impurity showed only a very low dependence of photosensitivity on temperature with a maximum near 173K and low conductivity pure CdS crystals had much greater variation of photosensitivity with temperature. Another work

by R.H. Bube [40] on CdS was related to the speed of response of photoconductivity for high intensity excitation.

During the same decade, study on photochemical effects in CdS crystals was done by Woods et al [41]. In this work they reported that Cd-rich crystals showed a trap level at 0.41, 0.83 and 0.63 eV below the conduction band. Trap levels in Cd-rich crystals disappeared when irradiated with white light at room temperature where as in sulphur rich crystals, these levels disappeared after heat treatment at 100°C. These effects were found to be reversible and a probable explanation for this was given in terms of associated defects. Photo induced chemisorption on insulating CdS crystals was also reported during the same period [42]. David C Look reported effect of high temperature annealing in electron irradiated CdS crystals [43]. Raman effect in CdS crystals was reported by Tell et al [44] and they determined the frequency and symmetry character of the fundamentals. Mary Church et al [45] studied the Cd:S ratio with the temperature dependence. They observed that heating in ultra high vacuum made the surface sulphur rich.

Cadmium Sulphide thin films can be prepared by a variety of techniques such as thermal evaporation [46,47], sputtering [48], chemical bath deposition [49,50], spray pyrolysis [51,52], molecular beam epitaxy [53] and screen printing [54]. In the following paragraphs we will briefly explain the properties exhibited by the samples prepared using different deposition techniques that are commonly used for the preparation of thin films of this material.

Stoichiometric CdS thin films can be prepared using vacuum evaporation. Dressner et al [46] reported the crystallanity and electronic properties of evaporated films. In this work, they reported that the electron mobility depends upon the re-orientation of the crystallites, but is only slightly affected by their size. The best films were having carrier mobility of

300 cm^2 V^{-1} s^{-1}, which was almost same as that of bulk crystal. They also reported that the resistivity of the high mobility films could be controlled by the addition of Cl or Ga at the proper stage of the processing. Khawaja et al [55] determined the optical constants (n and k) of evaporated CdS films.

"Photo angular effect" for polycrystalline CdS films obtained by vacuum evaporation was investigated by Porada et al [56]. The dependence of photoelectric voltage on the angle of incidence and wavelength of light was also reported in that work. Dawar et al [57] prepared thin films of CdS using vacuum evaporation having low resistivity and high mobility. X-ray diffraction studies showed that these films are well oriented with a preferential growth of crystallites in the <002> plane and the conductivity was in the range of 0.088 Ω^{-1} cm^{-1} to 1.34 Ω^{-1} cm^{-1}. Another publication by the same group [58] was about the effect of laser irradiation on structural and electrical properties of CdS thin films deposited by resistive heating technique. XRD studies revealed that the crystallanity of these films was improved on irradiation with a pulsed laser. But Hall coefficient and mobility increased with increase of energy density as well as the number of laser pulses. The effect of low temperature annealing on the thickness of the evaporated CdS films was reported by Chatterjee and Datt [59]. In that work they also showed that the optical absorption in the film decreases with increase in annealing temperature. They reported a decrease in film thickness (of about 5%) was occurring with increase in annealing temperature. Ashour et al [60] investigated the morphology of evaporated cadmium sulphide films using scanning electron microscopy. In this paper they reported that as-grown film of thickness less than 30 nm exhibited protrusions which were identified with films grown along c-axis. The structure of the deposited film was analysed using XRD pattern, with a particular emphasis to the effects of preparation condition on the orientation, crystallite grain size and residual microstrain.

Chemical bath deposition (CBD) is a low cost process and it is one of the techniques used to prepare large area thin films. It is possible to obtain stoichiometric uniform films with good adherence and reproducibility through this technique. Bath used for the preparation of CdS thin films consists of a suitable cadmium salt for providing cadmium ions and thiourea for sulphur ions. Triethanolamine is used as a complexing agent. The bath is made alkaline by adding ammonia and bath temperature is normally maintained at about 333K. Growth of CdS thin films by this method occurs either by an ion by ion condensation of Cd^{2+} and S^{2-} on the surface of the substrate or by the adsorption of colloidal particles of CdS on to the substrate [61]. The growth process has been discussed in detail by Kaur et al [62].

Cadmium sulphide thin films prepared using CBD are normally found to be either in the metastable cubic phase or as a mixture of cubic and hexagonal phases [63]. Sebastian et al [64] discussed the effect of post-deposition treatments on morphology, structure and opto-electronic properties of chemically deposited thin films of CdS. They found that good quality films can be obtained by choosing Cd : TEA : NH3 : TU molar ratio of about 1 : 3.75: 14.4 : 1 for the opto-electronic applications. They reported that the as-deposited films contained some organo-metallic impurities on the surface, which can be removed by etching the film surface in very dilute acetic acid. Jayakrishnan et al [65] reported the study of structural changes and physical properties of CdS thin films after multiple dip coating and rapid thermal annealing using XRD, SEM and electrical characterization. Rapid thermal annealing at 5×10^{-2} torr resulted in the reduction of resistivity from $10^{6}\Omega$ cm to 0.16 Ω cm, where as a slow annealing for 30 minutes in the same vacuum resulted in a resistivity of 10Ω cm. Observed reduction in resistivity upon annealing was attributed to the oxygen desorption. K.L Narayanan et al [66] also reported the drastic reduction in resistivity on cadmium sulphide thin films prepared by CBD, when annealed in

flowing air. They observed the reduction in resistivity only when substantial quantity of CdO phase was formed.

Hernandez et al [67] reported the thermal annealing studies of CdS thin films prepared using CBD, in which they reported the variation of optical and electrical properties of the films before and after annealing in sulphur atmospheres. They found that the absorption edge shifted towards the higher wavelengths, when the annealing temperature was increased, and this was attributed to the structural transformation. They also studied the band gap shift using photo-acoustic spectroscopy and the XRD measurements were carried out to confirm the phase transformation. Influence of thermal annealing in different ambient conditions on band gap and resistivity of CdS thin films prepared using CBD technique was studied by Thomas et al also [68]. It was found that the resistivity of the film reduced from $10^7\Omega$ cm in the as-deposited state to 0.15 Ω cm, when annealed in hydrogen atmosphere. Annealing in pure hydrogen (a process that has been applied to different types of CdS films) reduces the resistivity of the film by passivating the chemiabsorbed oxygen at the grain boundaries.

An extensive characterization of the chemically deposited CdS thin films was carried out by Kale et al [69]. They studied electrical and optical properties of the films by changing parameters like deposition temperature and dipping time. Depending upon the condition of deposition, chemically deposited CdS thin films showed a blue shift as high as 0.35 eV in the optical band gap. It was found that as the deposition temperature decreases from 358 to 273K, the band gap increases from 2.4 to 2.7 eV. They also mentioned that the decrease in band gap with increase in annealing temperature was due to the grain growth. Grain size attains a constant value of about 8 nm when the films were annealed at above 673K indicating saturation in the grain growth. Yu et al [70] characterized the CdS films prepared using CBD technique comprising of nano

particles and they confirmed the presence of quantum size effects based on blue shift in optical band gap of the films. The film structure was found to be hexagonal with a preferred <0002> orientation.

Pavaskar et al [49] described preparation of photoconductive CdS thin films using CBD process. Photoconductive rise and decay transients were studied by them in the temperature range of 130-310K with the view of identifying the nature of traps and to determine trap levels. Bhushan et al [71] carried out photoconductivity measurements of Y doped CdS thin films. They reported that the ratio of the photocurrent to the dark current was of the order of 10^5. They investigated the structural dependence of photoconductivity in Nd and Pr doped CdS thin films, using SEM, XRD and absorption measurements. Gupta et al [72] studied the dark and photo conductivity measurements of nano crystalline CdS thin films prepared using magnetron sputtering and observed that the conduction mechanism was dominated by the combined effects of thermionic emission, tunneling and variable range hopping. Carrier concentration and capture cross section of the trapped states were estimated to be ~ 10^6 cm^{-3} and ~ 10^{-18} cm^2 respectively.

Photocurrent response in chemically deposited cadmium sulphide thin films and a critical discussion of very high photoconductivity in those films had been reported by P.K.Nair et al [50]. They found that CdS films prepared using CBD technique can have high photosensitivity (σ_{photo} / σ_{dark} > 10^9), high photoconductivity (~ 10 Ω^{-1} cm^{-1}) and a very long photoconductivity decay time (13 hours per decade). Later the same group [73] reported the solar assisted chemical deposition of highly photosensitive cadmium sulphide thin films with optical transmission in the range 70-80% for wavelength above the band gap absorption. Optoelectronic characterization of these films prepared by chemical bath deposition was also reported by the same group [74]. Photocurrent decay

time of these films was depending on bath temperature and duration of storage. It ranged from a few seconds to 10^4 seconds per decade.

Ion implantation has a significant influence in the electrical and optical properties of semiconductors. This is one of the convenient techniques to introduce impurities into solids in a uniform manner. Effect of implantation of phosphorous ions in CdS crystals was reported in 70's [75]. Lattice disorder produced by ion implantation of CdS crystals with Bi^+, Kr^+, Ar^+ and Ne^+ had been studied using RBS/channeling and TEM technique [76]. Ratna Sagar et al [77] studied amorphisation of CdS thin films due to argon ion irradiation in dense plasma focus. Structural characterization of CdS single crystal platelets after Bi ion implantation with the help of TEM was reported by Govind and Fraikor [78]. In this work ion implanted CdS samples did not exhibit gross degradation of the wurtzite structure to amorphous zones. Implantation of Bi and Cu ions into CdS had been studied by Tell et al [79]. They studied various properties of the ion implanted CdS, which included optical absorption photoluminescence and photovoltage. Masafunni Yamaguchi [80] investigated annealing behaviour of the insulating layer in ion implanted CdS. It was observed that ion implanted CdS diodes show increase in resistivity and became photosensitive after annealing above 673K. Conductivity changes taking place in CdS, after irradiation with Co and Cs gamma rays at room temperature was reported by Chester [81]. Kitagawa and Yoshida [82] studied defect recovery in CdS crystals irradiated with 10MeV electron at 77K and observed at least three stages of recovery between 80 and 410K. Effects of low temperature annealing on defects created by 200keV electrons in CdS were also reported [83].

Spray pyrolysis technique had been developed by Chamberline and Skarman [51] for the deposition of thin films of sulphides and selenides and deposited CdS thin films using this technique. Chen-ho Wu and Bube [36] investigated electrical transport properties of sprayed CdS films. They found

that photoconductivity of solution sprayed film was caused primarily by an increase in electron mobility. Variation of electrical transport properties of sprayed CdS film as a function of substrate temperature had been co-related with variation in orientation, cubic/hexagonal phase ratio and morphology [52]. B.K. Gupta et al [84] reported electrical and photoconducting properties of sprayed CdS films. Values of activation energy calculated from the measurements of dark resistivity as a function of temperature were 0.03eV and 0.65 to 0.95eV for various samples. These values were attributed to chloride ions acting as donors and to complexes of associated Cd and sulphur vacancies in nearest neighbour sites respectively. A structural approach to the analysis of the electronic properties of chemically sprayed CdS films and cells were reported by H.L. Kwok [85]. He observed that although theoretically the mobility was found to be proportional to the ratio of grain to intergranular dimensions (L/d), it was not sufficient to explain measured changes in mobility in the case of chemically sprayed cadmium sulphide films. L. W. Chow et al [86] investigated the physical properties of the films as well as their condition of preparation and found that the substrate temperature played an important role in the grain size and the transport properties.

L. Escosura et al [87] studied effects of short heat treatments in vacuum on electrical, structural and optical properties of CdS thin films prepared using spray pyrolysis technique. It was found that electrical and structural properties changed remarkably under these treatments, but the optical properties did not vary significantly. Resistivity decreased from about 500 Ω cm to less than 1Ω cm due to annealing at 300°C while the electron mobility increased by two orders of magnitude. Nucleation, growth and microstructure of CdS film deposited using spray pyrolysis were investigated by Albin and Risbud [88]. In this work they identified the major mechanism of film growth as droplet impingement, surface pyrolysis and the incorporation of impurity phases.

A.G. Valyomana et al [89] studied influence of annealing temperatures on dark and photoconductivity properties of spray pyrolysed CdS thin films. They concluded that the annealing of films at 373K results in maximum conductivity where as annealing at 473K produces a minimum in its value. Influence of substrate temperature on optical absorption coefficient α and carrier density N of semiconducting CdS thin film prepared by spray pyrolysis technique was analytically studied by Jean Ebothe [90].

Sunny Mathew et al [91] studied optical and surface properties of spray pyrolysed CdS thin film. They studied the variation of real and imaginary parts of the refractive index with preparation temperature, using variable angle spectroscopic ellipsometry (VASE). They found that n and k increase with increase in substrate temperature. They also evaluated the surface roughness and found that it decreases with increase in substrate temperature and reaches a minimum in the range 280-300°C.

Zeenath et al [92] studied the trap levels in n- type CdS films prepared using spray pyrolysis. TSC measurements of the n-type CdS sample revealed the presence of only one peak under light excitation for a short period due to mobility of sulphur vacancies, but longer excitation could give evidence of one more level which was due to complex of cadmium and sulphur vacancies.

In the present work we used cadmium sulphide thin films prepared by spray pyrolysis technique. Details of the film preparation and characterization are given in the following section.

3.2.3. Preparation of CdS using spray pyrolysis

For the preparation of cadmium sulphide using spray pyrolysis, aqueous solution of cadmium chloride and thiourea are sprayed on to a heated substrate. The droplet undergoes pyrolytic decomposition to form a stoichiometric

cadmium sulphide film on the substrate. There are a number of reports giving the effect of variation of substrate temperature and carrier gas used. Details of the film preparation conditions for our purpose are discussed in the following paragraphs.

The SnO_2 films were given a thorough cleaning by detergent, distilled water and finally by the ultrasonic cleaning. These substrates were then placed on a hot plate made of thick iron block, which can be heated to the required temperature of 300°C with the help of a variac. Temperature on the glass substrate was measured using a digital thermometer. During spraying temperature of the hot substrate was kept constant with an accuracy of ± 5°C.

Aqueous solution of 0.02 M cadmium chloride (E.Merk, Darmstadt) and 0.02 M thiourea (Merk, Schuchardt) were prepared by dissolving these in doubly distilled water. They were mixed in the ratio 1:1 by volume. This solution was sprayed on to the heated SnO_2 coated glass substrate (with proper masking) to get thin films of CdS.

Thickness of the film prepared was measured by gravimetric method using a microbalance and also by stylus method. Later the thickness was verified when the depth profiling of these samples were done. In the present work, for all the cases, ~ 500ml solution was used for the spray which gave a film of thickness ~1μm. Rate of flow of solution for the spray was ~15 ml per minute and it was controlled with a valve. Size of the droplet was controlled by adjusting the pressure and the gas flow rate. This was done with the help of a gas flow valve. Angle of incidence of the solution over the hot substrate was ~ 70° and the distance between the spray head and the substrate was always ~ 25 cm. The films obtained were uniform in thickness, and this was achieved by the high scanning rate of the spray head over the substrate during the deposition process. Scanning rate in the present case was always ~ 110 per

minute. Cooling of the samples was allowed in a very slow rate i.e. 2°C per minute.

3.2.4. Characterization

Structural and optoelectronic properties of the semiconductor thin films depend to a large extend, on the film preparation technique and condition. So it is very necessary to characterize the film prepared using a particular technique. In the present work, we made use of a number of analytical techniques mentioned in the previous chapter to characterize the cadmium sulphide film deposited using spray pyrolysis technique. These analyses helped us to a very great extend, in optimising our technique and preparation conditions to deposit stoichiometric CdS films.

Structure of the cadmium sulphide films deposited was analysed by X-ray diffractometer using Cu k_α radiation at a slow scanning rate in the 2θ range 20-60°. The 'd' values obtained were compared with standard JCPDS values. Optical absorption was measured using a spectrophotometer. Electrical characterization of the samples was done by the Hall measurement.

3.2.4.1. Composition

Composition of the film is expected to depend on the kinetics of spray pyrolysis. Stoichiometry of the sulphide films generally does not vary much with the variation in metal to sulphur ion ratio in the spray solution [93]. But if the substrate temperature is lower so that the pyrolytic reaction is not completed some by-product or intermediate compound may be trapped as impurities in the film. Even if the substrate temperature is high, due to the cooling effect at the growing surface, a higher concentration of impurities is observed at the surface.

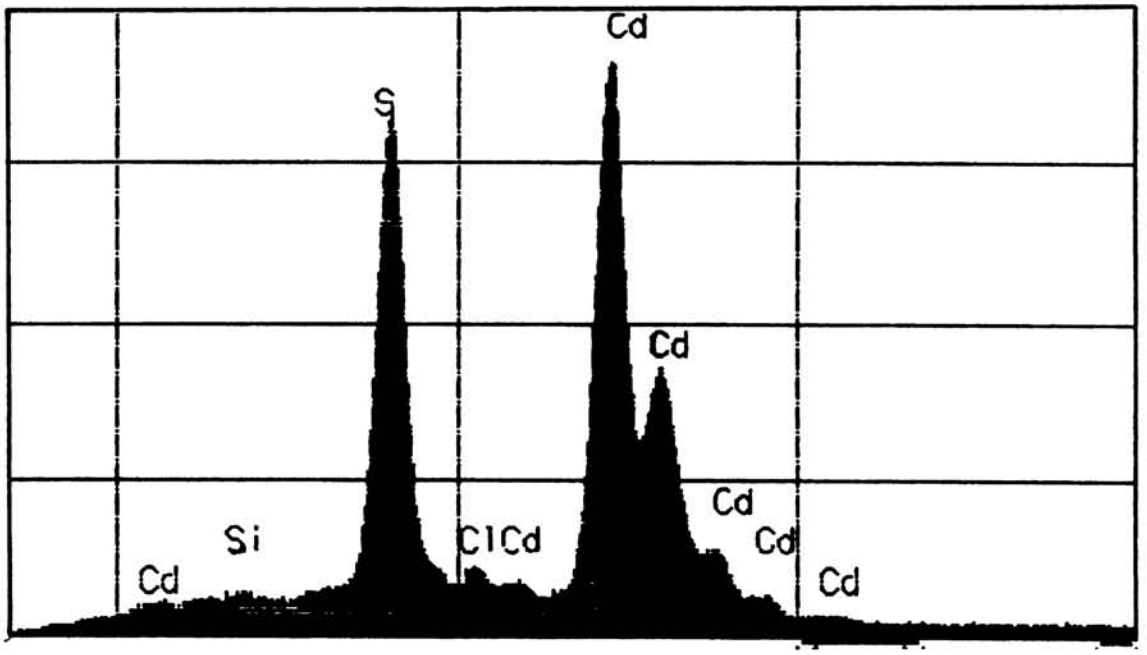

Fig. 3.3. EDAX Spectrum of as-prepared CdS film

EDAX spectrum of the CdS film prepared at a substrate temperature of 300°C is shown in Fig. 3.3. From this we can see that the sample shows the presence of cadmium, sulphur and the impurity chlorine. The chloride ion impurity present is from the spraying solution containing cadmium chloride. There is another peak corresponding to silicon, which is from the glass substrate used for the preparation of the film.

Composition of the film was analysed with a more advanced and sensitive analytical technique AES and the spectrum obtained is depicted in Fig. 3.4. In the figure we can see the characteristic peaks due to cadmium and sulphur. It also contains peaks corresponding to chlorine, carbon and oxygen. As mentioned earlier these impurities are derived from the starting materials and the ambient conditions. In order to know the variation of composition of the film along the thickness, the "depth profile" of the concentrations was obtained using ESCA and it is depicted in the Fig. 3.5. From the figure we can see that the composition of the film is uniform throughout the depth of the film, as far as cadmium and sulphur are concerned. Later depth profile of the entire cell showed clearly that the impurity concentration was very less along the thickness of the film (please refer Fig.4.10). Actually the impurities are residing on the surface of the film. Here carbon might have from thiourea while chlorine, as stated earlier, from $CdCl_2$. These are available on the surface only because surface temperature may be lower while spraying.

3.2.4.2. Structural Analysis

Structural characterization is one of the important factors, when we prepare a film by any method. Fig. 3.6 shows a typical diffraction pattern of the cadmium sulphide film prepared on SnO_2 coated glass substrate. The pattern shows the presence of a strong sharp peak at $2\theta = 26.5^{\circ}$. This could be indexed as <002> hexagonal. All other peaks are also due to hexagonal phase. It is very clear from the diffraction pattern that the films are crystalline and has

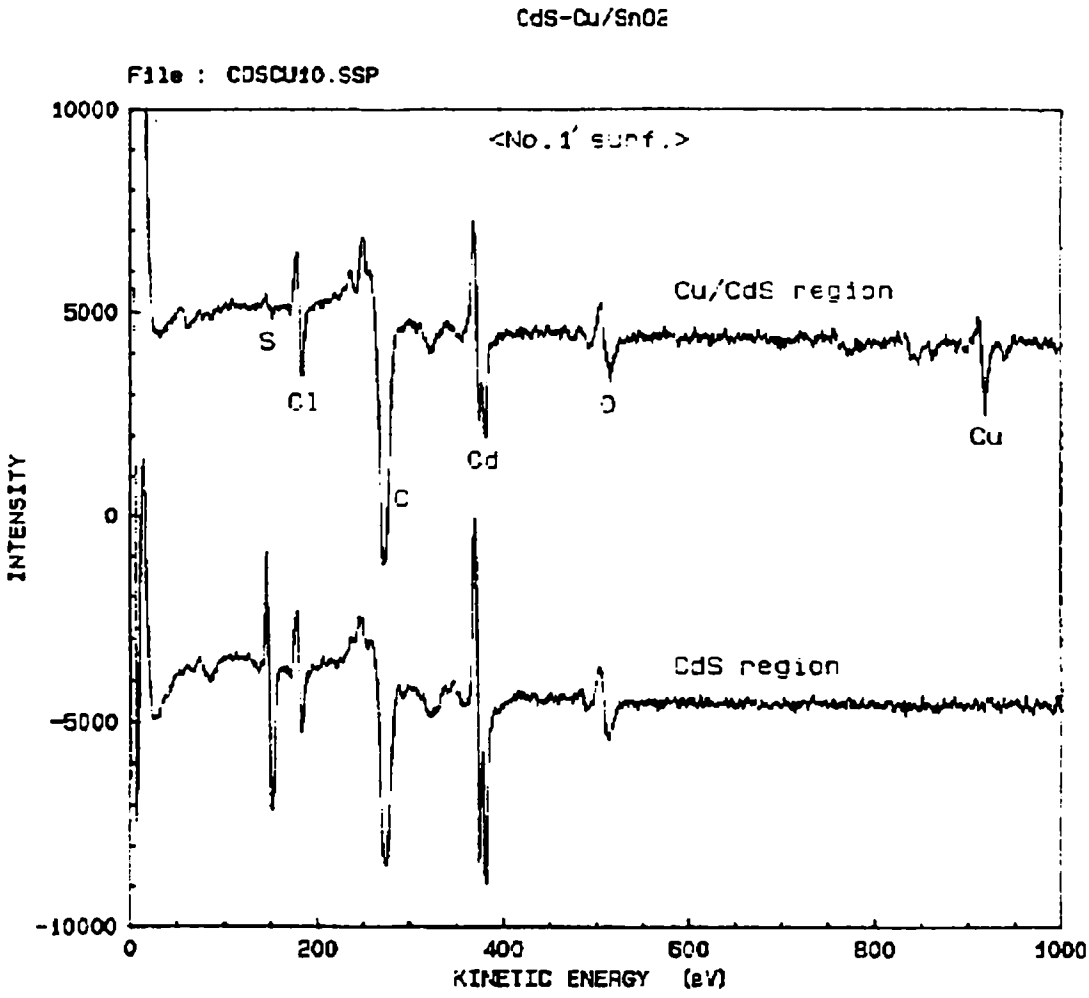

Fig. 3.4. AES surface profile of as-prepared CdS film and copper doped CdS film

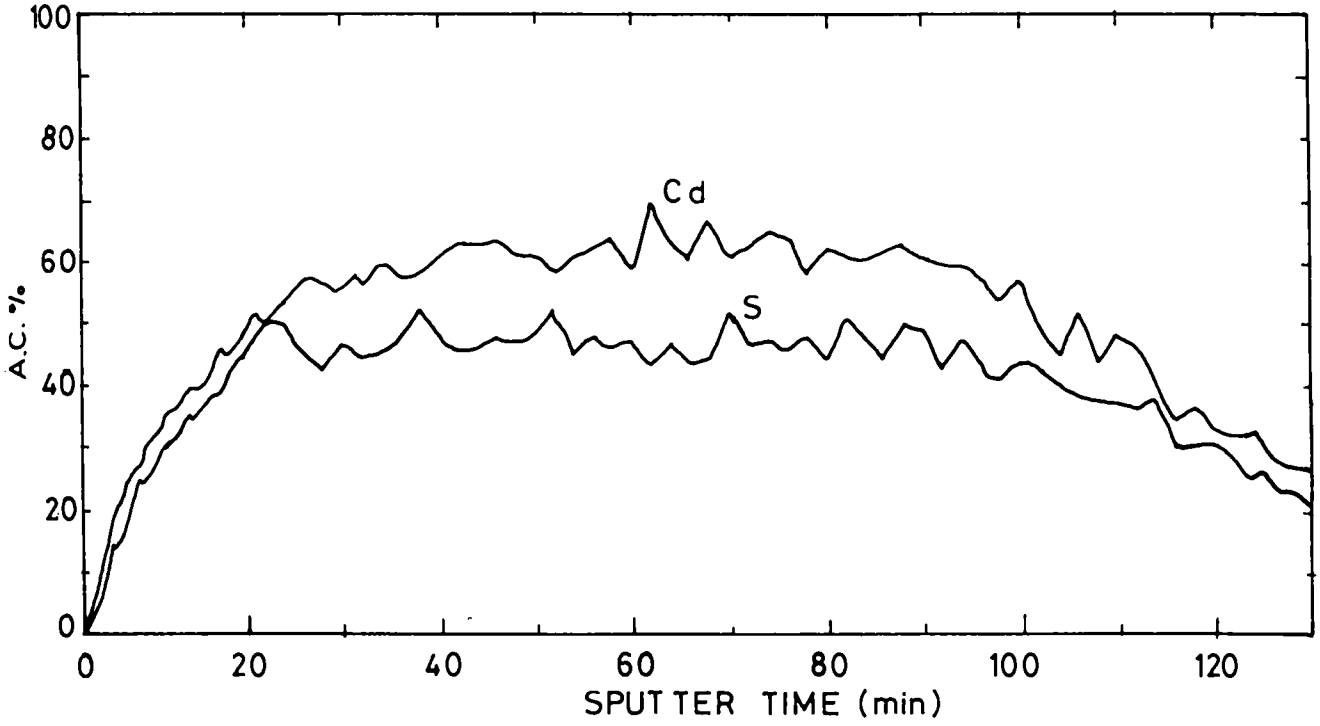

Fig. 3.5. ESCA depth profile of n-CdS sample

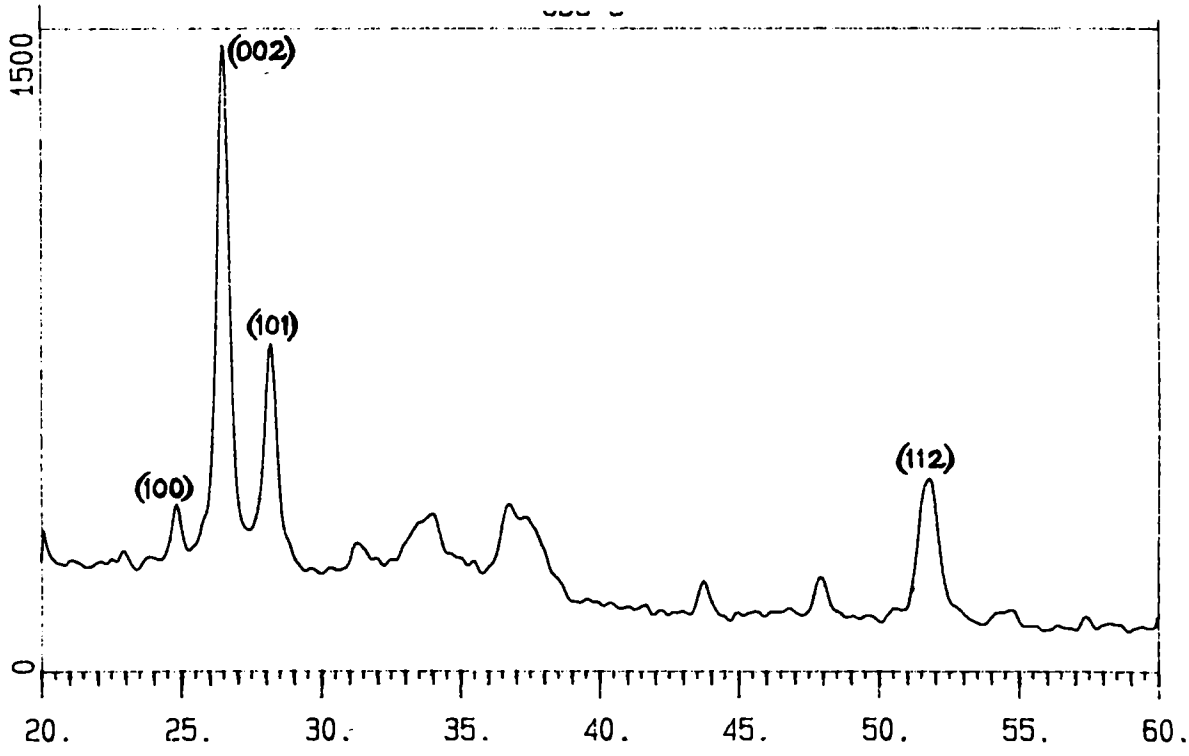

Fig. 3.6. XRD spectrum of n-CdS sample

preferential orientation along <002>. The 'd' values are compared with the standard JCPDS data and were found to be very close to the standard value. This result confirmed the crystallanity of the cadmium sulphide film deposited. Data obtained for XRD analysis is tabulated in Tab.3.4

Table 3.4

XRD data for the n-CdS film

Peak	2θ	d space A°		I (Rel)	plane
		observed	standard		
1	24.8	3.587	3.583	16.64	100
2	26.5	3.361	3.367	100	002
3	28.25	3.1565	3.16	49.82	101
4	51.75	1.7651	1.761	20.78	112

The microstructure of the film has a profound influence on the properties of the solar cells fabricated using the film. In order to fabricate good devices, grain size should be > 1μm. Usually SEM photograph of the samples can give such information accurately. Fig. 3.7 shows the SEM photographs of the cadmium sulphide films for a magnification of 3000. From the photographs the grain size of the films prepared was found to be 0.5 μm.

3.2.4.3. Optical

Optical absorption studies were carried out on the CdS films and absorption spectrum is depicted in the Fig. 3.8. These studies were carried out to find out the optical band gap of the semiconductor. From the figure we can see that the film has got a very sharp absorption edge. Cadmium sulphide is a direct band gap semiconductor. For an allowed direct band gap transition, absorption coefficient could be related to the photon energy $\alpha h\nu = A (h\nu - E_g)^{1/2}$

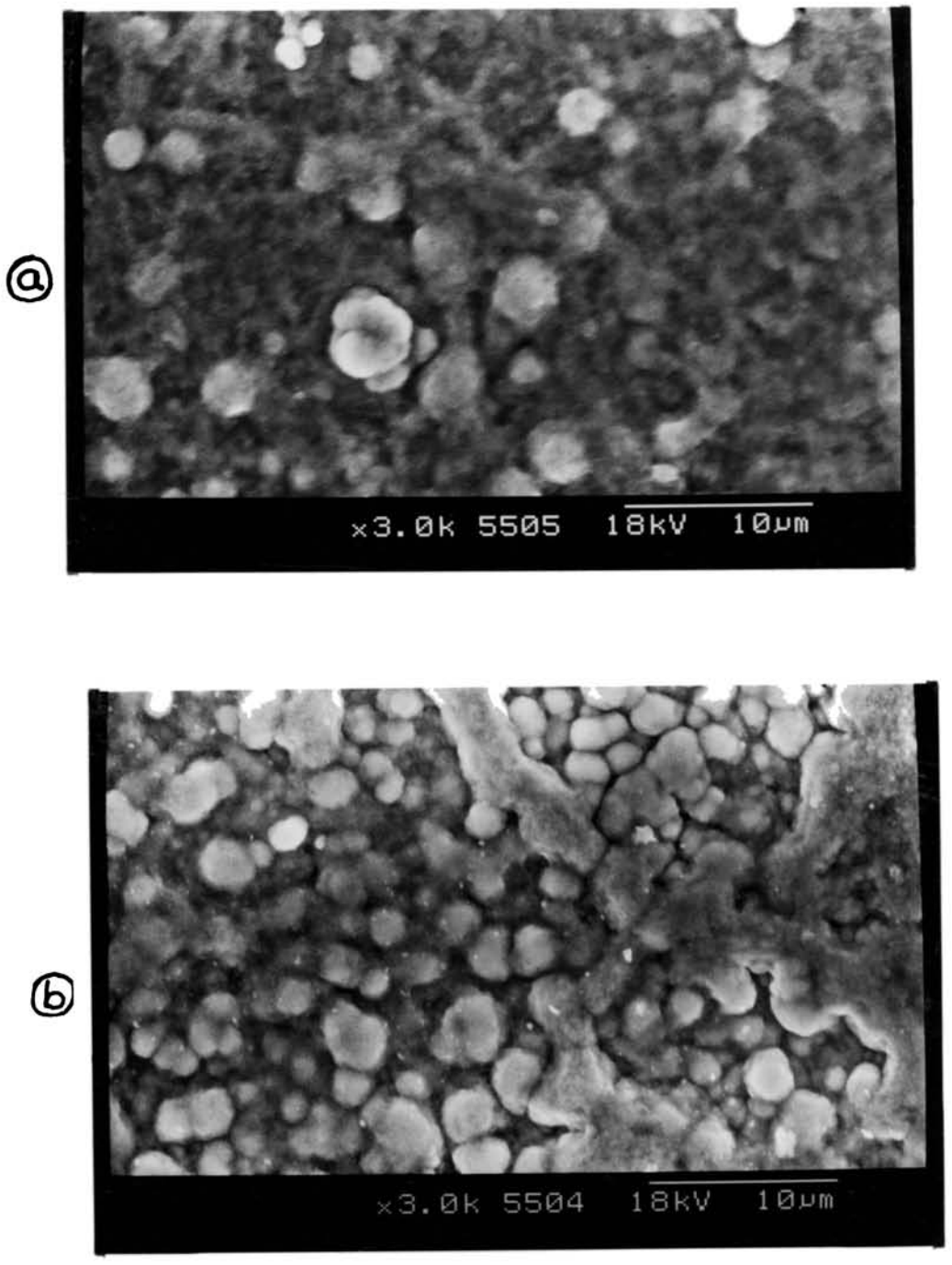

Fig. 3.7. SEM photographs of a) n-CdS sample b) copper doped CdS sample

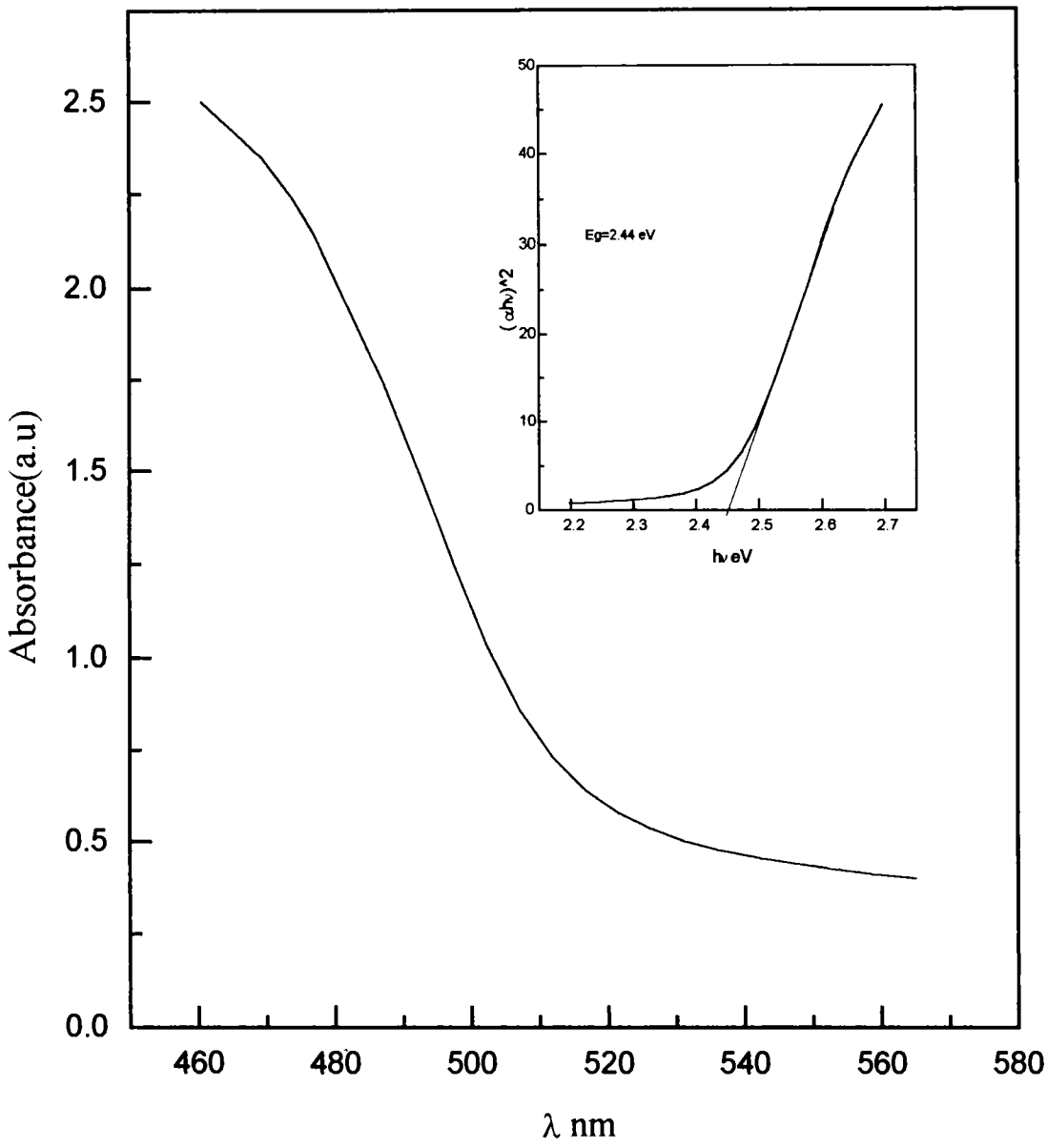

Fig. 3.8. Absorption spectrum of n-CdS sample

where α is the absorption coefficient and Eg is the energy band gap. Usually the optical band gap was calculated by plotting a graph between $(\alpha h\nu)^2$ Vs. $h\nu$. For a direct band gap semiconductor it will be a straight line. Such a graph is plotted and the graph is depicted in the inset of Fig. 3.8. It shows that the graph is a straight line in our case also proving that the material has a direct band gap. The value of the optical band gap is calculated from the graph by extrapolating the linear portion of the graph to the energy axis and found to be 2.44 eV, which is very near to standard value of the band gap for CdS.

3.2.4.4. Electrical Analysis

Electrical characterization is another important factor in developing a material for solar cell fabrication. This was done by Hall measurement using Vander Pauws techniques in square geometry for the CdS samples prepared. Details of the measurements of the sample prepared at a substrate temperature of 300°C are shown in Table 3.5. The sample analysed in this technique was prepared on glass, since the cadmium sulphide prepared on SnO_2 could not be analysed using this technique. From the table we can see that the sheet resistance is on the higher side. Carrier concentration is in the range 10^{14} cm^{-3}, which is in agreement with the reported values. The sample shows majority carriers as electrons in all the measurements.

Table3.5

Hall measurement values for n-CdS and P-CdS samples

Type of Sample	n-CdS	p-CdS
Resistivity Ωcm	250. 5923	31.4632
Mobility $cm^2 V^{-1}s^{-1}$	-310.507	17.85
Density cm^{-3}	1.02229×10^{14}	1.1114×10^{16}
Hall Coefficient cm^3/Coul	-77810.65	561.6169
Sheet Resistance Ω/ □	2.506×10^6	3.14×10^5
Type of carriers	Electrons	Holes

3.2.5. Conclusion

Cadmium sulphide films can be prepared using the low cost process, namely spray pyrolysis technique. Film is found to be stoichiometric and free from impurities, especially along the depth. The samples were characterized using structural, compositional, optical and electrical measurements.

3.3. Part III p-CdS

3.3.1. Introduction

It has been generally considered that the formation of p-type cadmium sulphide is very difficult because of self compensation effects due to sulphur vacancies. However, there are few reports on the attempt to form p-type CdS

crystals by compensation of donors with copper acceptors or by ion implantation of various acceptors. These authors had attempted to prepare p-n junctions and observed rectifying characteristics, photovoltaic effects and electroluminesence. Direct evidence of p-type conduction was confirmed by measuring a positive Hall coefficient and Seebeck coefficient. A brief report of the works on preparation and characterization of p-type cadmium sulphide is included in the following section.

3.3.2. Review of the works on conversion of n-CdS to p-CdS

Research works on type conversion in cadmium sulphide were started even in 1960's. Woods and Champion [94] were able to show that diffusion of copper produced p-conduction in cadmium sulphide. Later H.G Grimmeiss and R. Meming [95] reported the preparation of p- type CdS crystals by compensating donors with copper acceptors. In another publication by Grimmeiss and Memming [96] it was reported that p-type cadmium sulphide could be formed on vapour-deposited CdS film using copper diffusion. They showed photovoltaic effect on these films. Naturally this work on CdS encouraged a number of scientists to do doping with other materials such as phosphorous and bismuth. Anderson and Mitchell [97] implanted high energy phosphorous ions into cadmium sulphide single crystals and the implanted crystals were annealed for 10 minutes in saturated vapour along with an excess of CdS powder at various temperatures. Type conversion clearly observed after annealing at 450°C. Fred Chernow et al [98] reported the formation of high conductivity p-type cadmium sulphide, when they implanted bismuth into single crystal CdS. Hall measurements and lifetime studies were performed on the implanted layers.

During the 1990's a few reports were published on this topic, especially on thin films. Kashiwaba et al [99] reported the p-type characteristics of copper doped cadmium sulphide thin films prepared using vacuum evaporation. They

found that copper could easily diffuse into CdS film when it was deposited on a thin copper film at 200°C. They confirmed the p-type characteristics of cadmium sulphide film through Hall measurement and positive Seebeck coefficient. It was reported that the p-type cadmium sulphide thin films could be formed when CuCl solution is added to the bath containing cadmium acetate, triethanolamine (TEA), ammonia solution and thiourea for the preparation of cadmium sulphide by chemical bath deposition [100].

Sunny Mathew et al [101] reported the conversion spray pyrolysed cadmium sulphide thin films into p- type. In that work, they diffused copper atoms into CdS film using thermal annealing and they confirmed that the compounds like Cu_xS were not formed using the techniques like XRD, optical absorption, X-ray photoelectron spectroscopy (XPS) and variable angle spectroscopic ellipsometry. Later another group from Japan [102] also reported the preparation of p-type cadmium sulphide thin film, in which laser ablation was applied to a mixed target of cadmium sulphide and copper. As a part of the Ph.D thesis work, K.L. Narayanan [103] reported the conversion of CdS film prepared using chemical bath deposition by the ion implantation of nitrogen. Recently another report from Japan described the light emission of CdS (Cu) /CdS diode [104]

In the following section the preparation of p-CdS:Cu film and their characterization are reported.

3.3.3. Preparation of p-CdS:Cu film

The Cu/CdS bilayer films were prepared by vacuum deposition of copper film over the spray pyrolysed cadmium sulphide film at room temperature at a pressure less than 10^{-5} torr. The distance from source to substrate is kept at 25 cm. Thickness of the copper film was controlled by a quartz thickness monitor kept along the side of the substrate and rate of deposition was about

8A°/sec and this was achieved by adjusting the current through the molybdenum source at nearly 100A. Copper film was always coated on unannealed CdS samples. Different sets of bilayer films of Cu/CdS were prepared by depositing copper layers of different thickness. In all the cases, the thickness of the CdS film was kept constant nearly 1μm. Thickness of the copper film deposited over the cadmium sulphide film was in the range 25- 55 nm. These samples were labeled according to the thickness of the copper deposited as C25, C30, C35, C40, C45, C50, and C55. These represent the Cu/CdS samples with as prepared cadmium sulphide of thickness ~ 1μm and copper thickness 25, 30, 35, 40, 45, 50, 55 nm respectively and hereafter this notation will be used to refer to these samples.

3.3.3.1. Annealing

Annealing of the samples was done under high vacuum (10^{-5} torr) at a temperature of 300°C for 45 minutes. In all cases heating and cooling rates were fixed as ~ 2°C/minute. After the annealing samples were examined for the type conversion by hot probe method. In the samples C25 and C30 the type conversion was not observed whereas in the samples C35 and C40 the type conversion was observed. One common thing in the samples C25-C40 was that the whole copper deposited had diffused into the cadmium sulphide while for the samples C45, C50 and C55, it was found that a layer of copper was there on the top surface of cadmium sulphide. Type conversion was not consistent in these samples. For further investigations we selected the sample C40, which was found to be optimum.

3.3.4. Characterization

3.3.4.1. XRD analysis

Fig.3.9 gives the XRD pattern for the vacuum annealed sample C40. In this case main two peaks corresponds to <002> reflection of hexagonal phase and <101> reflection of the same hexagonal phase. All other peaks also

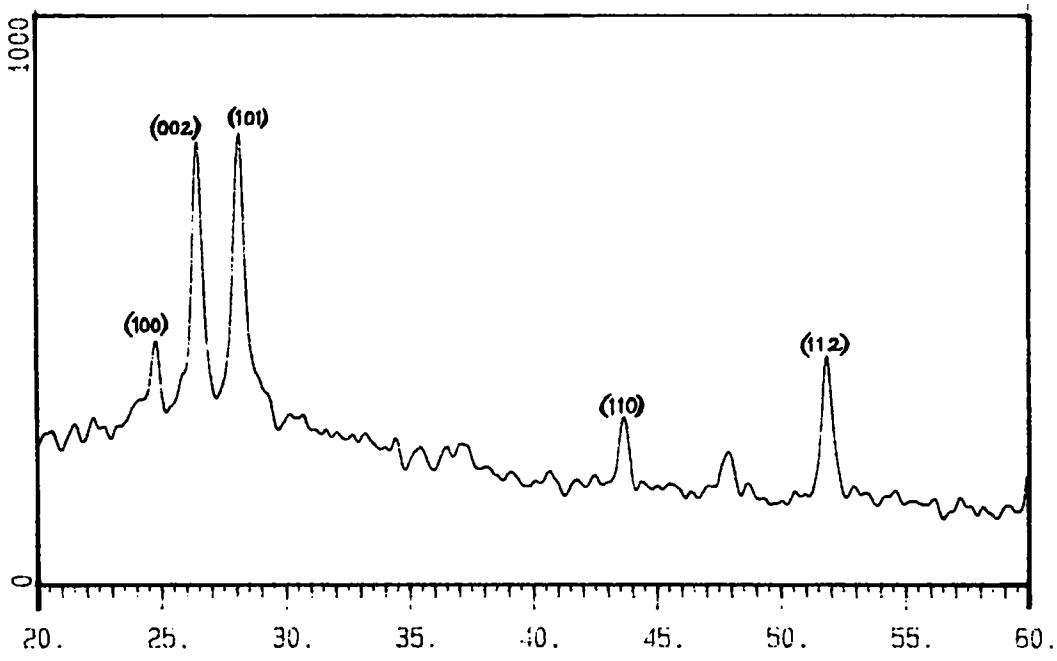

Fig.3.9. XRD spectrum of p-CdS:Cu sample

correspond to the stable hexagonal phase of cadmium sulphide. Chance for the formation of compounds like Cu_xS is high in this case, as there is CdS layer and Cu layer. Hence such compounds can be detected from the XRD pattern. It should be noted that there were no peaks corresponding to either pure copper or new compounds like Cu_xS formed by the chemical reaction between copper and sulphur. This confirmed that the whole copper was completely diffused into the cadmium sulphide layer and no chemical bonding is formed. The XRD data obtained from p-CdS is presented in Table 3.6

Table 3.6.

XRD data values for p-CdS

Peak	2θ	d space A°		I (Rel)	plane
		observed	standard		
1	24.8	3.587	3.583	42.68	100
2	26.45	3.367	3.367	100	002
3	28.15	3.1675	3.16	88.21	101
4	43.7	2.067	2.008	31.91	110
5	51.85	1.7619	1.761	65.09	112

Microstructure of the p-CdS:Cu film was analysed using SEM photograph at a magnification of 3.0 k and is presented in Fig.3.7. From this it is clear that average grain size of the film is far improved and it is found to be nearly 1μm. This is a quite good result as far the device fabrication is concerned. Again the film is found to be uniform.

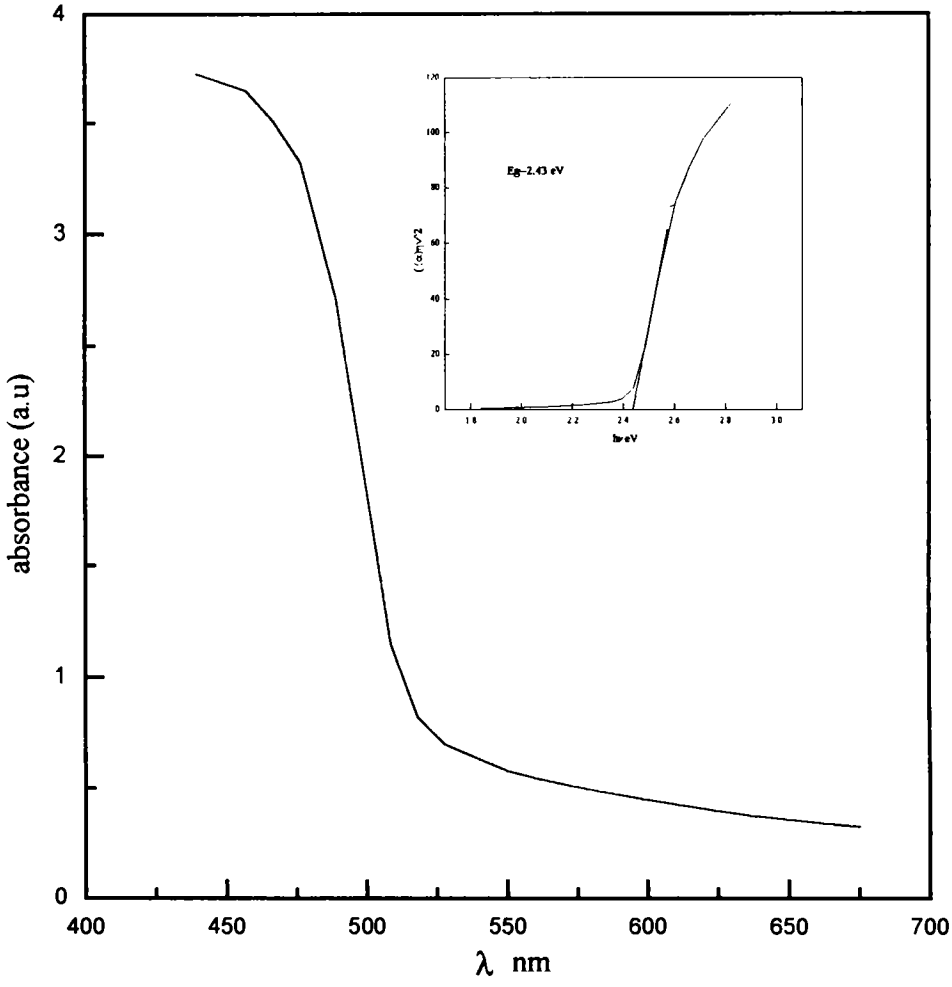

Fig.3.10. Absorption spectrum of p-CdS:Cu sample

3.3.4.2. Optical Analysis

Optical measurement is another important study for determining the band structure of semiconductors and it can also give an idea about the formation of new compounds. Fig. 3.10 shows the absorption spectra of vacuum annealed Cu/CdS bilayer film C40. Absorption spectra of this sample has the same characteristic as that of the as-prepared cadmium sulphide, except that an enhanced absorption starting, possibly due to some mid band gap defects created by doping of copper. Optical band gap was calculated by plotting $(\alpha h\nu)^2$ Vs $h\nu$ and it is shown in the inset of Fig.3.10. From the graph it was found to be nearly 2.43 eV, very near to the ideal value of cadmium sulphide films. Again it is to be specifically noted that no traces of Cu_2S (which has a band gap ~ 1.7 eV) was revealed from optical absorption studies.

3.3.4.3. ESCA analysis

XRD and the optical absorption studies showed that the copper completely diffused into the cadmium sulphide film due to annealing and these studies could not detect any trace of new compound formed between cadmium sulphide and copper. ESCA analysis would help us to know exactly the nature of copper atoms inside cadmium sulphide through the binding energy of copper (or sulphur). Fig. 3.11 depicts the ESCA depth profile of the copper annealed samples. It can be seen from the figure that the two peaks (932.7 eV and 953.5 eV) are corresponding to the binding energies of pure copper alone. The spectrum does not give any hints of shift in binding energy peaks. This also confirmed that no additional compounds like Cu_xS were formed as a result of diffusion of copper into CdS layer. The ESCA graph showing binding energy (B.E) of sulphur alone is shown in Fig.3.12. This peak corresponds to sulphur present at a depth of (approx.) 300 nm from the top surface. From this it is very clear that the peak is at 161.8 eV which is the binding energy corresponding to the sulphur in sulphide environment [105]. Similarly Fig.3.13 depicts the binding energy graph of cadmium in the same sample. This graph is also

obtained from the same depth. It is very evident that the binding energy corresponding to the major peak (405.2 eV) is representing cadmium in CdS environment [105]. These figures also show that there is no shift of the peaks, even to decimal point through out the depth of the film.

3.3.4.4. Electrical analysis

The electrical characterization is also an important tool. This was done by Hall measurements using Vander Pauws technique. Even though the type conversion was verified by the hot probe method, quantitative measurement is possible through the Hall measurements. Details of the measurement of a thermal annealed C40 sample is given in the table 3.5. From the table we can see that sheet resistance and resistivity of the film is decreased by an order, when we compare with the as-deposited cadmium sulphide. This may be partially due to the annealing by which the grain size of the film might have increased reasonably resulting in the increase of conductivity. Another important parameter to be noted in this connection is the carrier concentration. When the sample was converted into p-type, the carrier concentration was found to be increased by two orders of magnitude and the typical value obtained is 1.114×10^{16} cm^{-3}. These two may be the major reasons for decrease in sheet resistance. The sample showed holes as the majority carriers and positive Hall coefficient for different values of Hall currents.

TSC (Thermally Stimulated Current) studies were done on p-type C40 samples and the spectrum is shown in Fig. 3.14. Two peaks at (460K & 290K) were observed in this case irrespective of the duration of light excitation. Activation energies of these two peaks were calculated to 1.2eV (mobility of S vacancy) and 0.72-0.75eV. Since p-type sample is Cu doped, we expect a trap level of Cu impurity in this sample and we found that 0.77 eV is an acceptor level of Cu impurity [99]. It was reported [99] earlier that resistivity of Cu

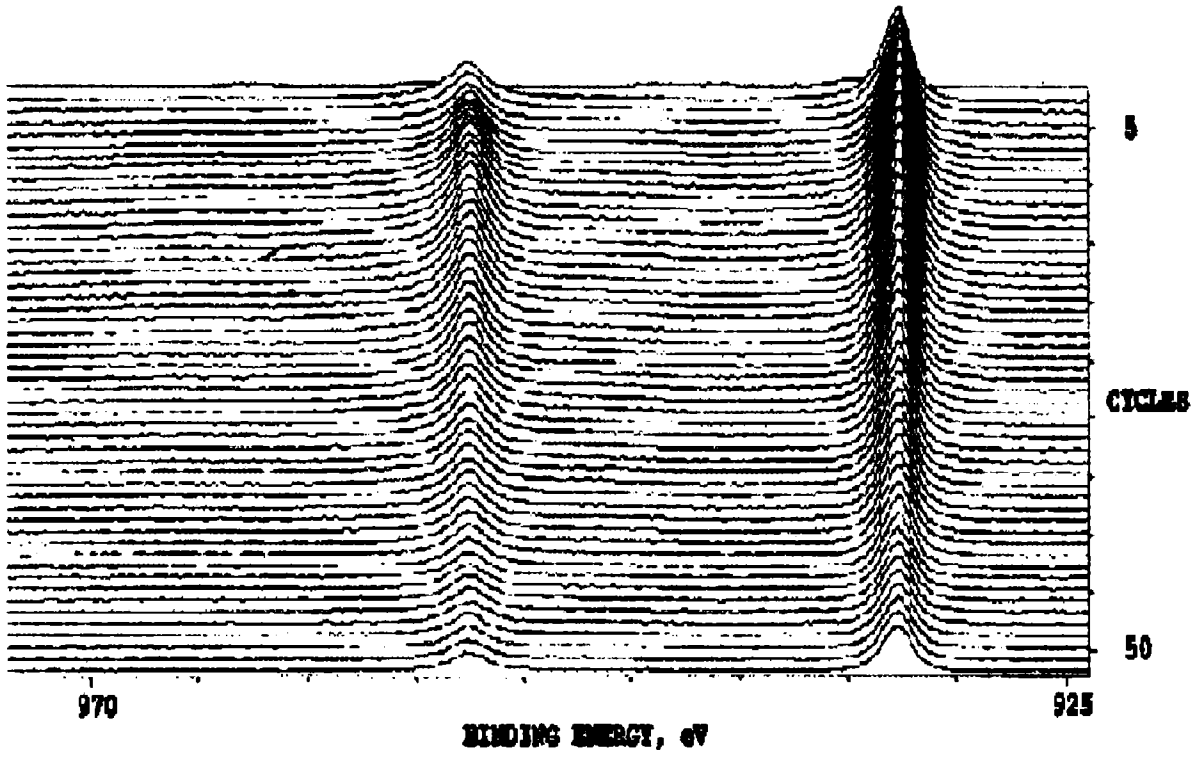

Fig. 3.11. ESCA depth profile of copper in p-CdS:Cu sample

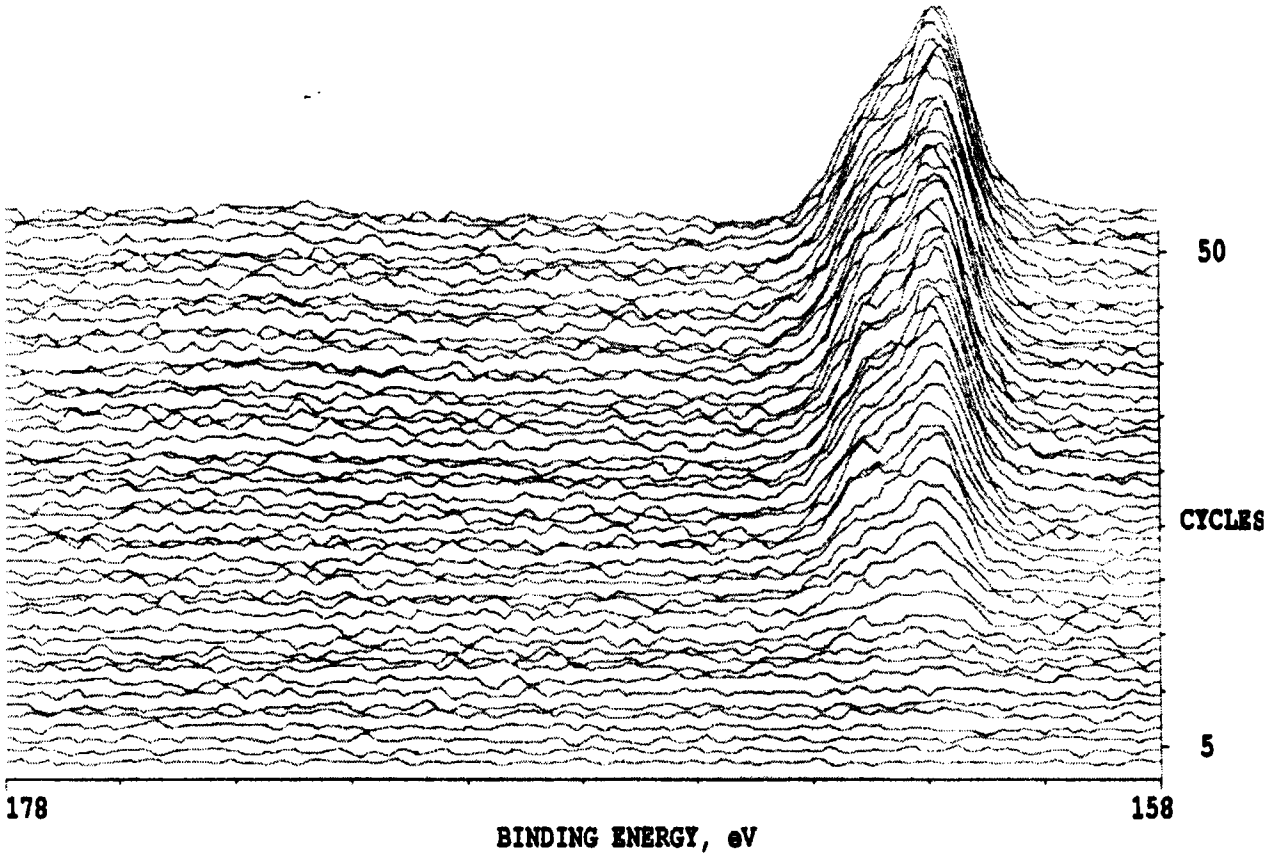

Fig. 3.12. ESCA depth profile of sulphur in p-CdS:Cu sample

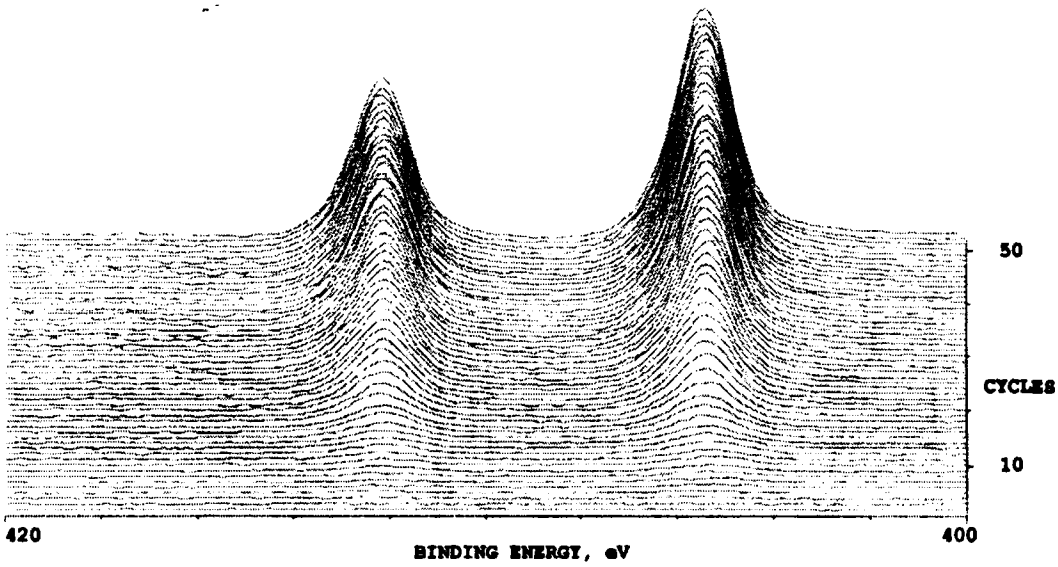

Fig. 3.13. ESCA depth profile of cadmium in p-CdS:Cu sample

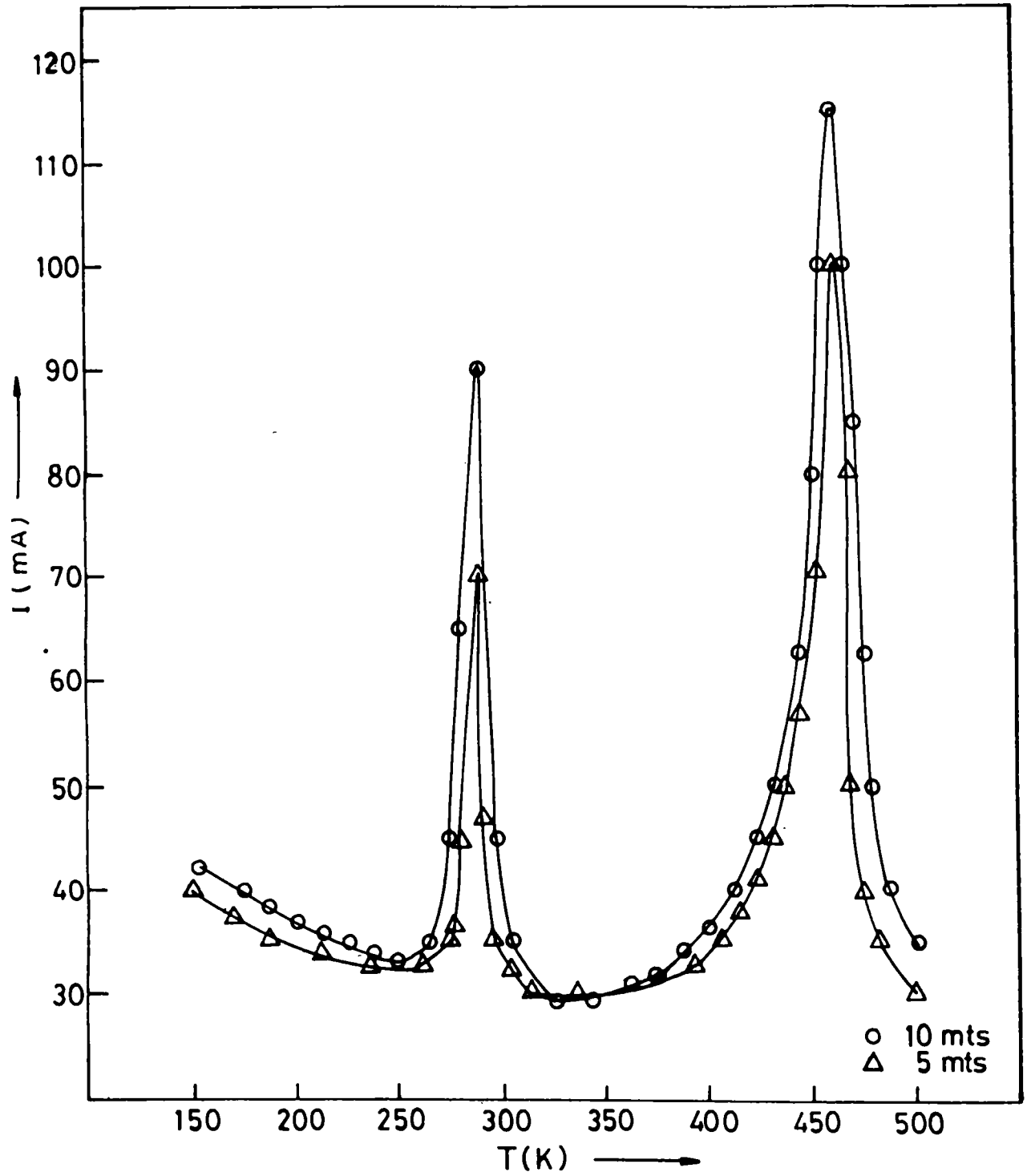

Fig. 3.14. TSC spectra of p-type CdS thin film under different excitation time

doped CdS sample first increases with increasing Cu concentration and shows an unmeasurably high value at about 0.5 at % of Cu. However, it shows a drastic decrease with further increase of Cu content upto about 25 at % of Cu. It was also reported that Cu atoms substituted for Cd sites acts as acceptors and according to Y. Kashiwaba et al, the increase of electrical resistivity to unmeasurably high value by Copper doping may be due to the compensation of donors which are probably due to sulphur vacancies [99]. They also suggested that the remarkable decrease of electrical resistivity above 0.5 at % of Cu is due to the increase of active Cu atoms substituted for Cd sites and this give rise to a p-type conductivity to the sample. In the present work, we could detect Cu impurity as such in the p-type sample and there is no trace of complexes of Cd and S vacancies even after 10 minutes light excitation. One can hence conclude that it may be the Cu impurity on Cd sites that gives the p-type conductivity to spray pyrolysed CdS films.

3.3.5. Conclusion

It is demonstrated that p-type cadmium sulphide can be prepared using copper doping by thermal annealing. The p-CdS formed by the diffusion of copper atoms is characterized for structural, compositional, optical and electrical properties. The AES depth profile of the sample confirms that no additional compounds like Cu_xS is formed due to the annealing of Cu/CdS bilayer film. Another valuable information obtained from ESCA analysis is only the top layer of the cadmium sulphide is converted into p-type, the bottom layer remained as n-type itself. So this gives a very strong support for the homojunction cell fabrication in cadmium sulphide.

References

1. Y.K.Fang and J.J. Lee, Thin Solid Films, **169** (1989) 51
2. H .W. Indischmann and P. Mark, J. Electrochem.Soc., **126** (1979) 627
3. K .H. Kin and C.G. Park, J. Electrochem.Soc., **138** (1991) 2408
4. P . Hedenqvist and A. Roos, Surface and Coating Technology, **48** (1991) 41
5. R .K. Latz Michel and M. Scerer, Jpn. J. Appl. Phys., **30** (1991) L149
6. M .H. Hohesiel, Mitwasky and C. Mrotzek, Phys.Status Solidi (a)., **123** (1991) 461
7. Y . Hamada, C. Adachi, T. Tsufsui and S. Saito, Jpn. J. Appl. Phys., **31** (1992)1812
8. H .L. Hartnagel, A.L.Dawar, A.K. Jain and C. Jagadish (Eds.) *Semiconducting transparent thin films*, IOP Publishing Ltd., London (1995) 316
9. J .L. Vossen in *Physics of thin films*, Academic Press, New York (1971) 9
10. H .L. Hartnagel, A.L.Dawar, A.K. Jain and C. Jagadish (Eds.) *Semiconducting transparent thin films*, IOP Publishing Ltd., London (1995) 22
11. W .H. Baur, Acta Crystallogr., **9** (1956) 515
12. A .K. Saxena, R. Thankaraj, S.P. Singh and O.P. Agnigotri, Thin Solid Films, **131** (1985) 121
13. K . Kim, T.G. Finstad, W.K. Chu, X.B. Cox and R.W. Linton, Solar Cells, **13** (1984-'85) 301
14. V . Vasu and A. Subramanyan, Thin Solid Films, **202** (1991) 283
15. E . Shanthi, A. Banerjee, V. Dutta and K.L. Chopra, J. Appl. Phys., **53(3)** (1982) 1615
16. K .H. Yoon and J.S. Song, Thin Solid Films, **224** (1993) 203
17. H . Demiryont and N. Tezey, Thin Solid Films, **101** (1983) 345
18. G . Beensh Marchwicka, L.K. Stephiewska and A. Misiuk, Thin Solid Films, **113** (1984) 215

19. K .L. Chopra, S. Major and D.K. Pandya, Thin Solid Films, **102** (1983) 1

20. H .L. Hartnagel, A.L.Dawar, A.K. Jain and C. Jagadish (Eds.) *Semiconducting transparent thin films*, IOP Publishing Ltd., London (1995)

21. A . Mani, N. Karuppiah and R. Mahalingam, Mater. Res. Bull. **25** (1990) 799

22. J . Proscia and R.D. Gordon, Thin Solid Films, **214** (192) 175

23. J . Geurts, S. Rau, W. Richter and F.J. Schmite, Thin Solid Films, **121** (1984) 217

24. J .C. Manifacier, M. De Murcia, J.P. Fillard and E. Vicario, Thin Solid Films, **41** (1977) 127

25. V . Casey and M.I. Stephenson, J.Phys.D: Appl. Phys., **23** (1990) 212

26. M . Watanabe, Jpn. J. Appl. Phys., **9** (1970) 1551

27. W .D. Munz, J. Heimbach and S.R. Reineck, Thin Solid Films, **86** (1981) 175

28. R .P. Howson, H. Barankova and A.G. Spencer, Thin Solid Films, **196** (1991) 315

29. A . De and S. Ray, J.Phys.D: Appl. Phys., **24** (1991) 719

30. H .L. Hartnagel, A.L.Dawar, A.K. Jain and C. Jagadish (Eds.) *Semiconducting transparent thin films*, IOP Publishing Ltd., London (1995) 72

31. A .K. Abass and M.T.Mohammed, J. Appl. Phys., **59** (1986) 1641

32. J .C. Manifacier, Thin Solid Films, **90** (1982) 297

33. W . Siefart, Thin Solid Films, **121** (1984) 275

34. P .K. Vidyadharan Pillai, *Ph.D Thesis*, Cochin University of Science and Technology, Cochin (1997)

35. T . Murnoi and M. Furukoshi, Thin Solid Films, **48** (1978) 309

36. C .Wu and R.H. Bube, J. Appl. Phys., **45** (1974) 648

37. K .L. Chopra and S.R. Das, *Thin Film Solar Cells*, Academic press, New York (1983) 297

38. D .C.Reynolds, G. Leiss, L.L. Antes and R,E. Marbuger, Phys. Rev., **96** (1954) 533

39. R .H. Bube, J.Chem. Phys., **23(1)** (1995) 18

40. R .H. Bube, J. Appl. Phys., **34(8)** (1963) 2390

41. J .Woods and D.A. Bright, *Proc.International Conf.*, Brussels (1958) 880

42. Peter Mark, J. Phys.Chem. Solids, **25** (1964) 911

43. David C. look, J. Appl. Phys., **45(1)** (1974) 492

44. B . Bell, T.C. Daman and S.P.S. Porto, Phys. Rev.,**144(2)** (1966) 771

45. M . Marychurch and G.C. Morris, Surface Science, **154** (1985) L251

46. J . Dresner and F.V. Shallcross, J. Appl. Phys., **34(8)** (1963) 2390

47. N . Romeo, G. Sberveglieri and L. Tarricone, Thin Solid Films, **43** (1977) L15

48. A . Piel and H. Murray, Thin Solid Films, **44** (1977) 65

49. N .R. Pavaskar, C.A. Menezes and A.P.B. Sinha, J. Electrochem. Soc., **124** (1977) 743

50. P .K. Nair, M.T.S. Nair and J, Campos, Solar Energy materials, **15** (1987) 441

51. R .R. Chamberline and J.S. Skarman, J. Electrochem. Soc., **113** (1966) 86

52. Yale Y. Ma and R.H. bube, J. Electrochem. Soc., **124(9)** (1977) 1430

53. J .L. Shay, S. Wagner, K. Bachman, E. Buchler and H.M. Kasper, *Proc.11th IEEE Photovoltaic Specilist Conference*, Phoenix AZ, IEEE, New York (1975) 503

54. N . Croitoru and S. Jakobson, Thin Solid Films, **56** (1979) L5

55. E . Khawaja and S.G. Tomlin, J.Phys.D: Appl. Phys., **8** (1975) 581

56. Z . Porada and E. Schabowska-Osiowska, Thin Solid Films, **175** (1989) 249

57. A .L. Dawar, P.K. Shishodia, Gayatri Chauhan, Anilkumar and P.C. Mathur, Thin Solid Films, **201** (1991) L1

58. A .L. Dawar, P.K. Shishodia, Gayatri Chauhan, Anilkumar and P.C. Mathur, J. Appl. Phys., **67** (1990) 6214

59. A .K. Chatterjee and S.C. Datt, Indian Journal of Pure and App.Phys., **31** (1993) 453

60. A . Ashour, R.D. Gould A.A. Ramdan, Phys.Stat Solidi (a)., **125** (1991) 541

61. W .J. Danaher, L.E. Lyons and G.C. Morris, Sol. Energy Mater., **12** (1985) 137

62. I .Kaur, D.K. Pandya and K.L. Chopra, J. Electrochem. Soc., **127** (1980) 943

63. A . Mondal, T.K. Chaudari and P. Pramanik, Sol. Energy Mater., 7 (1983) 431

64. P .J. Sebastian, J. Campos and P.K. Nair, Thin Solid Films, **227** (1993) 190

65. R . Jayakrishnan, S.R. Kumar and R.K. Pandey, Semicond. Sci. Tech., **9** (1994) 97

66. K .L. Narayanan, K.P. Vijayakumar, K.G.M. Nair and G.V.N. Rao, Bull. Mater. Sci., **20** (1997) 287

67. L . Hernandez, O. de Melo, O. Zelaya-Angel, R. Lozada-Morales and E. Puron, J. Electrochem. Soc., **141** (1994) 3238

68. S .A. Tomas, O.Vigil, J.J. Alvarado-Gil, R. Lozada-Morales, O. Zelaya-Angel, H. Vargas and A. Ferreira da Silva, J. Appl. Phys., **78** (1995) 2204

69. S .S. Kale, U.S. Jadhav and C.D. Lokhande, Indian Journal of Pure and App.Phys., **34** (1996) 324

70. I .I. Yu, Tetsuhiko Isobe and Mamoru Senna, Materials Research Bull., **30** (1995) 975

71. S . Bushan and S. K. Sharma, Appl. Phys. Lett., **57** (1990) 884

72. P . Gupta, R. Pal. D. Bhattacharya, S. Chaudhuri and A.K. Pal, Phys.Stat Solidi (a)., **148** (1995) 459

73. P .K. Nair, M.T.S. Nair, J. Campos and L.E. Sansores, Solar Cells, **22** (1987) 211

74. P .K. Nair, J. Campos and M.T.S. Nair, Semicond. Sci. Technol., **3** (1988) 134

75. W .W. Anderson and J.T. Mitchell, Appl. Phys. Lett., **12(10)** (1968) 334

76. W .R. Parikh, D.A. Thompson and G.J.C. Carpender, Radiation Effects, **98** (1986) 289

77. Ratnasagar and M.P. Srivastava, Phys. Lett.A, **183** (1993) 209

78. P .K. Govind and F.J. Fraikor, J. Appl. Phys., **42** (1971) 2476

79. B .Tell and W.M. Gibson, J. Appl. Phys., **40** (1969) 5320

80. Masafumi Yamaguchi, Jpn. J. Appl. Phys., **15** (1976) 723

81. R .O. Chester, J. Appl. Phys., **38** (1967) 1745

82. M . Kitagawa and T. Yoshida, Appl. Phys. Lett., **18** (1971) 41

83. M . Kitagawa and F.J. Bryant, Radiation effects, **33** (1977) 181

84. B .K. Gupta, O.P. Agnigotri and Ahmar Raza,Thin Solid Films, **48** (1978) 153

85. H .L. Kwok, J.Phys.D: Appl. Phys., **13** (1980) 1911

86. L .W. Chow, Y.C. Lee and H.L. Kwok, Thin Solid Films, **81** (1981) 307

87. L . Escosura, E. Garcia-Camarero, F. Arjona and F.Reuda, Solar Cells **11** (1984) 211

88. David S. Albin and S.H. Risbud, Thin Solid Films, **147** (1987) 203

89. A .G. Valyomana, K.P. Vijayakumar and C.Purushothaman, J.Materi.Sci.Lett., **9** (1990) 1025

90. Jean Ebothe, J. Appl. Phys., **77** (1995) 233

91. Sunny Mathew, P.S. Mukerjee and K.P. Vijayakumar, Thin Solid Films, **254** (1995) 278

92. N .A. Zeenath, K.P. Varkey and K.P. Vijayakumar, J. Phys.: Condens. Matter, **10** (1998) 2053

93. K .L.Chopra and S.R. Das, *Thin Film Solar Cells*, Academic Press, New York, (1983) Chap.5

94. Woods and J.A. Champion, J. Electronics and Control., **3** (1959) 243

95. Gremmeiss and R.Memming, J. Appl. Phys., **33** (1962) 2217

96. Gremmeiss and R.Memming, J. Appl. Phys., **33** (1962) 3596

97. W .W. Anderson and J.T. Mitchell, App. Phy. Lett., **12** (1968) 334

98. Fred Chernow,Graeme Eldridge, Guy Ruse and Lars Wahlin, App. Phy. Lett., **12** (1968) 339

99. Y . Kashiwaba, I. Kanno and T.Ikeda, Jpn. J. Appl. Phys., **31**(1992) 1170

100.P .J. Sebastian, App. Phy. Lett., **62(23)** (1993) 2956

101.Sunny Mathew, P.S. Mukerjee and K.P. Vijayakumar, Jpn. J. Appl. Phys., **34** (1995) 4940

102.S . Keitoku, H. Ezumi, H. Osono and M.Ohta, Jpn. J. Appl. Phys., **34** (1995) L 138

103.K .L. Narayanan, *Ph.D Thesis*, Cochin University of Science and Technology (1997)

104.T . Abe, Y. Kurobuchi, K. Ohta and Y. Kashiwaba, *Extended Abstracts;The 59 th Autumn Meeting of The Japan Society of Applied Physics*, (1998) p.1226

105.C .D. Wagner, W.M. Riggs, L.E. Davis and J.F.Moulder in *Hand book of Photoelectron Spectroscopy* (G.E. Muilenberg, Ed.), Perkin Elmer Corporation, Eden Prairie,MN (1979)

Chapter 4

Fabrication and characterization of CdS homojunction solar cells

4.1. Introduction

The history of cadmium sulphide cells begins with early 1950s. First report on the observation of a photovoltaic effect in cadmium sulphide with Cu, Ag, Au, or platinum contacts was from Reynolds et al [1]. They observed this as a contact effect and reported an open-circuit voltage of 0.4V and short-circuit current of 15 mA/cm^2 in direct sunlight with copper as electrode. They also reported the photovoltaic effect observed in pellets of CdS powder. Research on both single crystal and thin film cadmium sulphide continued through late 1950s. Single crystal cells were much superior in conversion efficiency, reaching over 5% in 1959, where as the efficiency of thin film cells remained below 1% [2].

Later Williams and Bube [3] studied the photovoltaic effect in cadmium sulphide crystals with electroplated junctions of several metals. The highest response was for the copper electroplated cell, making them argue that the photovoltaic current was due to the photoemission of electrons from copper metal into CdS crystal. During this time, Woods and Champion [4] explained the operation of the Cu/CdS cell by postulating the p-n junction formation due to either impurity band hole conduction or actual p-type CdS. Later Grimmeiss and Memming [5,6] joined with the idea of Woods and Champion and showed that in the copper diffused CdS crystal, the photovoltaic effect can be interpreted by a p-n junction formation. They studied the spectral distribution of

the short-circuit current, current-voltage characteristics at different illumination levels, temperature dependence of short-circuit current and open-circuit voltage.

During 1990s Kashiwaba et al [7] reported the photovoltaic effect in cadmium sulphide thin films prepared using vacuum evaporation technique. In this method they diffused copper atoms into cadmium sulphide by thermal annealing. They could obtain an open-circuit voltage of 0.45V, short-circuit current density of 31.4 mA/cm^2 and a conversion efficiency of 6.32%. They characterized the junction using the capacitance-voltage studies and studied the spectral dependence of short-circuit current of the cell. In this work, they proposed an i-n homojunction model for the formation of the potential barrier. Later the same group [8] proposed the p- type conversion of the cadmium sulphide by copper diffusion and the junction formed between copper doped CdS and undoped CdS showed rectification. Very recently another report from the same group described the light emission of CdS (Cu) /CdS diode occurring at liquid nitrogen temperature [9].

In the earlier reports on cadmium sulphide cell, generally single crystal was used. Later thin films of this material prepared using vacuum evaporation were used. As far as the device fabrication is concerned, large area film is a necessity. But at the same time it is rather difficult to have a large area film from vacuum evaporation. If we use chemical methods like 'spray pyrolysis' or 'chemical bath deposition', it is easy to obtain large area film. Moreover, these techniques are very cheap. It is with this idea that the spray pyrolysis technique was selected for the present work. In our laboratory we could successfully convert spray pyrolysed CdS into p-type and there are no reports on fabrication of junction using this type of CdS film. With this background we started working on the fabrication of homojunction in spray pyrolysed CdS film. Following section gives a detailed description of the junction fabrication and characterization.

Before entering into the device fabrication, we must know the basic mechanisms involved in the junction fabrication. An attempt is made in this direction and is presented in the following section.

4.2. Methods of p-n junction formation

In the present work, a homojunction is prepared by doping CdS with copper using thermal diffusion. So it will be better to give an idea of fabrication of junction using different process. Various authors have given the detailed account of junction formation [10,11]. In the following sections a brief descriptions on different techniques used for fabrication of junction are included.

4.2.1. Melt Grown Junctions

One of the easiest ways to make a p-n junction is the direct doping of the melt during growth of the crystal. If a n-type material is being grown from melt, add a larger amount of acceptor impurity than the donor impurity present in the melt at some point during the growth so that the crystal grown after the addition of the acceptor impurity will be p-type forming a p-n junction.

Another way of making p-n junction during growth from the melt is the rate growing method. In this method, both the acceptor and donor impurities are simultaneously present in the melt, and one of these predominantly incorporated in the growing crystal as determined by the rate of growth. The method of growing p-n junction from the melt is not suitable for large scale production.

4.2.2. Alloying

This involves heating of a semiconductor slice in contact with an impurity that becomes liquid at the temperature used for heating. After melting, it dissolves into the semiconductor making alloyed junctions. As the liquid is

cooled, the semiconductor re-crystallizes with impurity atoms substituted in the semiconductor lattice. p-n junctions can be made in n-type Ge by doping with indium using this method. This is a simple and efficient method of making p-n junctions. But the main disadvantage of this process is that it does not permit tight control on the area and the depth of the junction.

4.2.3. Solid-State Diffusion

It is the most widely used technique for making p-n junctions. Diffusion of dopant impurity atoms into a semiconductor is described by a second order partial differential equation known as Fick's law:

$$\frac{\partial N}{\partial t} = \nabla.(D\nabla N)$$

where N and D represent the concentration and diffusion coefficient of the diffusent, respectively. The above equation is usually simplified by making the assumption that D is constant. With this assumption and considering one-dimensional diffusion, we have

$$\frac{\partial N}{\partial t} = \mathrm{D}\frac{\partial^2 N}{\partial t^2}$$

The solution of this equation with appropriate boundary and initial conditions yields the impurity distribution in the semiconductor.

When a semiconductor is heated to a high temperature and a flux of impurity atoms is incident at its surface, the dopant atoms migrate into the crystal because of their concentration gradient. At a high temperature, many of the semiconductor atoms move out of their regular lattice sites creating a high density of vacancies. At the same time some semiconductor atoms move into the voids between the atoms and create self-interstitials. The impurity atoms diffusing into the semiconductor may occupy either the vacant lattice sites, or the voids between the atoms. The impurities that occupy the vacant sites replace the regular atoms in the lattice and are known as substitutional impurities, and

that occupy the voids are called interstitial impurities. When the crystal is cooled to the room temperature, interstitial atoms may return to the substitutional positions and become electrically active.

Diffusion may be carried out either in an open tube furnace or in an evacuated sealed tube system. The open tube diffusion is the preferred method, and in order to improve the controllability of the impurity profile, it is carried out in two steps: "pre-deposition" and "drive-in". During the pre-deposition step, a carefully controlled amount of the desired impurity is introduced into the semiconductor. The drive-in diffusion is performed after predeposition to reduce the surface concentration and to push the impurity atoms further away from the surface into the bulk of the semiconductor. Sealed tube diffusion is used for impurities, which cannot be diffused by the open-tube technique. In this method, a number of wafers are loaded into a boat and placed in a quartz tube together with the dopant source. The tube is then evacuated, sealed off, and placed in a diffusion furnace at a temperature at which the impurity develop sufficient vapour pressure to cause appreciable diffusion.

4.2.4. Ion Implantation

It is frequently used as an alternative to pre-deposition for introducing dopant atoms into the desired region of the semiconductor. The implanted impurities are then diffused further using a drive-in step. The major advantage of ion implantation is that it has the ability to precisely control the amount of dopant and its depth below the surface. Moreover, it is a low temperature process that eliminates deformation of semiconductor caused at high temperatures.

In this technique, a beam of ionized atoms is accelerated through a desired potential (10 to 500 KV) and is made to incident on a semiconductor target. In the ion implantation system, there is a chamber into which the gas or

vapour containing the atoms of the desired impurity is introduced, where the atoms are ionized by collision with high energy electrons. The ion beam emerging from the chamber contains not only the desired dopant ions, but also ions of unwanted species. The dopant ions are separated from the unwanted ions by passing the beam through a strong magnetic field (of precisely maintained intensity) that bends the desired ions through a calculated turn. The selected ions are then accelerated using an electric field and made to strike the semiconductor target, which is kept at ground potential. The beam is deflected horizontally and vertically so that it sweeps across the target in a raster pattern to ensure homogeneous doping. Both the target and beam are maintained in high vacuum. When the accelerated ions enter the semiconductor, they lose their kinetic energy through collisions with the electron cloud of the semiconductor atoms as well as the positively charged nuclei of the atoms and finally come to rest.

Ion implantation produces damage in the crystal target by displacing atoms from their regular lattice sites. Then, a highly disordered layer is created near the surface of the semiconductor. This radiation damage is annealed out by a heat treatment in the 400-800^{o}C. Ion implantation is essentially a shallow doping process and cannot be used in devices where deep diffusion is required.

Recently, K.L. Narayanan et al [12] reported optical absorption studies of Ar^{+} implanted CdS thin films. Raman scattering studies in these films was also been reported by them. Post implantation annealing of CdS thin films prepared using CBD showed a more stable hexagonal phase. Effect of irradiation induced disorder on the optical absorption spectra of CdS thin films was reported by the same group [13]. They also used positron annihilation technique to analyse the effect of ion implantation in CdS [14]. The effect of implantation of argon ions on CdS film prepared using CBD was studied by K.L. Narayanan and it was observed that there is a progressive reduction of

band gap with an increase in the irradiation dose. He also observed persistent photoconductivity on nitrogen implanted CdS film [15].

4.3. Device fabrication

Fabrication of thin film solar cells, even in laboratory scale, involves several steps of thin film deposition and characterization. Fig. 4.1 shows the "process-flow chart", employed for the fabrication of thin film homojunction CdS solar cells. Each process is discussed in detail in the following sections. But the details of the film deposition process are given in earlier chapter.

4.3.1. Film preparation

The tin oxide coated glass substrates were cleaned with dilute alkaline detergent solution and then using ultrasonic cleaning. These samples were dried and cadmium sulphide was deposited over the SnO_2 layer using spray pyrolysis. Above the CdS layer, a thin layer of pure copper was deposited using vacuum evaporation over an area 1 × 0.7 cm^2. This was annealed to 300^{o}C for 45 minutes under high vacuum (10^{-5} torr). The top layer of cadmium sulphide was converted into p-CdS by the diffusion of copper atoms by thermal annealing. The detailed description of the deposition process and characterization of SnO_2 layer, cadmium sulphide layer and p-CdS layer are included in chapter 3.

4.3.2. Device Optimization

Optimization of the homojunction device fabricated by this method in the laboratory is the next aspect to be described here. Thickness of the cadmium sulphide is an important parameter controlling the properties of the junction. This is so sensitive that the photovoltaic effect may not be even "visible", if the thickness is not optimum.

Since thermal diffusion technique was used to introduce copper into cadmium sulphide for conversion into p-type, there should be a clear idea about the depth of diffusion of copper atoms due to annealing at a temperature of

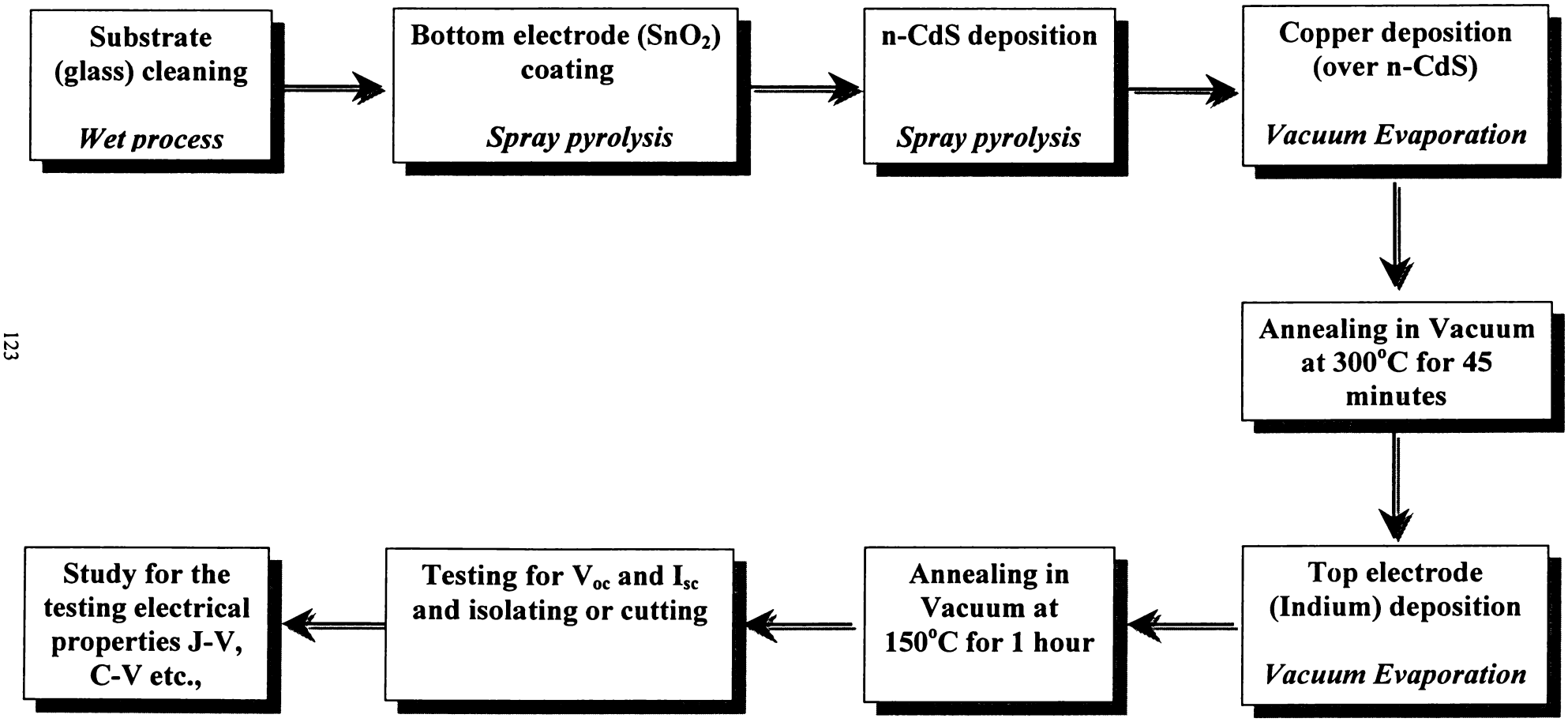

Fig. 4.1. Flow chart of the process of fabrication of CdS homojunction thin film solar cell

300°C. Earlier studies in our laboratory [16] in this matter had revealed that copper diffused to a depth of 500 nm when the annealing temperature was 300° C. Hence in the present work the thickness of the cadmium sulphide layer was kept greater than 500 nm, so as to ensure the presence of a layer of undoped pure CdS at the bottom. Thickness of the cadmium sulphide layer was varied in the range 400 nm to 1000 nm and the junction parameters like open circuit voltage and short circuit current density were noted. Optimum thickness, which gave maximum response, was found to be nearly 1μm.

Another parameter to be controlled was the thickness of copper layer deposited over cadmium sulphide. This was also varied in the range 25 nm to 55 nm and the details are included in chapter 3. Finally for the better performance of the junction, thickness of the copper film was fixed at 40 nm. The third parameter to be optimized in this work was the annealing temperature of the sample. This was varied from 250°C to 350°C and the results obtained are included. The optimum value was found to be 300°C.

The material and structure of the top electrode were found to have a good control over cell performance. In this work indium was used as the top electrode. It was coated as a film of thickness 300 nm over the p-CdS. An annealing was found to be necessary for the better performance of the cell. This annealing temperature was to be optimized and finally the temperature for the annealing was fixed at 150°C. This was also done under high vacuum (10^{-5} torr). After the selection of electrode material, it was the area of the electrode, which was to be optimized next. Photovoltaic activity was found to be the lowest when the whole area of p-CdS was covered with the top electrode. This may be due to micro shunts (microscopic local areas of shunting) and also due to spatial non-uniformity of composition of the film. After several trials, the electrode area was restricted to 5×5 mm^2 to get good photovoltaic activity. Therefore from

each cell, the area that gave the maximum response was selected for characterization.

4.3.3. Characterization

The J-V characteristics under dark and illuminated conditions were studied. The photograph of the experimental arrangements used for this purpose is shown in Fig.4.2. The sample was mounted in a vacuum cell provided with a sample holder made of thick copper block having arrangements for controlled heating. Measurements were carried out in vacuum of 10^{-1} torr. The samples were illuminated in the backwall configuration (illuminating from window side) with a tungsten lamp that gave an optical power of 60 mW/cm^2 (corrected for transmission through the SnO_2 side) on the test cell. This input power was measured by a power meter (Suryamapi, A-136 model supplied by CEL). The distance between the lamp and sample was always 15 cm. There was no appreciable change in the temperature of the sample due to heating by incident light. So the cooling arrangements were not given. The voltage across the cell was measured using a 4½ digit autoranging multimeter (APLAB model 1087). Voltage across the standard resistor was measured by another multimeter (Keithley 2000) and hence the current was calculated. The solar cell parameters like open circuit voltage (V_{oc}), short circuit current density (I_{sc}), fill factor (FF) and efficiency (η) were estimated from these illuminated J-V characteristics. The relative spectral response of the device was plotted for different wavelengths in the range 450 to 800 nm using a monochromator. This was done by noting the short circuit current for different wavelengths and by using the spectral response graph of the lamp source, the normalized short circuit current was plotted for different wavelengths.

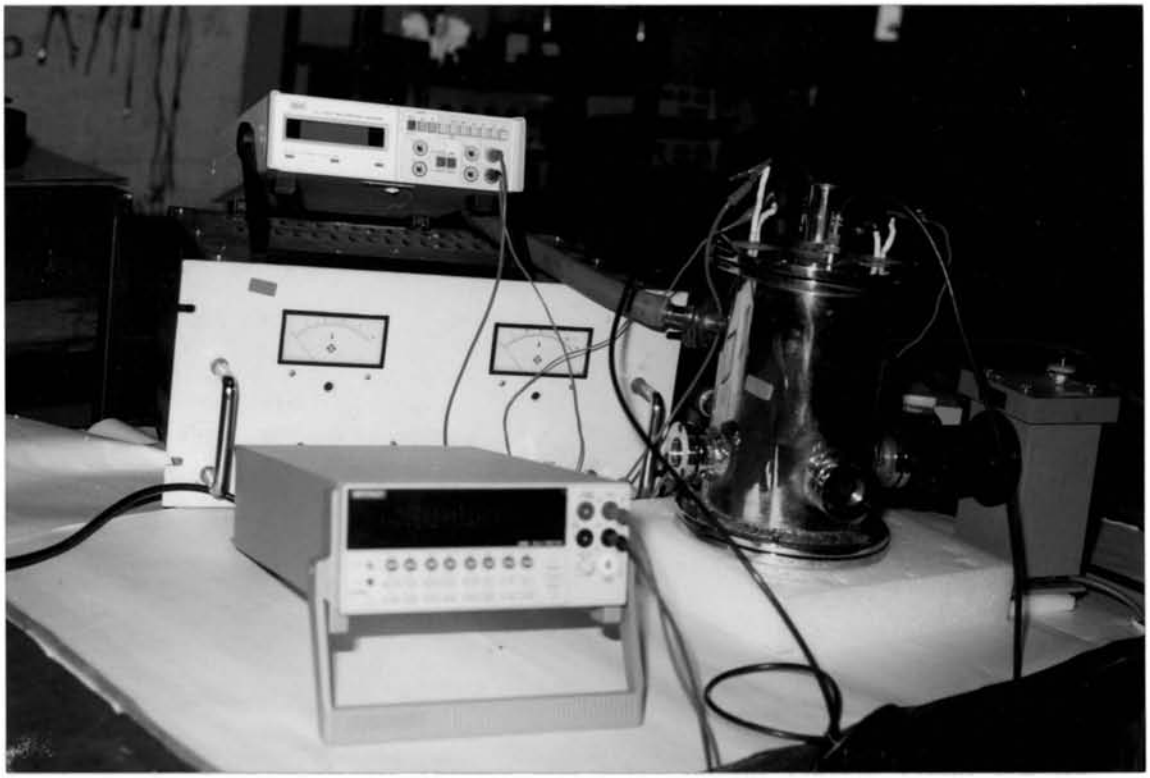

Fig. 4.2. Photograph of the experimental setup used for the characterization of solar cells

4.3.4. Results and Discussions

4.3.4.1. Effect of variation in annealing temperature

In order to know the effect of annealing temperatures on the junction formation, we measured the open circuit voltage and short circuit current density of the cells, in which the annealing after the copper deposition were conducted at different temperatures in the range 250 to 350°C. The results are given in Table 4.1.

Table 4.1.

Variation of cell parameters with annealing temperature

Annealing temperature (°C)	Open Circuit Voltage (mV)	Short Circuit Current Density (mA/cm^2)
250	-	-
275	-	-
300	191	4.93
325	196	4.96
350	198	4.97

From the table one can see that when the annealing temperature was below 300°C, open circuit voltage and short circuit current could not be measured. This may be due to the fact that temperature of annealing was not sufficient to diffuse the copper atoms into the CdS layer for the conversion into p-CdS. So the junction would not have been formed. It is also interesting to see that there was no practical variation in the values of open circuit voltage and short circuit current density for annealing temperatures above 300°C. This may be because, almost all copper atoms have diffused into the CdS layer converting it to p-type and hence by just increasing the temperature there was no further increase in acceptor density.

4.3.4.2. Effect of CdS thickness

Another argument about this was that it might have formed with a structure, p-CdS:Cu/n^+ SnO_2. In order to rule out this possibility, we fabricated the junction in CdS films of different thicknesses (in the range 400 to 1000 nm) deposited over the SnO_2 layer. In all these films thickness of the copper deposited was kept constant (40 nm). All these samples were annealed at a temperature of 300°C for 45 minutes in high vacuum. Values of the open circuit voltage and short circuit current density for these cells are presented in Table 4.2.

Table 4.2.

Variation of cell parameters with thickness of CdS layer

Thickness of CdS layer (nm)	Open circuit Voltage (mV)	Short Circuit Current Density (mA/cm^2)
400	-	-
500	20	-
600	156	2.9
700	178	4.0
800	191	4.93
900	197	4.95
1000	185	4.8

It was found that the junction was not formed when the thickness of the CdS layer was less than 500 nm. It is worth mentioning here that variable angle spectroscopic analysis studies on similar samples had clearly indicated the depth of penetration of copper atoms into CdS was 500 nm [16]. So it became evident that the junction was formed only when the CdS layer had a thickness of at least 500 nm ensuring that there was a layer of n-CdS below the copper diffused

p-CdS layer. This result proved beyond any doubt that the junction was formed in CdS itself. On the other hand, if the junction formation was between SnO_2 and p-CdS there could not have been dependence of thickness of CdS layer in forming the junction.

Later this was confirmed by taking the ESCA depth profile of the sample and it is depicted in Fig.4.3. From the figure it is very clear that copper is not diffused along the full depth into the CdS layer and at the bottom there is a layer of pure CdS without the trace of copper atoms. At the same time we can see the depth profiles of tin and oxygen from the tin oxide coated over the glass substrate. This was a solid proof for the homojunction formation.

4.3.4.3. J-V Characteristics

The J-V characteristic under dark condition is depicted in the Fig.4.4. The series resistance of the cell was calculated using the slope of the straight portion of dark forward characteristics and it was found to be 400 Ω. Even though this value is high, this is reasonably good and compares well with other reported values. For example, Ristova and Ristov [17] reported a value of 1170 Ω for CdS/SnS_x cell under dark conditions. Diode quality factor of the cell fabricated was calculated from the slope of the log J Vs. V plot which is depicted in the inset of the Fig.4.4 and this was found to be 2.6. This value seems to be high for the junction, but there are reports of values of 3 or even 4 [18].

Fig. 4.5 shows the J-V characteristic of the homojunction under illuminated condition. For the best sample prepared, the open circuit voltage obtained is 200 mV, the short circuit current density $5mA/cm^2$, fill factor was found to be 0.44 and the efficiency was calculated as 0.73%. The low fill factor and low efficiency may be due to the following reasons. First, the series resistance of the cell was high and this might have affected the fill factor.

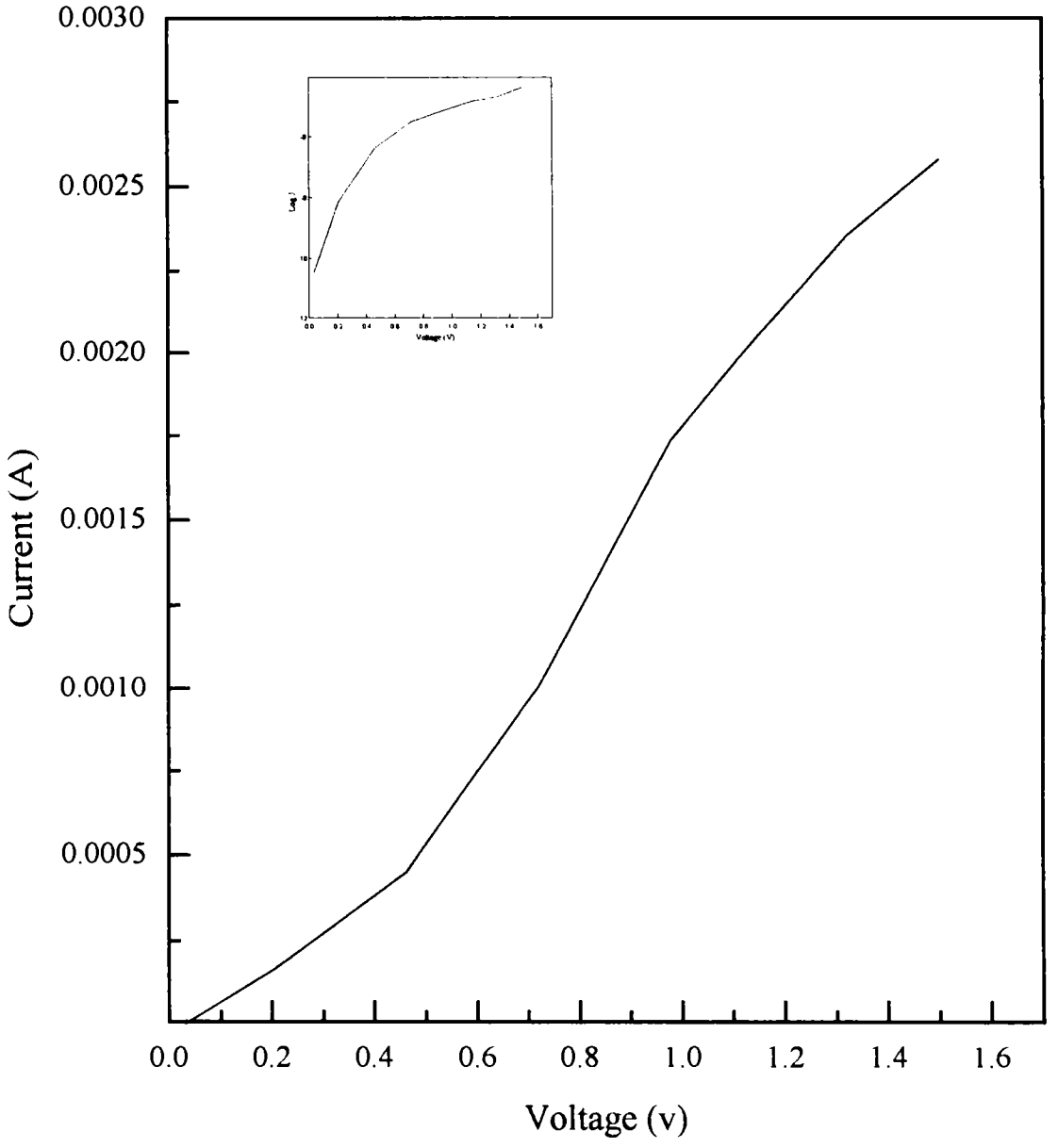

Fig. 4.3. J-V characteristics of the cell under dark condition

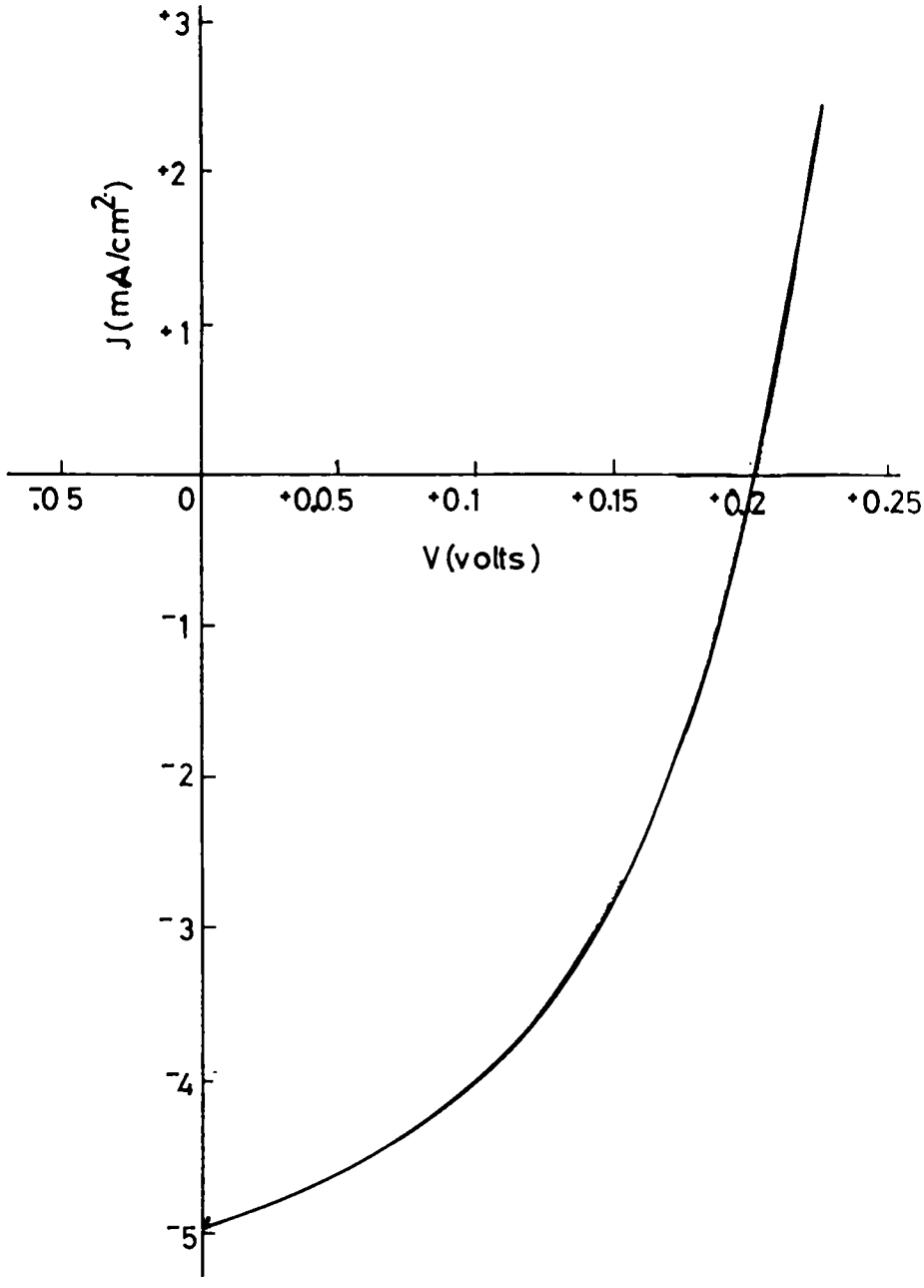

Fig. 4.4. J-V characteristics of the cell under an illumination of 60 mW/cm^2

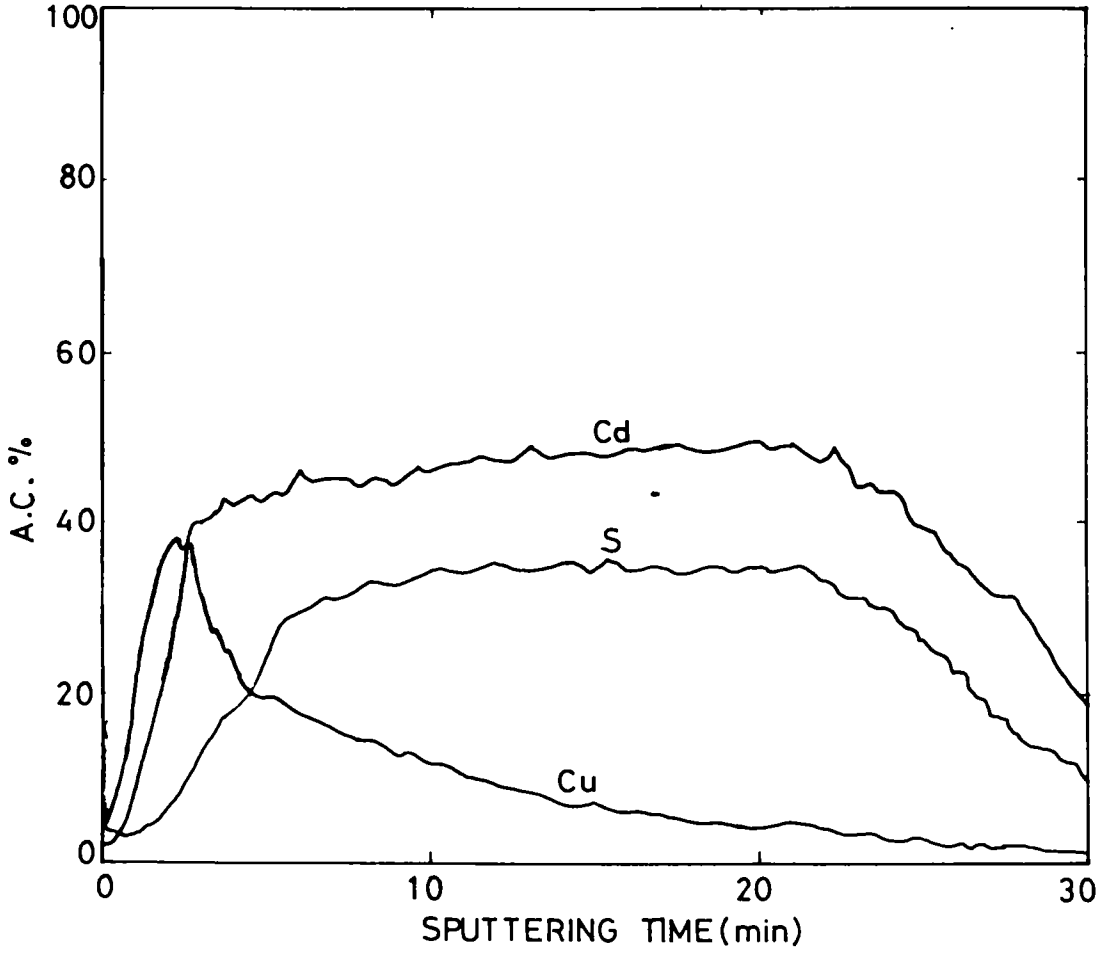

Fig. 4.5. ESCA depth profile of the copper diffused sample

Another reason is that the junction formed may be shallow, so that the minority carriers might have been lost.

4.3.4.4. Spectral response

The spectral response curve of the cell is shown in Fig. 4.6. It shows that the higher wavelength response ceases at about 800 nm while the shorter wavelength response extends upto 500 nm. The sharp cut off at the shorter wavelength side may be due to the distance of the junction from the n-CdS/SnO_2 interface. Hence the carriers due to the absorption of high energy photons near the interface may not be reaching the junction.

4.3.4.5. Stability of the cell

The major advantage of this homojunction solar cell is its stability, compared with the Cu_2S/CdS cell. The V_{oc} and J_{sc} values remain more or less constant for one year, when we place the cell in ordinary lab conditions, even without any encapsulation. For the best cell fabricated, the parameters are included in table 4.3.

Table 4.3.

Cell parameters for the best cell fabricated

Open Circuit Voltage	200 mV
Short Circuit Current Density	5 mA/cm^2
Fill Factor	0.44
Efficiency	0.73%
Series resistance	400Ω
Diode Quality Factor	2.6

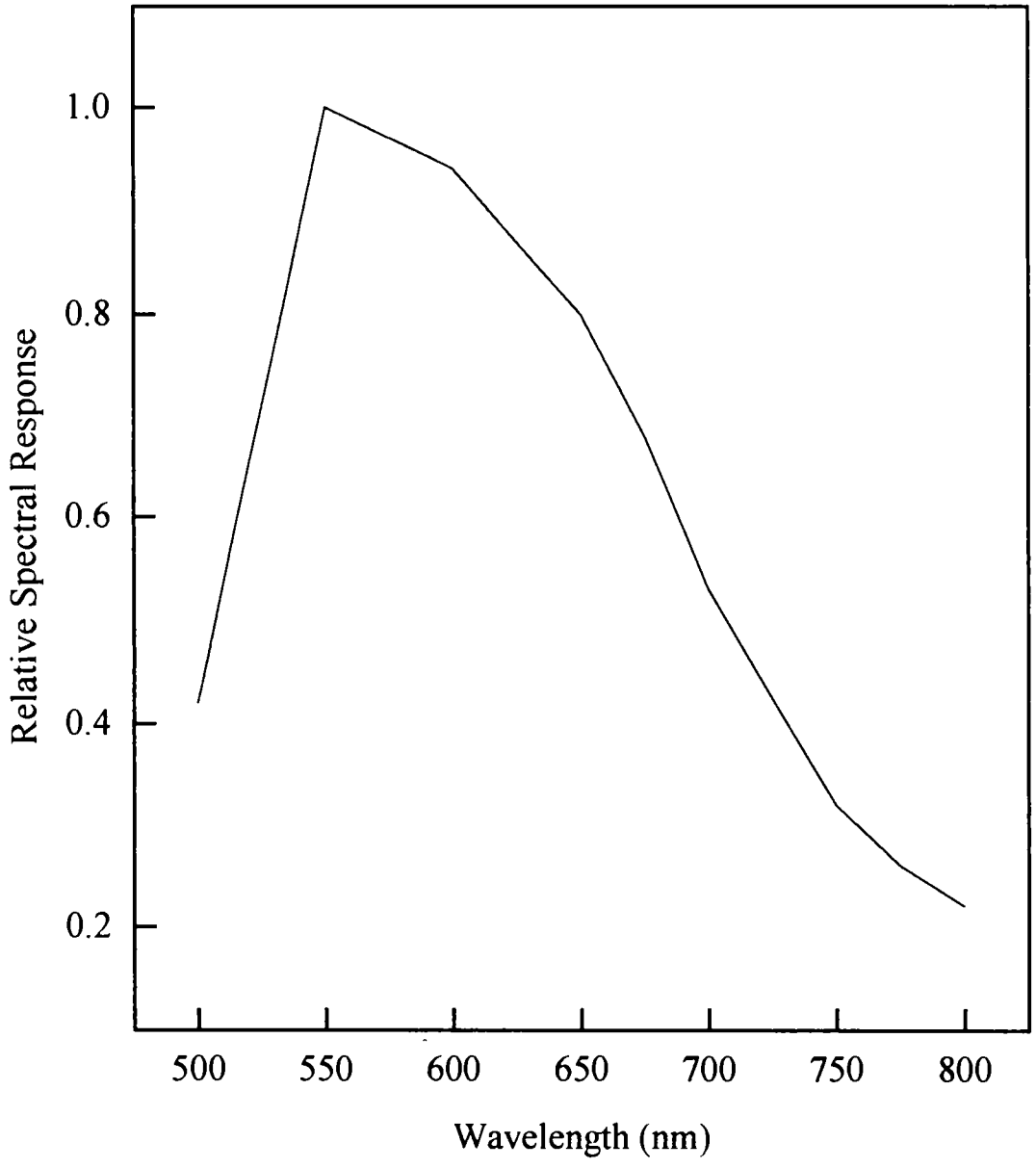

Fig. 4.6. Relative spectral response of the solar cell fabricated

4.3.5. Conclusion

For the first time, it is found that the homojunction can be fabricated in spray pyrolysed CdS thin film. This is an important result as it can be used for fabrication of tandem cells. This gains more importance in the case of $CuInSe_2$/CdS cells prepared using only chemical bath deposition with CdS forming the top layer [19].

4.4. Fabrication of a cell with improved performance

In the earlier section we had seen the performance of CdS homojunction solar cells. But the main problem with the above one was that it was having low efficiency. For a viable solar cell, efficiency has to be improved. Detailed analysis of the junction was done using ESCA depth profile. The result of this is depicted in Fig 4.5. From this figure it is clear that the copper distribution over the top layer of CdS was not uniform. This had a maximum value at about a depth of 200 nm from the top surface. Since the maximum copper content existed very near to the top surface, the junction was far away from the illumination surface (i.e. the SnO_2/CdS interface) resulting in the loss of the photogenerated carriers. This might have been the major cause for the low efficiency. Another important factor is that the junction formation may not be well defined, since the copper distribution is not uniform. This ultimately affects the open circuit voltage and short circuit current, which in turn affects the efficiency.

4.4.1. Sample Preparation

In order to keep the copper distribution on the top layer of CdS to be uniform to a larger depth and also to have a junction away from the top surface, more copper was diffused into the Cadmium sulphide film. In this case the samples with more thickness of CdS layer were selected (~1.3 μm). For the fabrication of cell, another thin layer of pure copper (25 nm) was deposited over the earlier samples (in the same region where copper was diffused earlier) using

vacuum evaporation. The sample was again annealed at 300°C for 45 minutes in high vacuum. Preliminary investigation showed that all the copper atoms had diffused into the CdS layer and the cell showed good photovoltaic activity. Indium was coated as the top electrode. The area of the electrode was $0.2cm^2$ and the thickness of the electrode was exactly the same as that in previous case (300 nm). Annealing of the electrode was also done. The details of analysis and discussions are included in the following sections.

The J-V characteristics of the cell were done under an illumination of 80 mW/cm^2 on the sample surface. Here we used a source of higher illumination than the previous case. The arrangement for this is exactly the same as that used for the earlier analysis. Another important analysis was the ESCA depth profile of the sample. This was mainly to get a better knowledge about the distribution of copper on the top layer of CdS. This analysis would also help us to know whether any new compounds like Cu_xS has been formed as a result of any chemical reaction between cadmium sulphide and the diffused copper.

Optical absorption studies have been done, to know the formation of any new compound. The short circuit current at different wavelengths of the incident light was found out and a relative spectral response curve was drawn by taking the normalized value. The value is normalized by taking the spectral graph of the source and the value corresponding to the maximum is taken as 1. The capacitance-voltage characteristics were studied by superimposing a signal of frequency 100 kH_Z over a steady voltage. Capacitance was measured with a LCZ meter (Hewlett Packard 4277 A model) for different bias voltages. This was done at a temperature of 303K and the area of the cell was $0.2cm^2$. The built-in voltage and acceptor state density were calculated from the C^{-2} Vs V graph.

4.4.2. Results and discussions

4.4.2.1. J-V characteristics

J-V characteristics under dark condition were drawn and it is depicted in Fig.4.7. From the forward characteristics, the series resistance of the cell was calculated and it was 305 Ω. This value is reduced by 25 % when compared with that of the previous cell and this may be one of the reasons for improving the efficiency. Diode quality factor was calculated from the slope of the log J Vs.V graph which is depicted in the inset of the Fig.4.7 and it was found to be 1.9. This value is better than the previous case and comparable with the usual values (between 1 and 2).

From the illuminated J-V characteristics, given in Fig.4.8, open circuit voltage and short circuit current density were obtained as 400 mV and 12 mA/cm^2 respectively. Fill factor was 0.49 and conversion efficiency was calculated to be 3%. When we compare with the earlier results, this is most encouraging, but still the fill factor is low. Again the reason for that may be the high series resistance. Increase in open circuit voltage and short circuit current density is commendable and this may due to the well defined junction formed slightly away from the top surface.

4.4.2.2. ESCA depth profile

Fig. 4.9 shows the depth profile of the sample obtained using ESCA technique. We can see that the distribution of copper was more or less uniform to a larger depth of the film than the previous cell, since the atomic percentage of copper is more uniform than the previous case. Again the ESCA analysis gave insight to the structure of the solar cell fabricated. The structure should be Glass/SnO_2/n-CdS/p-CdS:Cu, since we can see that there is a layer of pure n-CdS (of thickness ~ 300 nm), without the trace of copper atoms, below the top

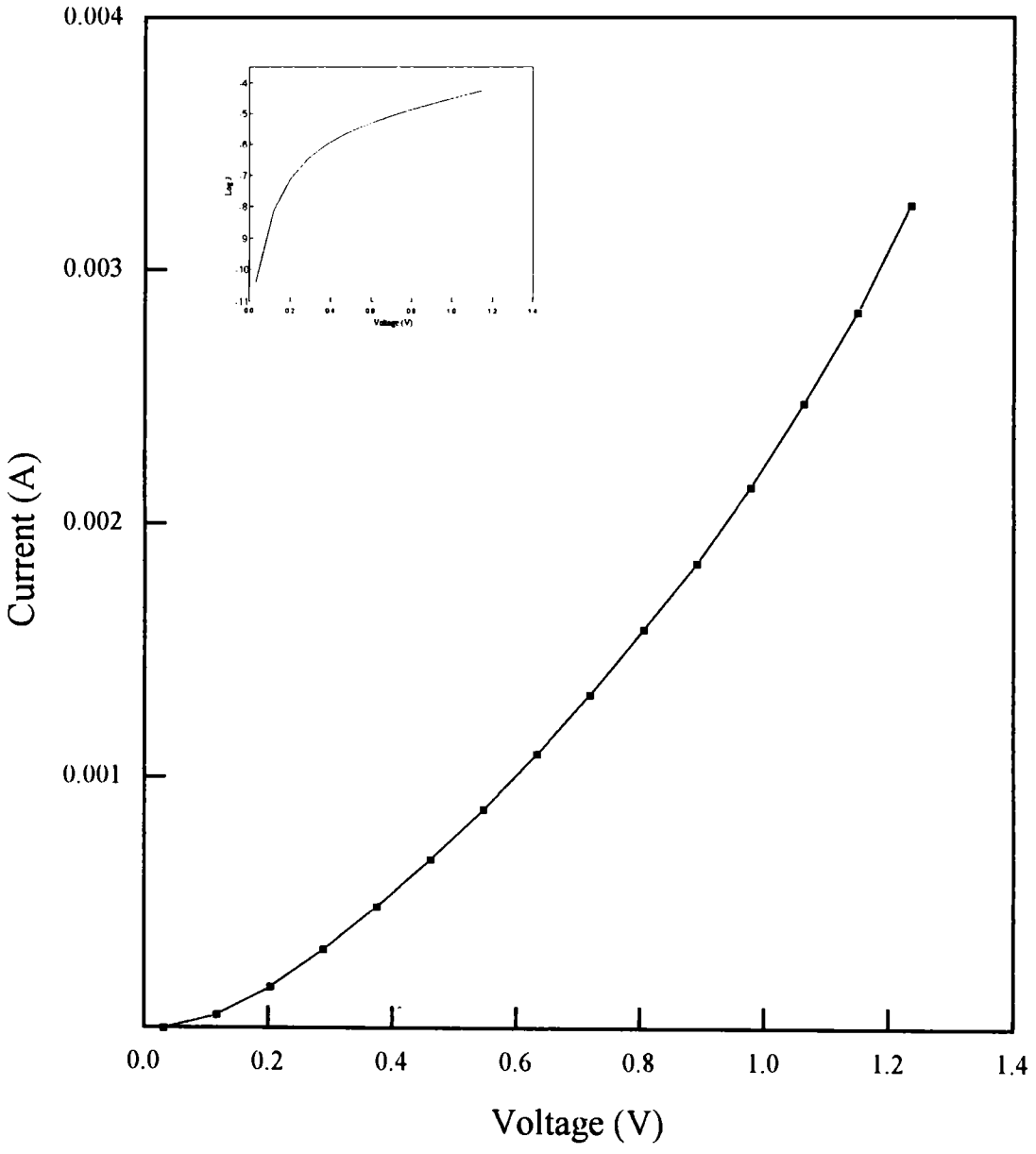

Fig. 4.7. J-V characteristics of the improved cell under dark condition

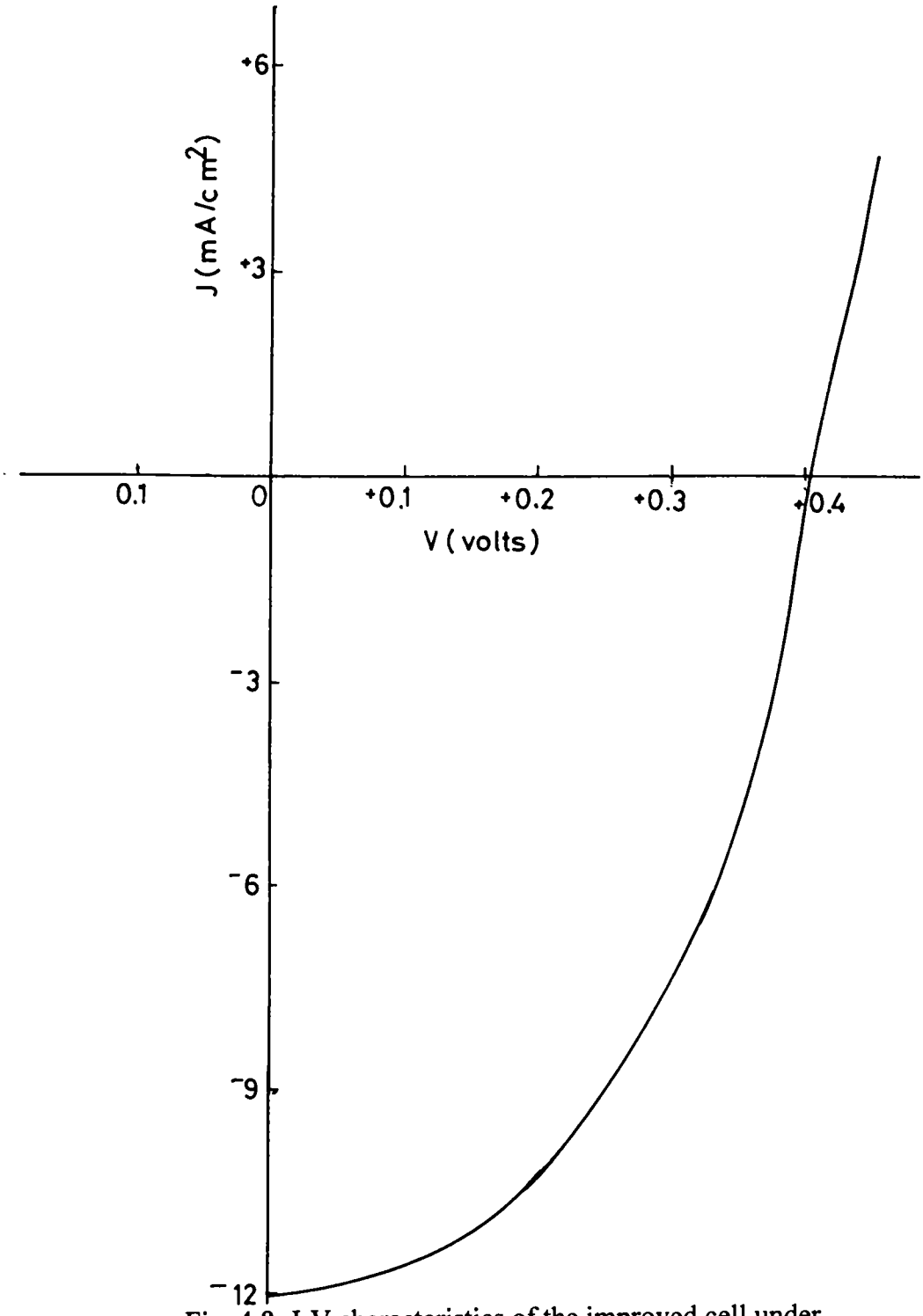

Fig. 4.8. J-V characteristics of the improved cell under an illumination of 80 mw/cm^2

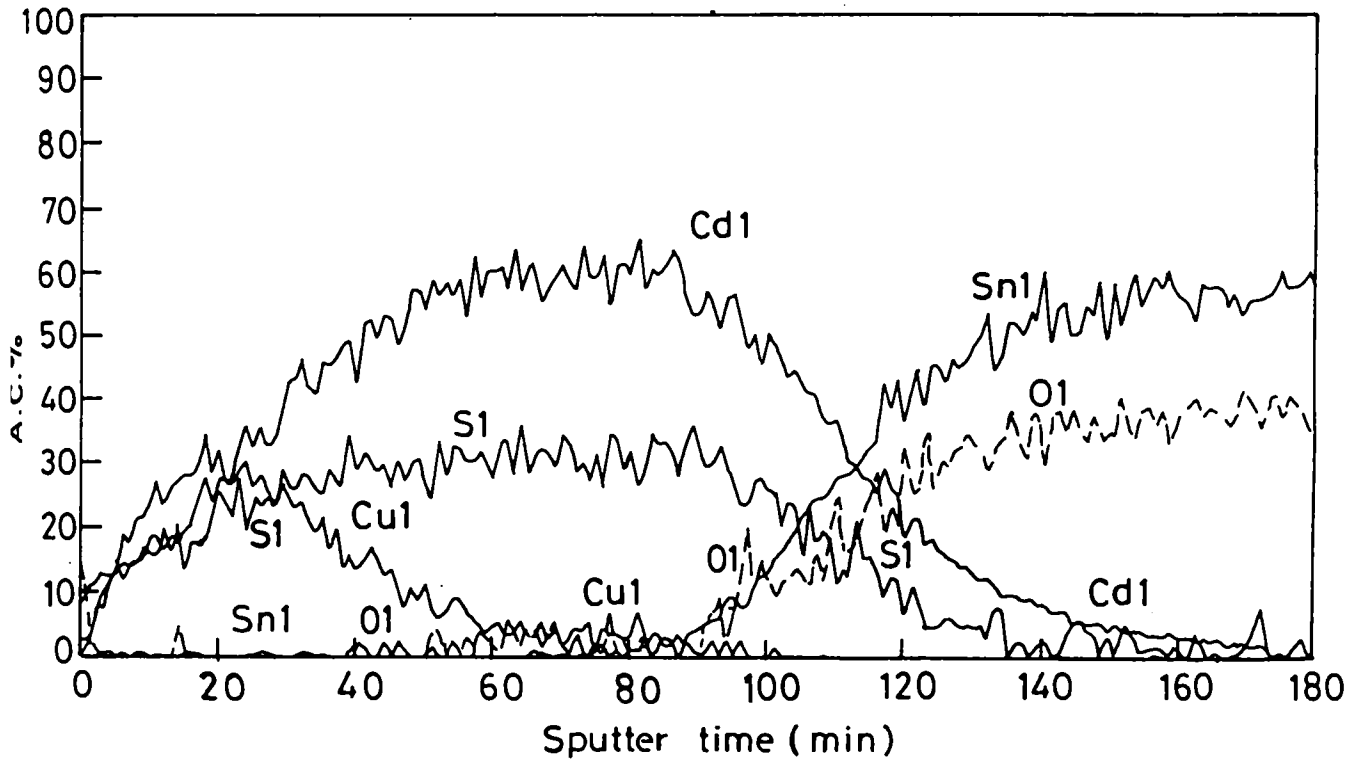

Fig.4.9. ESCA depth profile of the "more copper diffused" sample

layer of p-CdS:Cu. This was again verified from the depth profile of the improved cell, which is depicted in the Fig.4.10. From this it is very clear that copper was not fully diffused into the CdS. Peaks of tin and oxygen start where the CdS layer ceases, i.e. from the bottom electrode of tin oxide.

Another important result is that, even after diffusing more quantity of copper into the CdS film, there was no evidence indicating the formation of any new copper compounds. This is very vivid from the ESCA depth profile of the copper depicted in Fig.4.11. In the figure the two peaks (932.7 and 952.5 eV) are corresponding to the binding energies of elemental copper. There is no shift in binding energy throughout the thickness of the sample i.e. in any depth of the sample, no new compound formation was taking place.

4.4.2.3. Optical absorption studies

The optical absorption spectrum for the n-CdS and p-CdS layer were taken separately and it is given in Fig.4.12. From this $(\alpha h\nu)^2$ Vs $h\nu$ graph was plotted in the same graph and is depicted in Fig. 4.13. This is very useful, since optical absorption reveals the formation of Cu_xS as a result of reaction between the diffused Cu and CdS. This gains importance in this case, as the quantity of copper was enhanced this time. If Cu_xS had been formed, we can expect a change in optical absorption corresponding to the band gap (1.7 eV) of Cu_xS. From the figure it is clear that, the graphs are identical and there is only a slight decrease in band gap (0.2 eV) for copper diffused CdS. A similar case of shift in absorption edge due to copper doping in CdS film (prepared using CBD) was reported earlier [20].

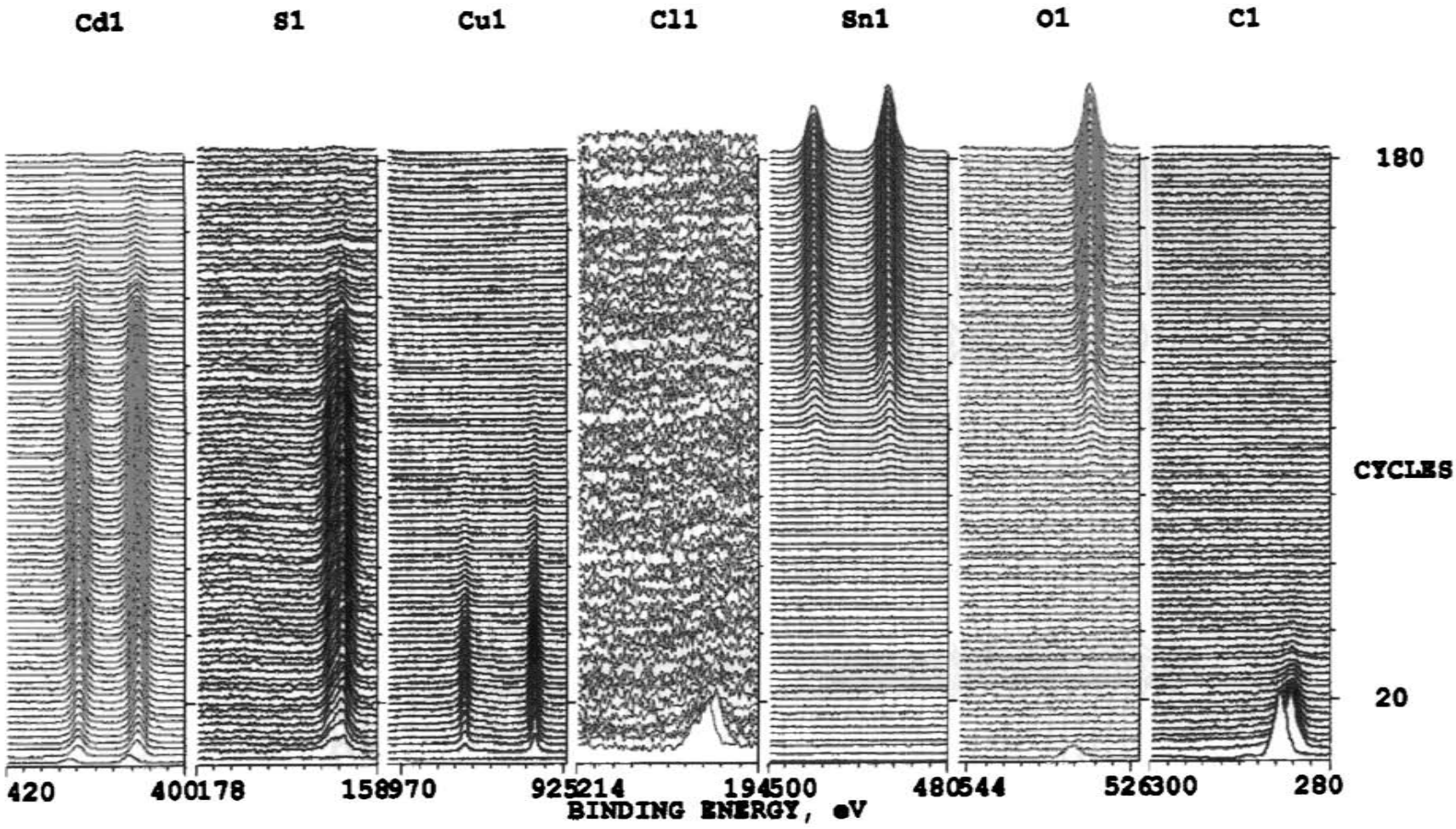

Fig. 4.10. ESCA depth profile of the improved CdS homojunction cell

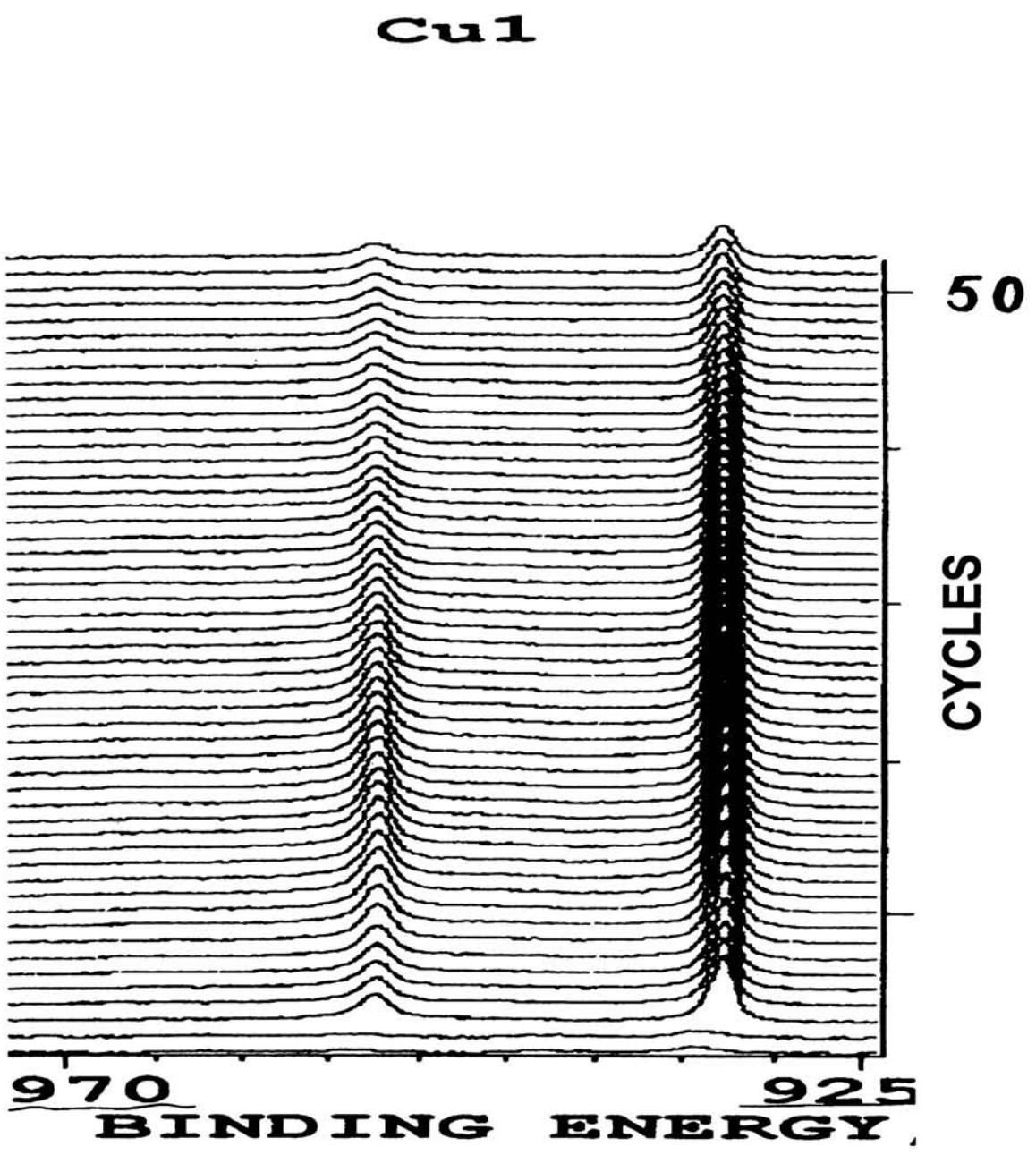

Fig. 4.11. ESCA depth profile of copper in improved cell

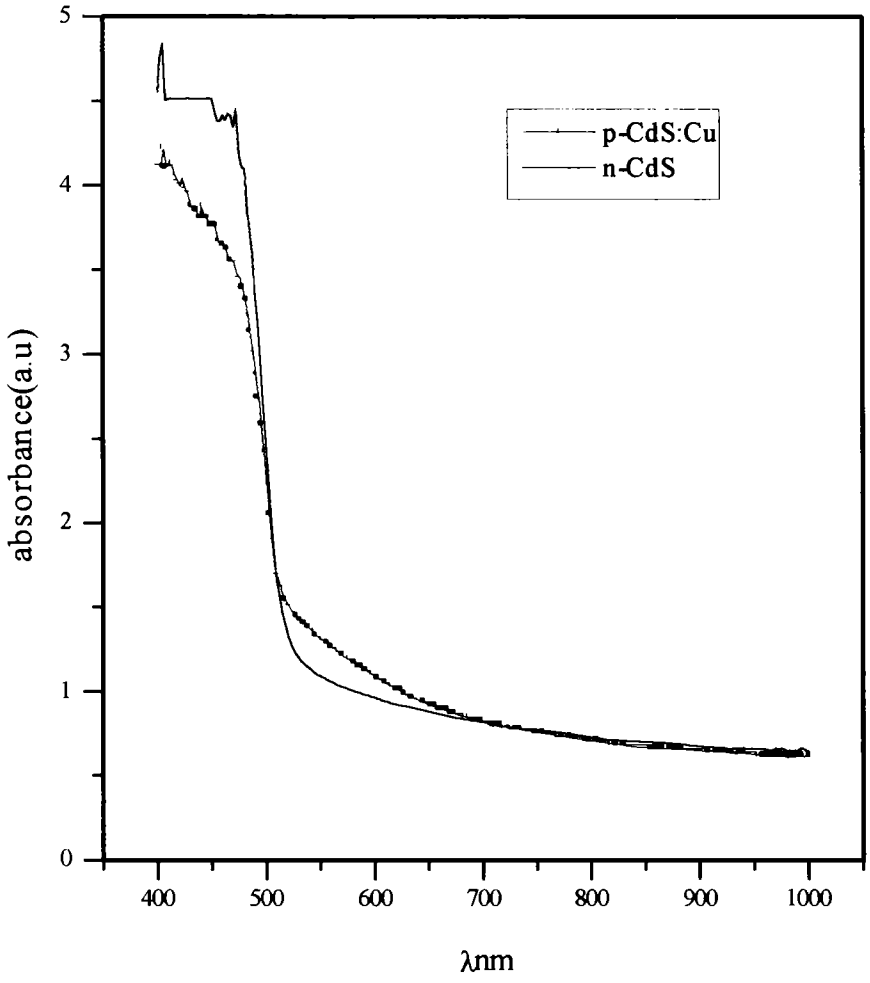

Fig.4.12. Optical absorption spectra of n-CdS and p-CdS:Cu (improved cell)

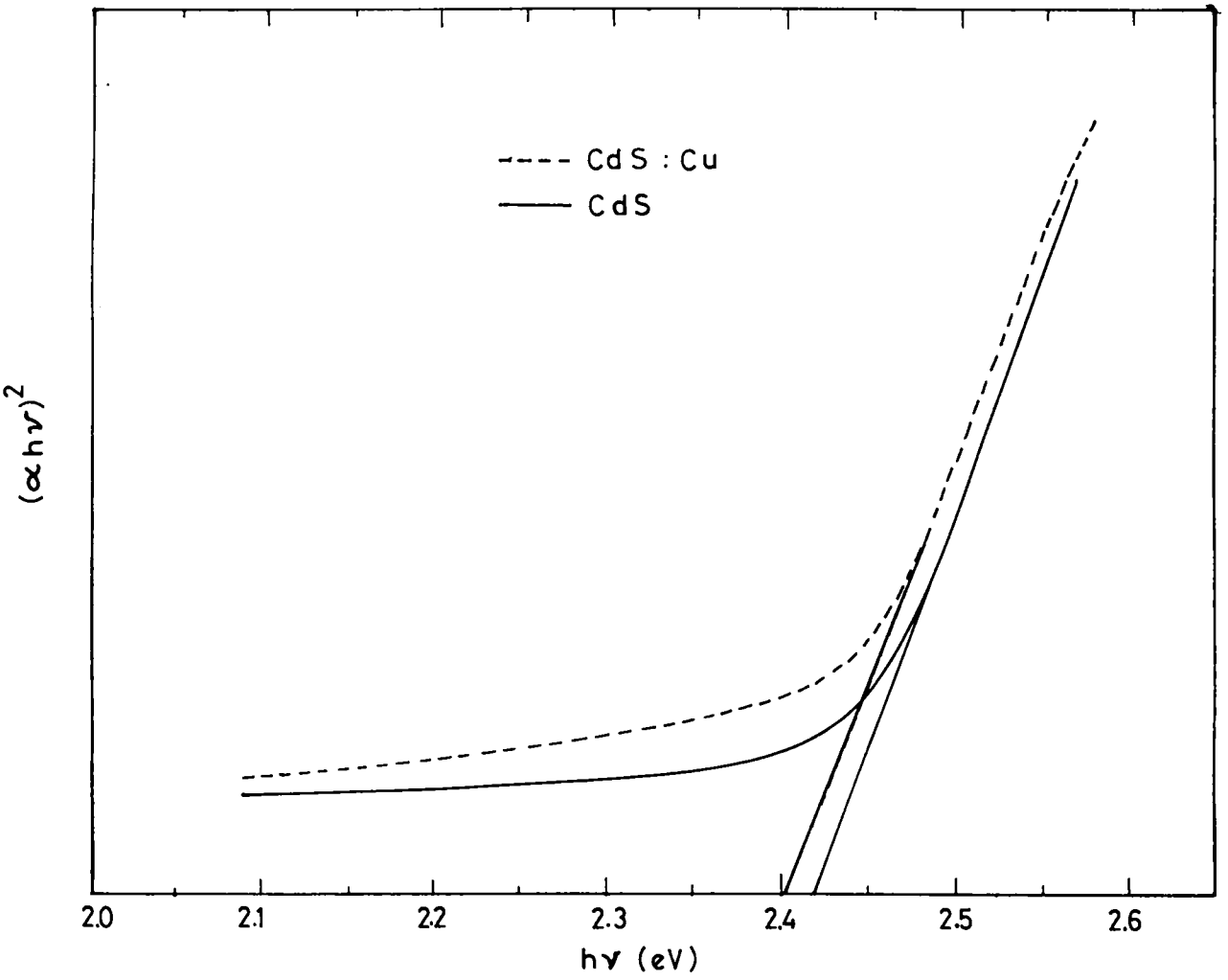

Fig. 4.13. $(\alpha h\nu)^2$ Vs. hν plott of n-CdS and p-CdS:Cu (improved cell)

4.4.2.4. Spectral response

The spectral response of the cell prepared is another important parameter while we characterize the cell. The curve is drawn by measuring the short circuit current for different wavelengths using a monochromator and this was normalized by considering the spectral graph of the source. This is given in Fig. 4.14. From the figure it can be seen that the response is higher at the absorption region of CdS and falls sharply to the higher energy side. The tailing of the response towards the red region of the spectrum may be due to the existence of acceptor level in the CdS band gap created by the diffused copper atoms.

4.4.2.5. Studies on capacitance variation

The C^{-2} Vs V graph for the cell is shown in Fig. 4.15. and it is more or less a straight line. This shows that the junction formed is more or less an abrupt one. The built-in voltage which is the difference between work functions of n and p-side, was evaluated from the extrapolated intercept on voltage axis and it was found to be 0.58 V. The acceptor density was calculated from the slope of the graph and it was found to be 1.23×10^{14}. Parameters of the best cell prepared are given in Table 4.4.

Table 4.4.

Cell parameters for the improved cell

Open Circuit Voltage	400 mV
Short Circuit Current Density	12 mA/cm^2
Fill Factor	0.49
Efficiency	3%
Series resistance	305Ω
Diode Quality Factor	1.9
Built-in Voltage	0.58V
Acceptor State Density	1.23×10^{14} cm^{-3}

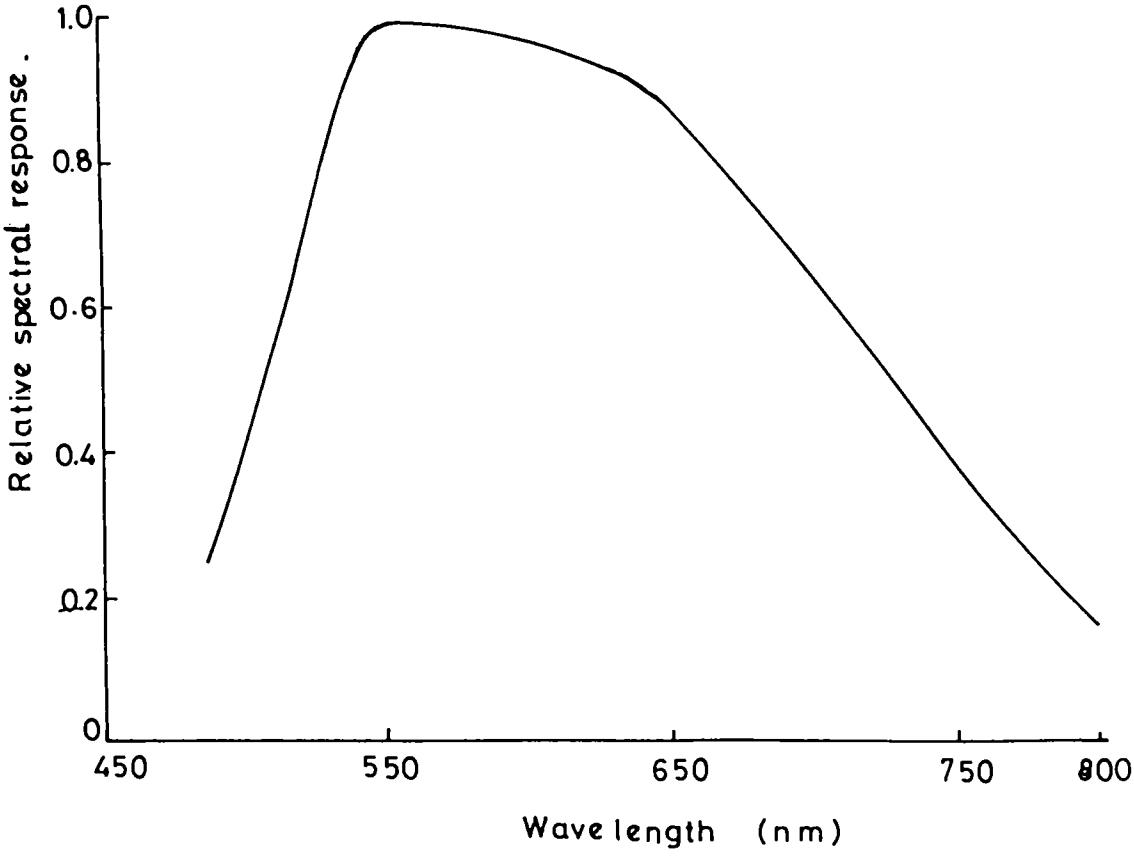

Fig. 4.14. Relative spectral response of the improved cell

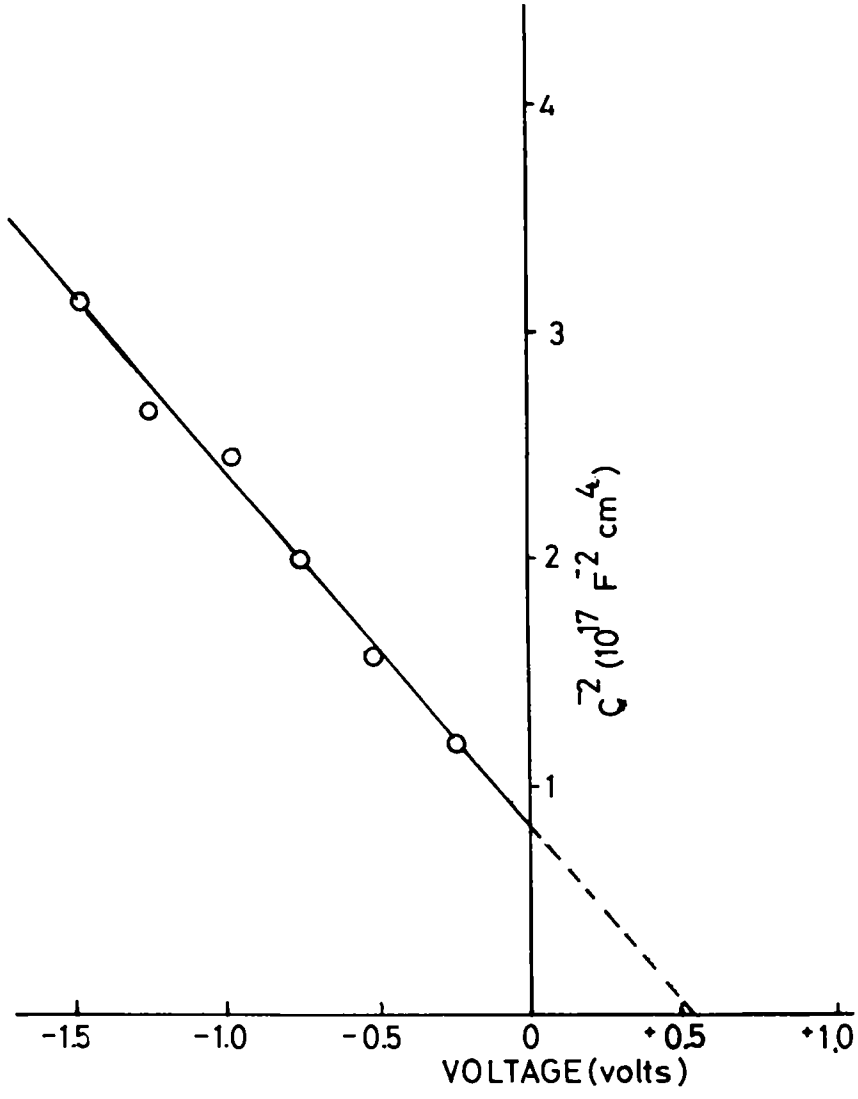

Fig. 4.15. C^{-2} Vs. V graph of the improved homojunction cell

4.4.3. Conclusion

Homojunction solar cells with moderate efficiency were fabricated. This is achieved by the uniform distribution of copper on the top layer of cadmium sulphide. The absorption and ESCA studies proved beyond doubt that there are no additional copper compounds due to the diffusion of more copper atoms into cadmium sulphide.

4.5. Indium doped CdS cell with better efficiency

In the earlier cases of cell fabrication, one can see that major defect to be a low fill factor as evident from the J-V characteristics. This ultimately affects the solar cell efficiency. One of the reasons for the low fill factor may be high series resistance of the cell resulting from high resistivity of cadmium sulphide films. Hence the reduction in the resistivity can lead to the reduction of series resistance of the cell, improving the fill factor. Such an attempt was made in this work, by doping the cadmium sulphide films with indium.

4.5.1. Brief review on doping of CdS

There is a growing interest in preparing doped CdS layer to use as window material in heterojunction solar cells. An effective way to obtain CdS thin films with low resistivity is to add indium as impurity (capable of acting as donors) into the films during the time of deposition. Several researchers had reported the properties of indium doped CdS films. Among these reports, there are studies on the effect of varying the doping concentration of indium. L.D. Partain et al [21] reported that doping of n-type CdS (containing excess Cd) with indium could raise the free-carrier concentration by an order of magnitude over the 77–300K temperature ranges. But they found that the increase in carrier concentration is only a small fraction of total concentration of indium impurities added as dopants. Neelkanth G. Dhere [22] et al reported that doping with indium, even at the lowest doping level utilized, resulted in the desired reduction of resistivity from 10^{5} to 10^{-2} Ωcm. The films were n-type with

electron concentration of 10^{18} to $10^{19} cm^{-3}$ and mobility of 14 to 75 $cm^2 V^{-1} s^{-1}$. Shi Yul Kim et al [23] studied the structural, electrical and optical properties of indium doped CdS thin films which were vacuum evaporated. Analyses were done by using XRD, SEM, Hall effect and optical transmittance spectra. They reported that the electrical conductivity, carrier concentration and Hall mobility at first increased with increasing In concentration and started decreasing after a level of doping. E. Bertran et al [24] studied the transparency of indium doped CdS films and they found that there was a change in band gap due to variation of indium concentration. They conducted these experiments in order to increase the electrical conductivity and transparency so that the efficiency of the cell can be increased. A. Kuroyanagi and T. Suda [25] reported the variation of resistivity of CdS thin films (prepared using ionized deposition on glass substrates) by indium doping. Jagger and Seipp [26] reported the shift of absorption edge in evaporated indium doped CdS layers, due to the variation of carrier concentration.

In the present work, the spray pyrolysed CdS films were doped with indium and the variation in resistivity, carrier concentration etc.were measured. Using these doped samples we fabricated homojunction solar cells. The details of the work are presented in the following section.

4.5.2. Preparation of CdS films doped with indium

100 ml solution of 0.02 M cadmium chloride and 100 ml of 0.02 M thiourea were mixed and into which $InCl_3$ solution (0.02 M, 10 ml) was added so that the percentage of indium doping was 10% by volume. This solution was sprayed into the hot substrate (SnO_2 coated glass) kept at a temperature of 300°C, keeping other spraying conditions exactly the same as those for the CdS preparation described in detail in chapter 3. Then 150 ml solution of 0.02 M cadmium chloride and 150 ml solution of 0.02 M thiourea were mixed and sprayed over the same film, again keeping the same spray conditions. The total

thickness of the CdS film in this case was in the range 1.1 to 1.3 μm. CdS films with different percentage of doping (5% and 8%) were also prepared.

These films, with different doping concentration were characterized first by taking XRD for structural analysis and then using Hall measurements for electrical characterization. Optical absorption studies were performed to have the $(\alpha h\nu)^2$ Vs. $h\nu$ graph from which optical band gap was calculated. Later chemical composition was confirmed by taking the ESCA depth profile. Details of the results from these analyses are described in the following sections.

4.5.3. Characterization

4.5.3.1. XRD Analysis

The XRD spectra of the samples with different doping concentrations are shown in Fig. 4.16. The films show excellent crystalline structure with all peaks characteristic of CdS and the <hkl> planes are marked in the figure. Films with 5% and 8% doping have preferred orientation along <002> direction, just like that of the undoped CdS film. But the film prepared with a doping of 10% has the preferred orientation along <101> direction. All the films are hexagonal in structure.

4.5.3.2. Hall measurement

The electrical characterization is important for the present work, since we are interested in films of low resistivity. This was done using Hall measurements. Here we used Vander Pauws techniques in square geometry and the details are presented in the Table 4.5.

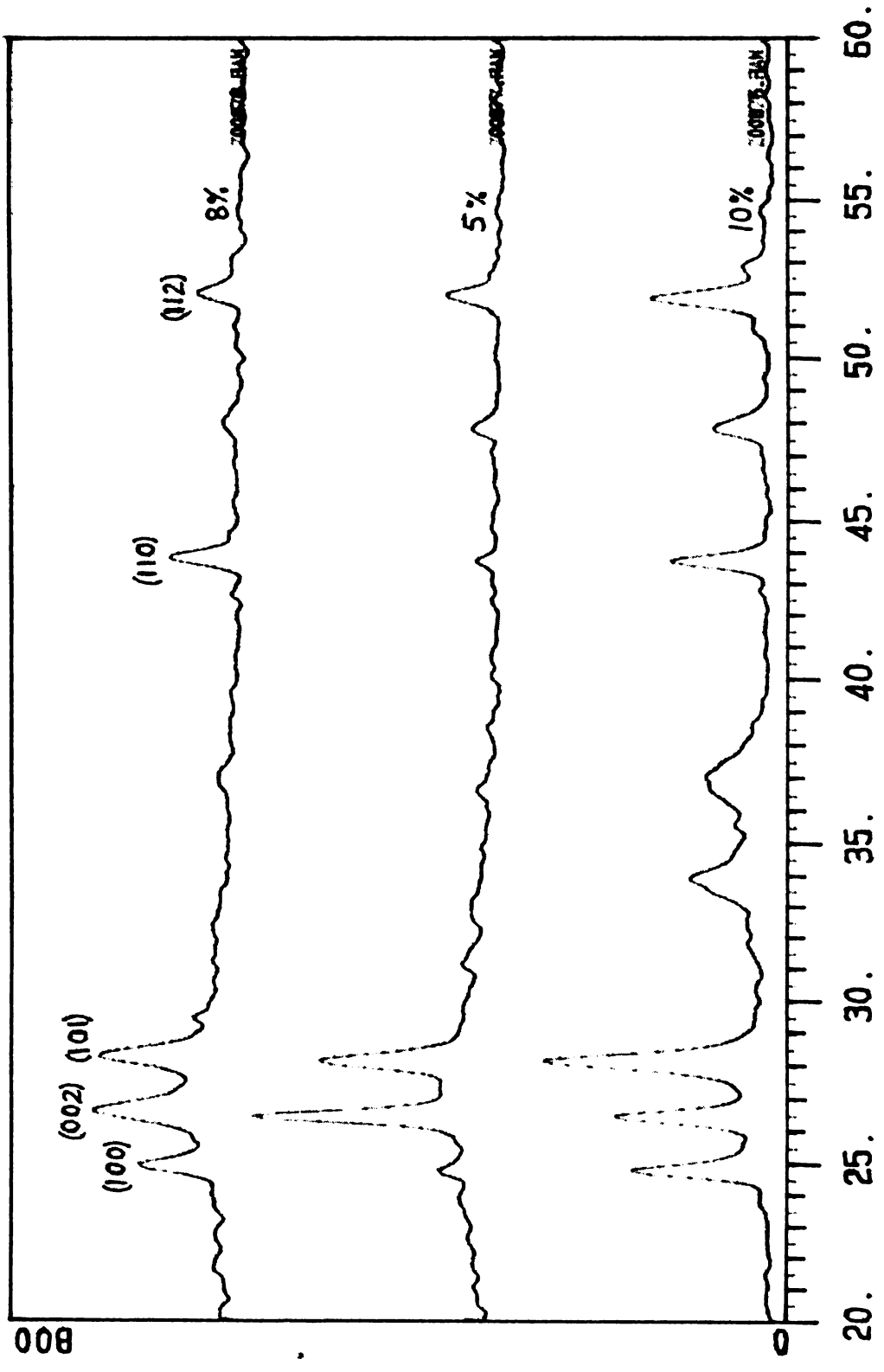

Fig.4.16. XRD spectra of indium doped CdS samples

Table 4.5.

Hall measurement values for CdS films with different percentage of In doping

% of Doping	5 %	8%	10%
Resistivity Ωcm	215.5826	169.1561	83.78191
Mobility $cm^2V^{-1}s^{-1}$	-315.9374	-166.5901	-59.066
Density cm^{-3}	-1.165×10^{14}	-2.215×10^{14}	-1.261×10^{15}
Hall Coefficient cm^3/Coul	-68110.3	-28179.73	-4948.7
Sheet Resistance Ω / □	2.156×10^{6}	1.691×10^{6}	8.378×10^{5}
Type of carriers	Electrons	Electrons	Electrons

It was found that the electrical resistivity decreased by one order, whereas the carrier concentration was increased by one order in comparison with the undoped CdS samples. Among the samples with different percentage of doping, 10% indium doped samples were better and we selected these for fabricating the device.

4.5.3.3. ESCA analysis

ESCA analysis of the sample with 10% indium doping was done and it is depicted in Fig.4.17. From the figure it is very clear that indium is present in the CdS sample. Again the stoichiometry of the film is not at all affected. It was found that indium had diffused into the top layer where copper is present. The atomic percentage of indium was found to be 10 on the top layer and it is gradually decreases. Eventhough solution containing indium was sprayed first so that doped layer was expected to be at the bottom, ESCA analysis revealed that the indium is present at the top layer. This may be due to the diffusion of indium, since the temperature applied to the sample is high during spraying.

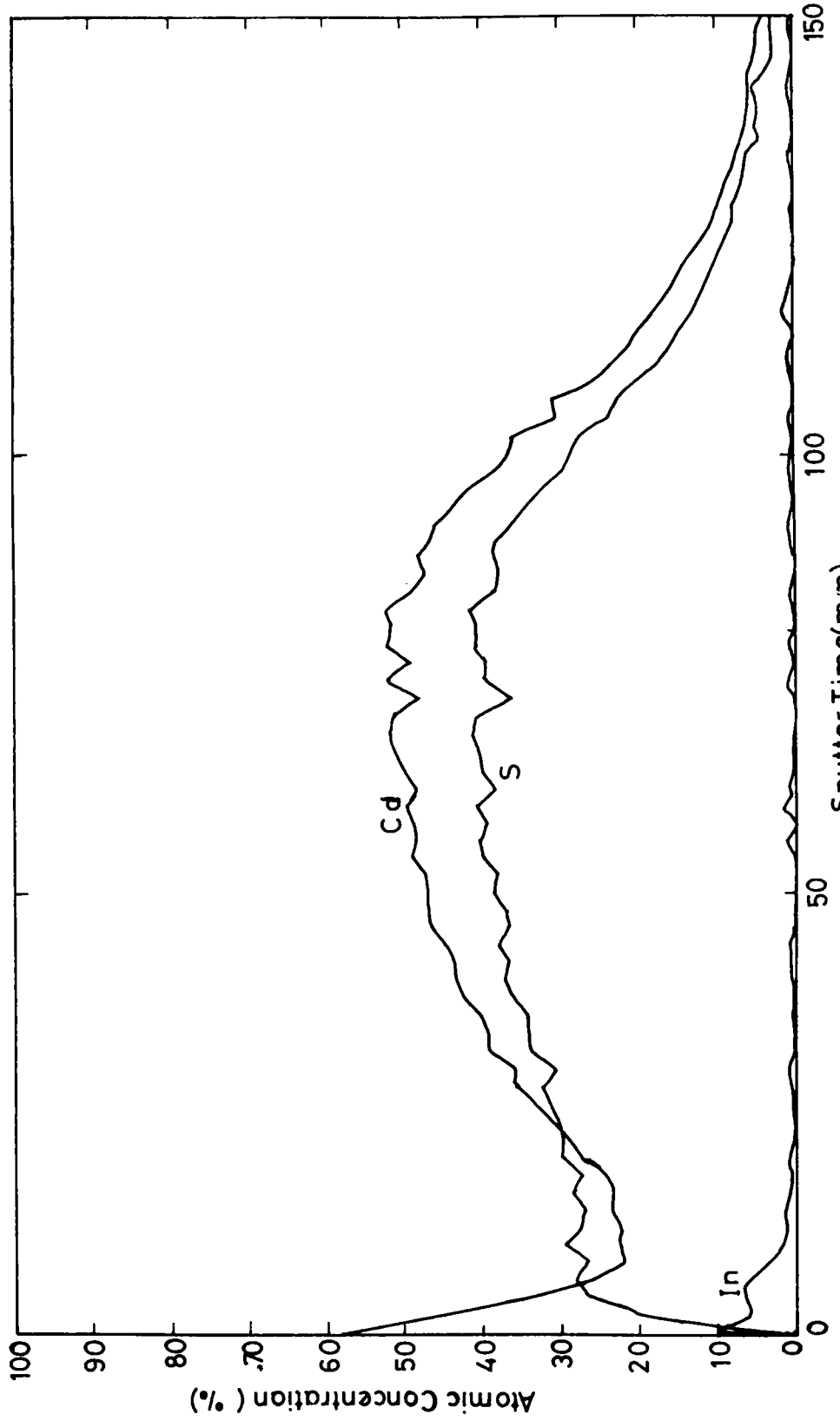

Fig.4.17. ESCA depth profile of 10% indium doped CdS sample

4.5.3.4. Optical absorption studies

The optical absorption studies were done on the samples and the spectrum is depicted in Fig.4.18. $(\alpha h\nu)^2$ Vs. $h\nu$ graph was drawn which is depicted in the inset of the Fig.4.18. From this the optical band gap was calculated to be 2.47 eV. Value of the band gap of the sample was found to be slightly greater than the standard value of CdS films, but an increase of the bandgap was reported in indium doped samples [24]. Optical absorption spectrum of the copper doped p-CdS sample was also taken and it is presented in the Fig.4.19. Bandgap was calculated by plotting $(\alpha h\nu)^2$ Vs. $h\nu$ graph, which is depicted in the inset of the Fig.4.19 and found to be 2.46 eV, which is slightly less than the n-CdS. This is valid when we compare with the earlier results. Here also optical absorption studies revealed that no traces of Cu_xS was present.

4.5.4. Cell fabrication

For the fabrication of homojunction in the doped CdS samples, we diffused copper into the CdS twice as in the previous case. This was done by annealing the copper deposited samples at a temperature of 300°C for 45 minutes, in high vacuum. Here the thickness of copper deposited was exactly the same in the previous case (first, 40 nm and then 25 nm). Then indium was coated as the top electrode and it was annealed. The area of the top electrode was 0.2 cm^2. The characterization of the cell fabricated was done by taking the J-V measurements, spectral response and capacitance-voltage measurements.

4.5.5. Results and Discussions

4.5.5.1. J-V Characteristics

The forward dark J-V characteristic was also drawn and it is presented in Fig.4.20. From its slope, the series resistance of the cell was calculated and it was 130 Ω. This value seems to be reasonably good for a solar cell and it is far improved when we compare with the previous cases. This value supports the idea that the series resistance can be reduced by reducing the resistance of the

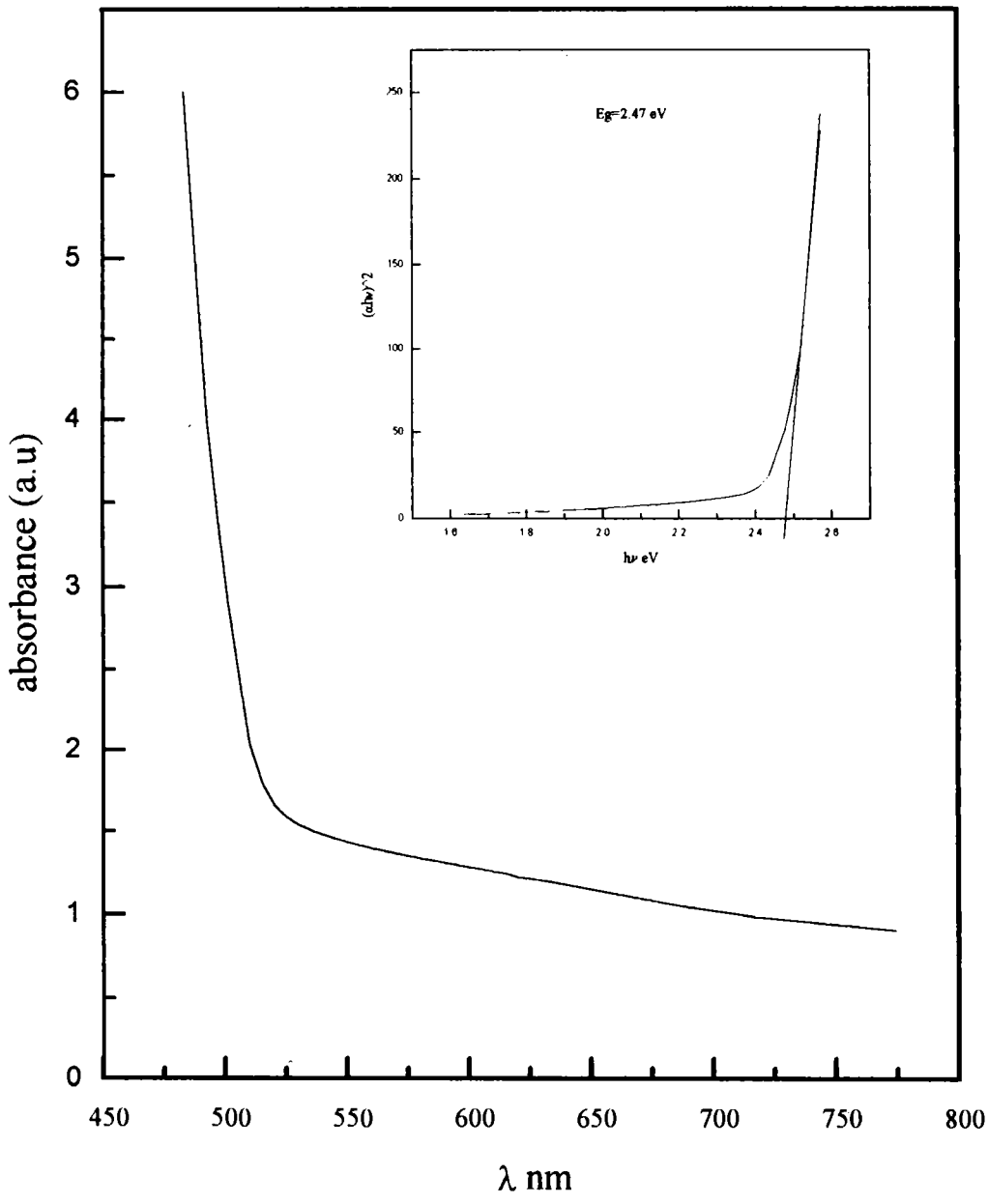

Fig.4.18. Absorption spectrum of indium doped n-CdS sample

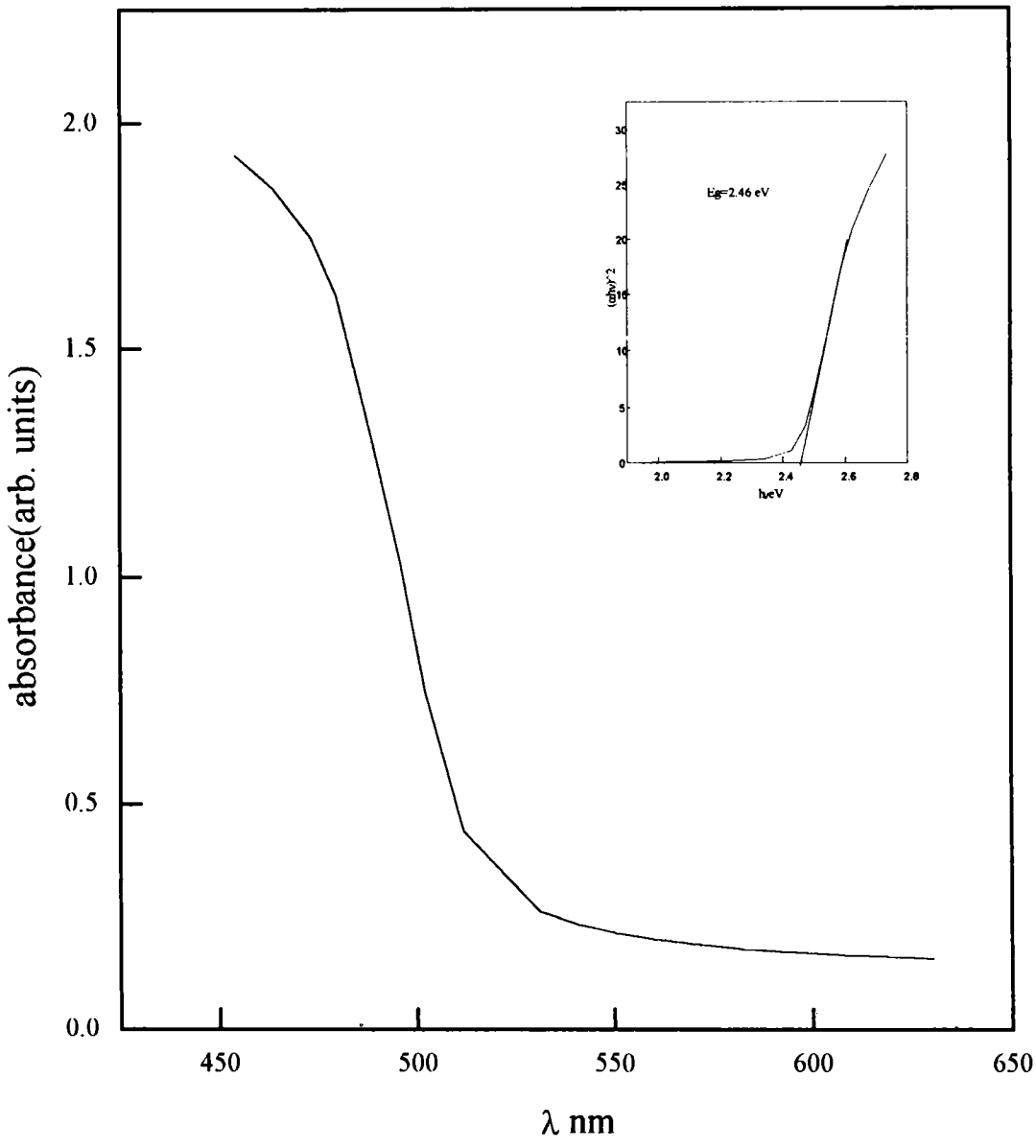

Fig.4.19. Absorption spectrum of indium doped p-CdS:Cu sample

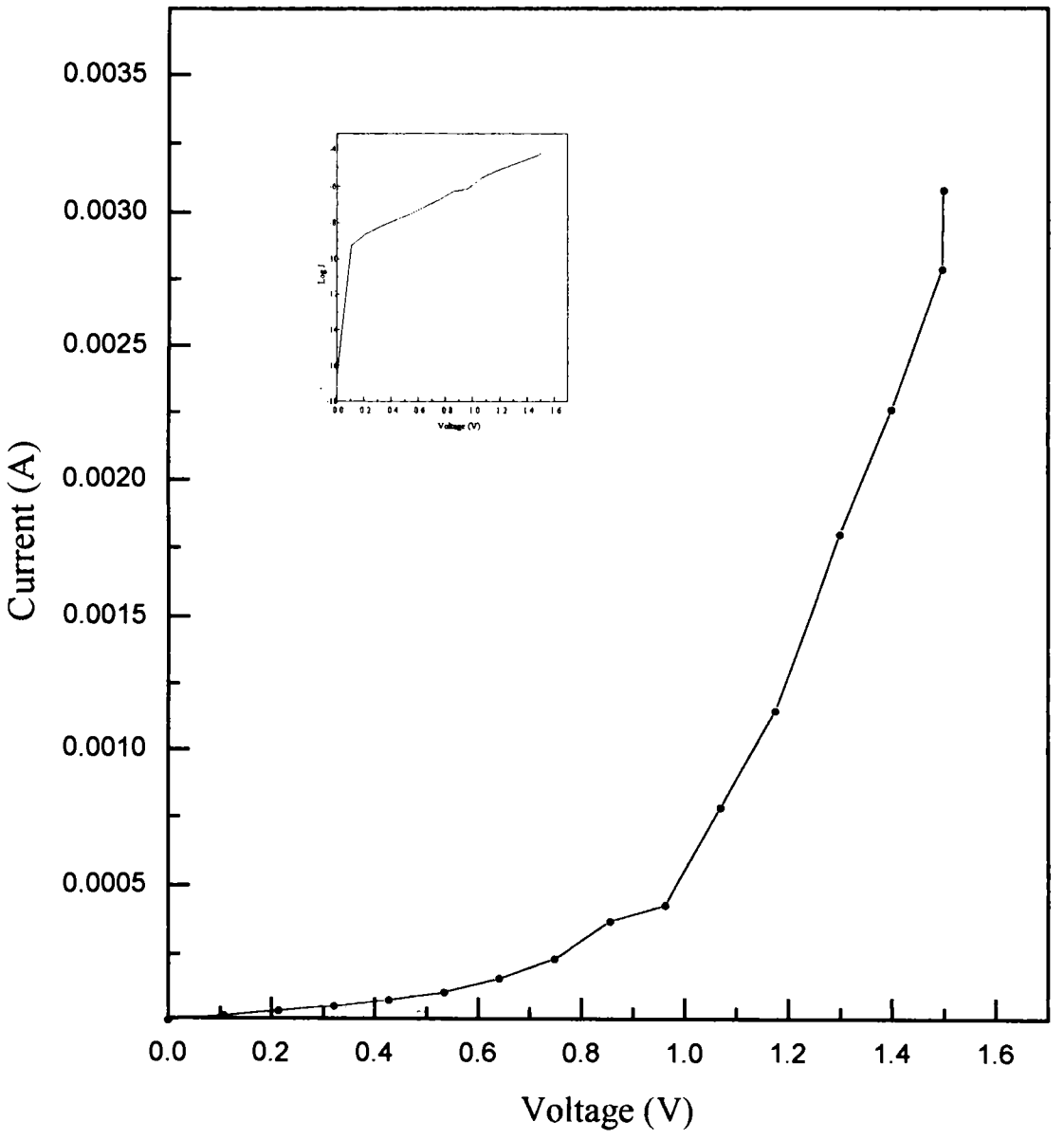

Fig.4.20. J-V characteristics of indium doped cell under dark condition

sample. Diode quality factor was calculated from the slope of the log J Vs. V plot, which is depicted in the inset of Fig.4.20. This value was found to be 1.7, which is also improved in this case. These may be the reasons for a better efficiency in this case.

The J-V characteristic of the homojunction solar cell fabricated is shown in the Fig. 4.21, under an illumination of 80 mW/cm^2 on the sample surface. The set up was exactly the same one used for the earlier cell studies. From this characteristic, the open circuit voltage and short circuit current density was found to be 390 mV and 13 mA/cm^2 respectively. The fill factor was calculated to be 0.55 and the efficiency was found to be 3.5%. The noticeable parameter in this case is the increase in fill factor. There is an increase of 12 % in fill factor when compared with that of undoped (improved) CdS cell. The increase in fill factor becomes 25 % when compared with the first cell. Similarly the short circuit density shows an increase of 8.3%. This resulted in an increased efficiency (3.5% in this case). The major increase is in the fill factor and this may be due to the decrease in resistivity of the CdS film by doping.

4.5.5.2. Spectral response curve

The spectral response curve was drawn by measuring the short circuit currents for different wavelengths. The graph was drawn using normalized value. This is depicted in Fig. 4.22. The curve is exactly similar to the previous curves for undoped samples showing the maximum at the absorption region of CdS and falls sharply to the lower wavelength region. But there is an enhanced response towards the lower wavelength side and a slightly higher value on the greater wavelength side.

4.5.5.3. Capacitante study

The C^{-2} Vs V graph was drawn from C-V measurement data and it is depicted in Fig. 4.23. This was done at a temperature of 303K and the area of

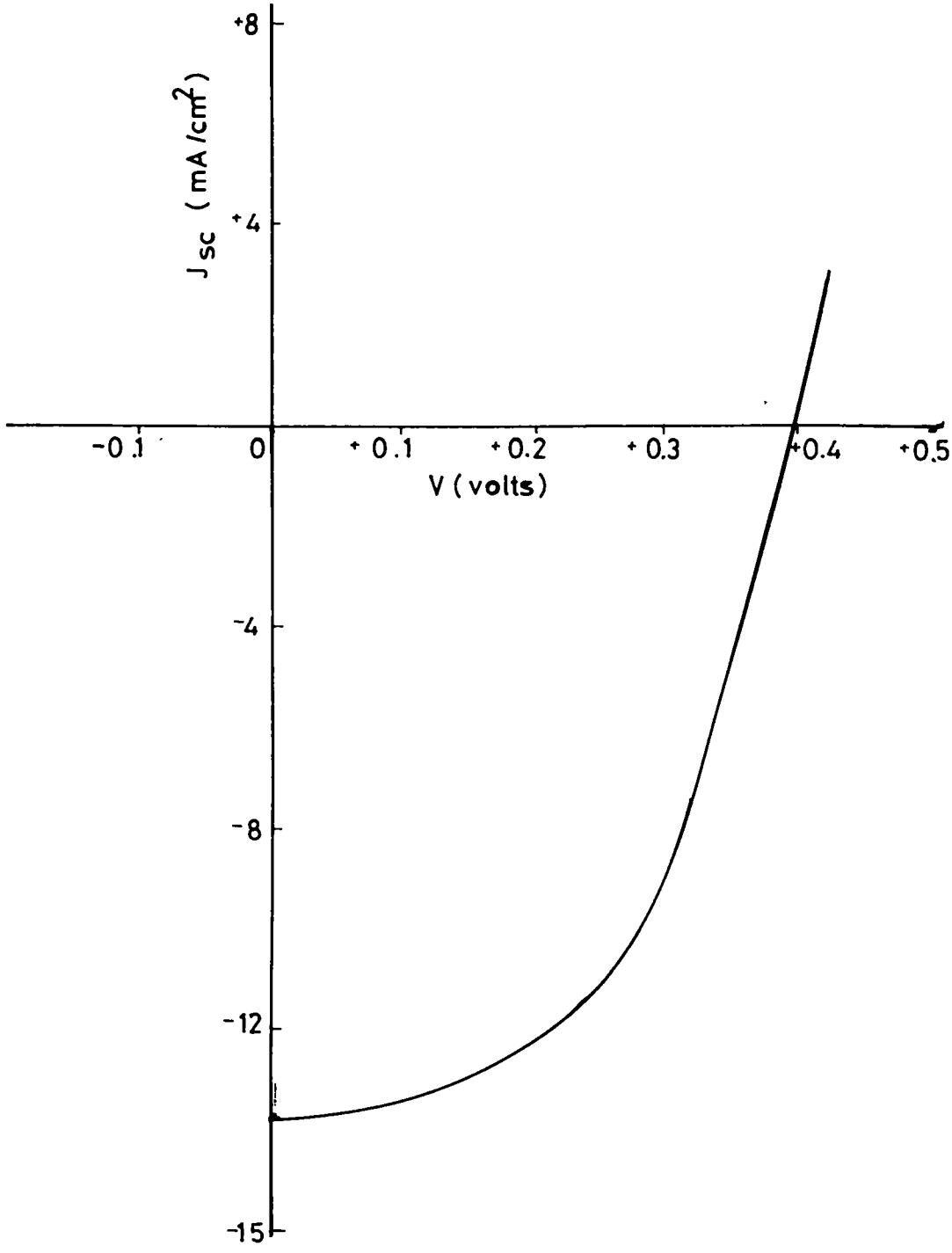

Fig.4.21. J-V characteristics of indium doped cell under an illumination of 80 mW/cm^2

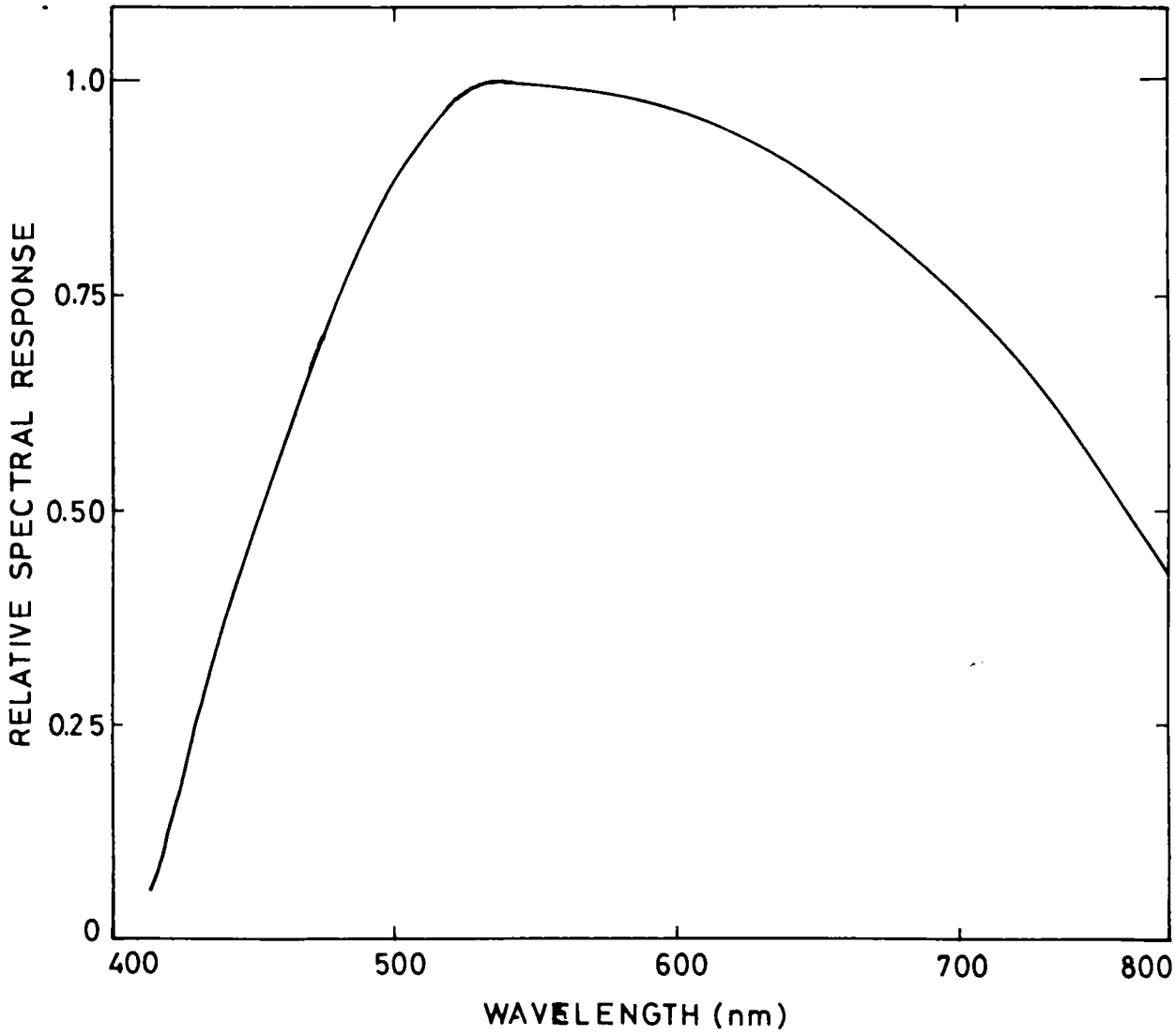

Fig.4.22. Relative spectral response of indium doped cell

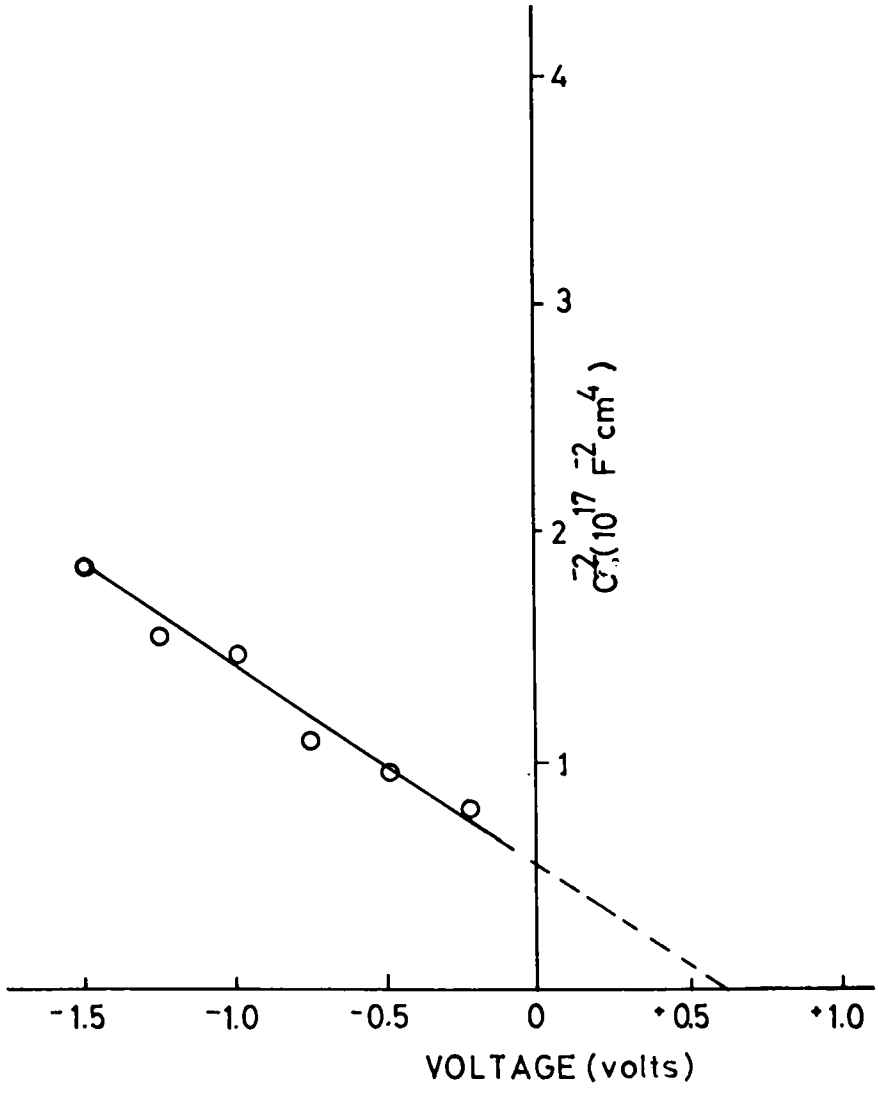

Fig.4.23. C^{-2} Vs. V graph for indium doped CdS homojunction cell

the cell was 0.2 cm^2. Just like the previous case, this is more or less straight line in behaviour. The built- in voltage was found to be 0.6V, which is more or less the same value for the previous cell. Again the acceptor density was calculated from the slope of the graph and it was found to be 1.725×10^{14} cm^{-3}. This value is comparable with the value obtained for the previous cell, but here it is slightly on the higher side.

4.5.5.4. ESCA analysis

ESCA depth profile of the cell was done and it is shown in Fig.4.24. From the figure it is very clear that there is no shift in binding energy for the copper throughout the thickness of the sample. The two peaks are corresponding to the binding energy of the pure copper. Similarly we can see that there are no shift in binding energies for sulphur and cadmium also. This confirms that there are no copper compounds formed due to the diffusion of copper in indium doped samples. For the best cell fabricated, parameters of the cell are given in Table 4.6.

Table 4.6.

Cell parameters for the indium doped cell

Open Circuit Voltage	390 mV
Short Circuit Current Density	13 mA/cm^2
Fill Factor	0.55
Efficiency	3.5 %
Series Resistance	130 Ω
Diode Quality Factor	1.7
Built-in Voltage	0.6V
Acceptor State Density	1.725×10^{14} cm^{-3}

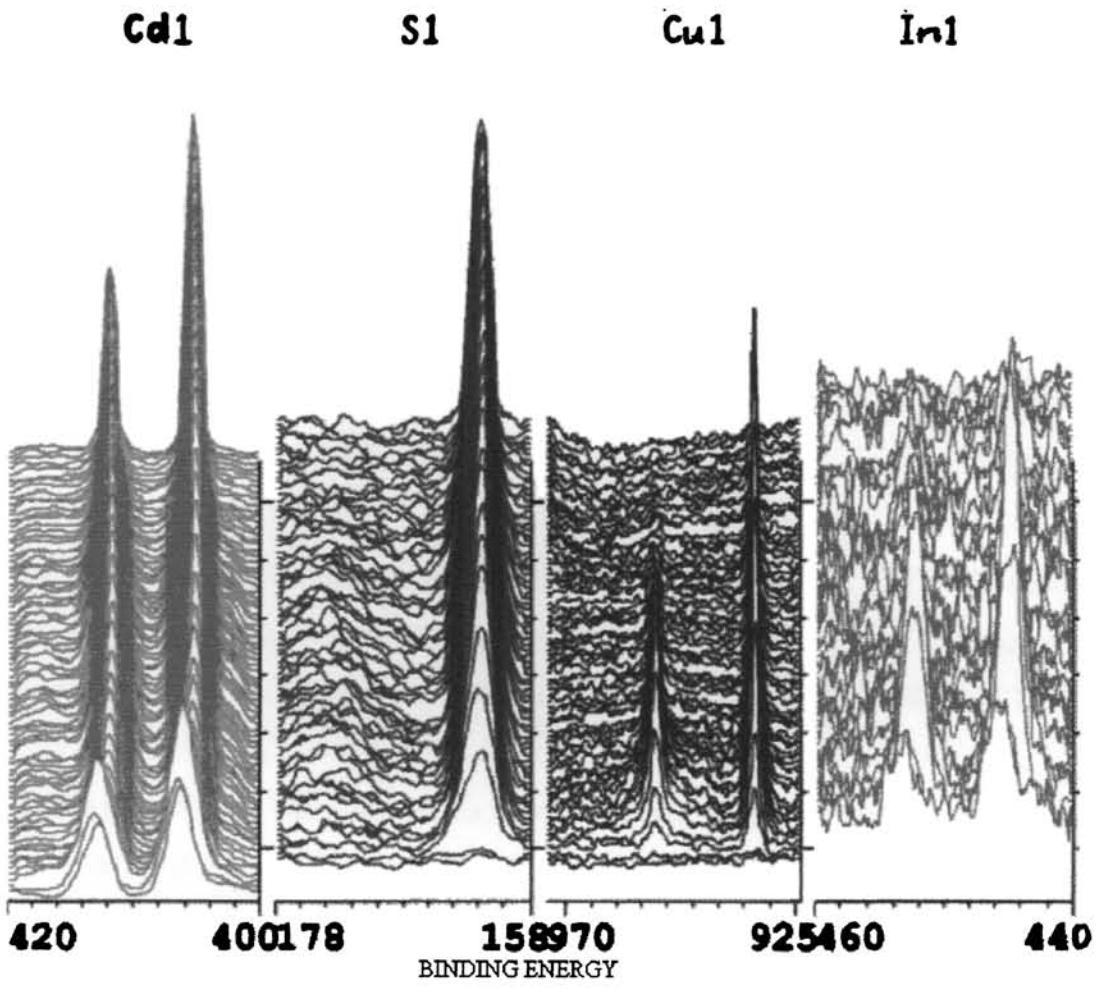

Fig.4.24. ESCA Depth profile of Indium doped cell

4.5.6. Conclusion

Indium doped CdS films with different doping concentrations have been prepared and characterized. Films doped with 10% of indium are found to be better in electrical properties. Homojunction in indium doped CdS thin film was fabricated. The fill factor for the cell fabricated was found to be better than the case of undoped samples and have better value of diode quality factor. This cell could give a moderate efficiency.

References

1. D .C.Reynolds, G. Leies, L.L. Antes and R.E. Marburger, Phys. Rev., **96** (1954) 533
2. T .J. Coults and J.D. Meakin (Eds.), *Current Topics in Photovoltaics*, Academic press (1985) 224
3. R .Williams and R.H. Bube, J. Appl. Phys., **31** (1960) 968
4. J .Woods and R.A. Champion, J. Electron Control., **7** (1960) 243
5. H .G. Grimmeiss and R. Memming, J. Appl. Phys., **33** (1962) 2217
6. H .G. Grimmeiss and R. Memming, J. Appl. Phys., **33** (1962) 3596
7. Y . Kashiwaba, H. Kirita, H. Abi and T. Ikeda, Jpn. J. Appl. Phys., **29** (1990) 1733
8. Y . Kashiwaba, I. Kanno and T. Ikeda, Jpn. J. Appl. Phys., **31** (1992) 1170
9. T . Abe, Y. Kurobuchi, K. Ohta and Y. Kashiwaba, *Extended Abstracts;The 59 th Autumn Meeting of The Japan Society of Applied Physics*, (1998) p.1226
10. M .S. Tyagi, *Introduction to Semiconductor Materials and Devices*, John Wiley & Sons (1991)
11. K .W. Boer, *Survey of semiconductor Physics*, Vol.2, Van Nostrand Reinhold, New york (1992) 820
12. K .L. Narayanan, K.P. Vijayakumar, K.G.M. Nair, B. Sundrakkannan, G.V.N. Rao and R. Keshavamoorthy, Nucl. Instr.Meth.Phys.Res., **B132** (1997) 61
13. K .L. Narayanan, K.P. Vijayakumar, K.G.M. Nair and N.S. Thampi, Phys.Stat Solidi (b)., **240** (1997) 8
14. G . Venugopal Rao, G. Amarendra, B. Viswanathan, K.L. Narayanan and K.G.M. Nair, Solid state Physics (India) **39C** (1996) 219
15. K .L. Narayanan, *Ph.D Thesis*, Cochin University of Science and Technology (1997)
16. Sunny Mathew, P.S. Mukerjee and K.P. Vijayakumar, Jpn. J. Appl. Phys., **34** (1995) 4940

17. M . Ristova and M. Ristov, Solar Energy Materials and Solar Cells, 53 (1998) 95
18. H .J. Hovel, Semiconductors and Semimetals, **Vol.11**, Solar Cells, Academic press, New York (1975) 65
19. P .K. Vidyadharan Pillai, K.P. Vijayakumar, P.S. Mukerjee, J. Mater. Sci. Lett., **13** (1994) 1725
20. P .J. Sebastian, App. Phy. Lett., **62(23)** (1993) 2956
21. L .D. Partain, G.J. Sullivan and C.E. Birchenall, J. Appl. Phys., **50(1)** (1979) 551
22. Neelkanth G. Dhere, Helio R. Moutinho and Ramesh G. Dhere, J. Vac. Sci. Technol., **A 5(4)** (1987) 1956
23. Shi Yul Kim, Dong Seop Kim, Byung Tae Ahn and Ho Bin Im, Thin Solid Films, **229** (1993) 227
24. E . Bertran, A. Lousa, M. Varela, M.V. Garcia-Cuenca and J.L. Morenza, Solar Energy Materials, **17** (1988) 55
25. A . Kuroyanagi and T. Suda, Thin Solid Films, **176** (1989) 247
26. H . Jager and E. Seipp, J. Appl. Phys., **52(1)** (1981) 425

Chapter 5

Summary and Conclusions

5.1. Introduction

As an alternative to the conventional energy sources, the PV technology has to be improved. If it is to be used for the terrestrial applications, this has to be popularised. In order to achieve this, we have to develop solar cells and modules at reasonable prices, affordable to common man and this can be achieved by a strong interaction between Scientists and Engineers. First thing to be done in this direction is to study about the factors affecting the performance of the existing solar cells and this will result in the enhancement of efficiency of the cells. At the same time it is equally important to have R&D works on developing new photovoltaic devices and processes which are less expensive for large scale production. The work presented in this thesis is such an attempt.

CdS is an important binary compound semiconductor, which is very useful in the field of photovoltaics. Works on this material started almost at the same time when research on silicon was started. Moreover, it is very easy to prepare large area CdS thin films. Considering these points, CdS was selected for the present work. But it is to be specifically mentioned here that the work presented here fully concentrates on the fabrication of a homojunction in CdS. In earlier chapters of this thesis, a detailed review of works on this material and a description of relevant theory of p-n junction are included. Later chapters contain the experimental aspects of the work including material analysis. Finally a brief description of environmental and health problems, on large scale usage of CdS is also given.

In order to fabricate thin film homojunction cadmium sulphide cells, we prepared and characterized SnO_2 thin film as the lower electrode, p-CdS as the active layer and n-CdS as window layer.

5.2. Tin Oxide (SnO_2)

For the fabrication of solar cells presented in this work, SnO_2 films prepared on ordinary glass substrate using spray pyrolysis technique was used as the lower electrode. This process was standardized to get highly conductive and transparent films. The structural, optical and electrical characterizations were also carried out using different analytical techniques such as XRD, spectrophotometer and Hall measurements and the results are summarized in the next paragraph.

SnO_2 coated on glass substrates using spray pyrolysis technique is highly adhesive and stable. At first the spray parameters like, rate of spray, concentration of solution, the angle of incidence of spray, pressure etc., were optimized. Regarding the substrate temperature we found that there was an optimum value at which the sheet resistance became minimum. In the present study this temperature was 475° C and the resistivity obtained was 5.68×10^{-4} Ω cm for undoped films. Using Hall measurements the films were found to be n-type and carrier concentration were found to be in the order of 10^{20} per cm^3. Even though doping of the films with flourine reduced the sheet resistance, it was not used in the present study. Flourine doping affected the percentage of transmission of SnO_2 films. Transmission of the film used in the present work was 80% in the visible region. The films were found to be highly crystalline with preferred orientation along <211> direction. These films having the above mentioned properties were used for the cell fabrication as the lower electrode.

5.3. n-CdS

CdS films were deposited using spray pyrolysis technique, which is ideal for large area thin film preparation. Moreover spray pyrolysed films are found to be stoichiometric. Another advantage of this method was that doping could be done effectively. After a number of trials, the different spray parameters were standardized for getting good quality films. The best films were characterized by using different analytical techniques.

XRD results gave a picture about the chemical composition and structure of the film. Films prepared were found to be crystalline with preferred orientation along <002> direction. Optical absorption studies were done and from the $(\alpha h\nu)^2$ Vs $h\nu$ graph, band gap was calculated as 2.44 eV, very near to the standard value of the bulk material. Composition of the films was analysed by EDAX and was later confirmed using ESCA results. Electrical characterization of the films was done using Hall measurements, from which it was found that the films prepared were n-type and the electrical resistivity was about 250 Ω cm. Carrier concentration for the best film was found to be 1.02229×10^{14} cm^{-3}. Using SEM microstructural analysis was done.

5.4. p-CdS

The main thrust of the present work was on the preparation and characterization of p- type CdS films. For the preparation of p-CdS, a thin layer of pure copper (40 nm) was deposited on the as prepared CdS film. This copper layer was completely diffused into CdS by thermal annealing under high vacuum at 300°C for 45 minutes. It was found that the copper diffused region of CdS was converted into p-type. This was verified first by hot probe method, and later by Hall measurements.

XRD pattern of the p-CdS showed the peaks to be exactly the same as that of the n-CdS itself. Film had hexagonal structure with <002> as the preferred orientation. It is to be noted that there were no peaks corresponding to Cu_xS. Optical absorption studies gave value of the band gap to be 2.43 eV. ESCA analysis of p-CdS was also done to confirm that no compounds like Cu_xS were formed. Depth profile analysis indicated that there was a layer of n-CdS below the p-CdS. From the electrical characterization, it was found that the resistivity decreased by one order when compared to that of n-CdS and the carrier concentration was found to be 1.114×10^{16} cm^{-3}.

5.5. CdS homojunction solar cells

Homojunction solar cells were fabricated with the structure Glass/SnO_2/ n-CdS/p-CdS:Cu/In. Parameters like annealing temperature, CdS layer thickness etc. were optimized by varying them in wide range. J-V characteristics of the best cell fabricated were V_{oc} = 200mV, J_{sc} = 5mA/cm^2, FF = 0.44 and η = 0.73%. In this case, annealing temperature was 300°C and the thickness of CdS was nearly 1μm. Cell was characterized by drawing the spectral response curve also. From the dark J-V characteristics, "diode quality factor" was calculated as 2.6. Series resistance of the cell under dark conditions was found to be 400 Ω.

5.6. Homojunction solar cells with improved performance

Depth profile of the earlier cell revealed that copper distribution over the p-CdS layer was not uniform and the depth of diffusion of copper atoms was also less (500 nm). The junction formation was not well defined and this might have been the reason for low efficiency. So another layer of copper (25nm) was coated in the same region where copper was diffused earlier. This was again annealed at 300°C for 45 minutes in high vacuum. These samples also formed homojunction with the same structure as that of the first one. Depth profile of the sample was done and

found that the copper distribution on the top layer of CdS was uniform. Copper was present up to a depth of 700 nm in this case. It also revealed that there were no additional compounds like Cu_xS, due to the diffusion of more copper atoms. It also showed that there was a layer of n-CdS below the p-CdS:Cu layer in this case also. J-V characteristics under illumination and dark conditions were drawn. From the cell characteristics under illumination, the open circuit voltage was found to be 400mV and short circuit current density was obtained as $12mA/cm^2$. Fill factor in this case was 0.49 and the efficiency was calculated as 3%. Diode quality factor and series resistance of the cell were found to be 1.9 and 305 Ω respectively, from the J-V characteristics under dark condition. Again, the cell was characterized from the spectral response curve and C-V measurements. Acceptor density was calculated to be 1.23×10^{14} cm^{-3}. These results show that there is considerable improvement in the cell parameters when the quantity of copper diffused into CdS was increased.

5.7. Cell fabrication in the indium doped CdS samples

In the earlier sections we summarized the results obtained from the characterization of two homojunction cells fabricated using CdS. Here one can see that fill factor was low for both the cases. This might have been due to the high series resistance of the sample, since the CdS film prepared had high electrical resistivity. In order to reduce this, indium was doped in CdS thin films in different percentages. These were again characterized using XRD and Hall measurements. CdS films containing 10% indium (by volume of spray solution) showed good electrical properties. ESCA analysis on these samples also confirmed the presence of indium. In these types of films copper was diffused two times, just like the previous case to fabricate homojunction cell. The J-V characteristics under illumination and dark conditions were drawn. Here open circuit voltage and short circuit current density were 390mV and $13mA/cm^2$ respectively. Fill factor was

calculated to be 0.55 and efficiency was 3.5%. From the forward characteristics obtained under dark condition, diode quality factor and series resistance of the cell were calculated. These values were 1.7 and 130 Ω respectively. The cell was again characterized by drawing the spectral response curve. The capacitance variation with the applied voltage was also studied. From the C^{-2} Vs. V graph, the acceptor density was calculated and it was found to be $1.725 \times 10^{14} cm^{-3}$. It is very clear that due to indium doping, there is considerable improvement in the fill factor (12%) while the diode factor and series resistance got decreased.

5.8. Environmental and other related problems

One may be interested in knowing whether problems related to environmental, health and safety (EH&S) may become very serious in the event of large scale production of these cells using cadmium. These aspects are briefly discussed below.

Cadmium material used for the fabrication of homojunction solar cells is highly toxic. The major damages due to continued exposure to low levels of cadmium are on the kidneys, lungs and bones. In the body, Cd accumulates in renal cortex, where it is effectively retained. Chronic exposure to excessive cadmium levels may also cause bone diseases characterized by softening, bending and reduction in bone size.

The real advantage of spray pyrolysis process is that there is no emission of any toxic gases during the deposition. Again a powerful airflow can take the waste gases to distant places through pipe. Very low concentration of the chemicals is needed in this process. So long as the operators keep good laboratory practices in handling the chemicals, the risk involved from this material is very low, though they are toxic. On large scale usage it may become necessary that the cells after

their life, should be bought back by the companies to retrieve the chemicals like cadmium. This will reduce environmental problem and also the material wastage.

References

L .D. Partain (Ed), *Solar Cells and their Applications*, John Wiley & Sons, Inc., New York (1995)